

UCSF

UC San Francisco Electronic Theses and Dissertations

Title

Transcriptional control of subtype switching ensures adaptation and growth of pancreatic cancer

Permalink

<https://escholarship.org/uc/item/5cx3t1b6>

Author

Adams, Christina

Publication Date

2019

Peer reviewed|Thesis/dissertation

Transcriptional control of subtype switching ensures adaptation and growth of pancreatic cancer

by
Christina Adams

DISSERTATION

Submitted in partial satisfaction of the requirements for degree of
DOCTOR OF PHILOSOPHY

in

Biomedical Sciences

in the

GRADUATE DIVISION

of the

UNIVERSITY OF CALIFORNIA, SAN FRANCISCO

Approved:

DocuSigned by:

Jayanta Debnath

Jayanta Debnath

51C29AC261CD4F0...

Chair

DocuSigned by:

Rushika Perera

Rushika Perera

DocuSigned by:

Matthias Hebrok

Matthias Hebrok

DocuSigned by:

Tien Peng

Tien Peng

256E38508AB94C9...

Committee Members

Dedication

This work is dedicated to my Abuelitos who always saw me as “number 1”, to my Tía who I miss dearly, and to Andrew - without whom I would not be blessed with my Jessamine.

Acknowledgements:

The work herein would not be possible without the guidance, mentorship and support from many people. It takes a village and I will forever be grateful.

First and foremost, I would like to thank my graduate advisor, Rushika Perera, for her constant mentorship and guidance. Her willingness to design a research program appropriate for where I was in my graduate school training made it possible for me to stay on track and remain engaged in the work. Her enthusiasm for conducting solid and exciting science provided constant motivation and I am grateful for all that she taught me.

I would also like to thank my thesis committee members Jayanta Debnath, Matthias Hebrok, and Tien Peng for their time, feedback and support. I am appreciative of their constructive remarks and outside perspective that helped to strengthen this story. I am especially indebted to my committee chair Jayanta Debnath who served as an immense source of support during my graduate studies even before I joined the Perera lab. His engagement in this story from the beginning has shaped how I think about a scientific problem, and I am grateful for the many opportunities I had in presenting this work to him and his group.

I would like to thank all the members of the Perera Lab who have made working in the lab such a joy. Their input during lab meetings and everyday discussions has helped hone my scientific thinking and helped to push this project forward. In particular I would like to thank Aprilgate Wang, who was a technician in the lab that helped me establish the foundation of this story during a time when the finished product was still far off and hard to realize. Thank you to Megan Montoya, a talented SRTP summer student (and

now a current BMS graduate student) who contributed substantially to this project despite her short tenure in the lab. Thank you to Denna Kwang (Htet Htwe Htwe) who provided essential technical support to this project in its final stages, and who very bravely took on the mouse experiments that elevated this story to its final state. Many thanks to the other members of the lab (Julian Yano, Anthony Venida, Suprit Gupta, and Zeynep Cakir) who I have called on for favors now and again, and for their constant support and senses of humor. They are truly a wonderful group of people and I will cherish the memories made in the midst of trying to do good science.

Before starting at UCSF, I attended Cal State Fullerton where the mentors and teachers there made this entire academic journey possible. In particular the mentorship from Amybeth Cohen, Marcelo Tolmasky and Chandra Srinivasan was key in introducing me to scientific research, and I am so thankful to them for showing me that I was capable of getting a PhD at a place like UCSF.

A huge thank you to the BMS program and my classmates and friends who provided distraction, humor and support throughout my graduate school journey. I am very lucky to have become friends with such brilliant and talented people, and I have benefited immensely from knowing them.

I am extremely fortunate to have such a deep support network in my family. I am so grateful for their enduring love and support. Thank you to my parents, sister, grandparents, aunt and uncles, all of whom have shaped how I think and have been instrumental in keeping me sane.

Finally, thank you is not adequate enough a sentiment to my partner, Andrew, who has gone beyond all in holding me up and who took on fatherhood with strength,

fearlessness and vulnerability. To my 8-month old daughter Jessamine, thank you for humbling me and giving me a large dose of perspective – you are the most important person in my life always.

Contributions to presented work

The work described in this dissertation was done under the direct supervision and guidance of Dr. Rushika Perera.

Contents in Chapters 1-3 are modified from the following publication:

Adams CR, Htwe HH, Marsh T, Wang AL, Montoya ML, Subbaraj L, Tward AD, Bardeesy N, Perera RM. Transcriptional control of subtype switching ensures adaptation and growth of pancreatic cancer. 2019. *eLife*. 8:e45313

Lakshmipriya Subbaraj and Aaron Tward performed the analysis for overall and progression-free survival and the accompanying cox proportional hazards regression models shown in Figures 2.1, 2.2 and 2.3. Christina Adams performed all other experiments.

Transcriptional control of subtype switching ensures adaptation and growth of pancreatic cancer

By: Christina Adams

Abstract:

Pancreatic ductal adenocarcinoma (PDA) is a heterogeneous disease comprised of a basal-like subtype with mesenchymal gene signatures, undifferentiated histopathology and worse prognosis compared to the classical subtype. Despite their prognostic and therapeutic value, the key drivers that establish and control subtype identity remain unknown. Here we demonstrate that PDA subtypes are not permanently encoded and identify the GLI2 transcription factor as a master regulator of subtype inter-conversion. GLI2 is elevated in basal-like PDA lines and patient specimens and forced GLI2 activation is sufficient to convert classical PDA cells to basal-like. Mechanistically, GLI2 upregulates expression of the pro-tumorigenic secreted protein, Osteopontin (OPN), which is especially critical for metastatic growth in vivo and adaptation to oncogenic KRAS ablation. Accordingly, elevated GLI2 and OPN levels predict shortened overall survival of PDA patients. Thus, the GLI2-OPN circuit is a driver of PDA cell plasticity that establishes and maintains an aggressive variant of this disease.

Table of Contents:

Chapter 1	Introduction	1
	Pancreatic ductal adenocarcinoma	2
	Disease development and progression	2
	Genetic alterations in pancreatic cancer	6
	Targeting mutant KRAS	7
	Stromal contributions to disease pathogenesis	7
	Identification of pancreatic cancer subtypes	9
	Transcriptional profiling revolutionizes subtype identification in cancer	9
	Pancreatic cancer subtypes	12
	EMT contributes to tumor cell plasticity and subtype conversion	17
	EMT promotes cancer cell plasticity	17
	The role of EMT in basal-like pancreatic cancer	21
	Contributions of EMT to drug resistance in cancer	24
	Subtype switching underlies features of aggressive disease	25
	The role of hedgehog signaling in pancreatic cancer	28
Chapter 2	GLI2-OPN mediated subtype switching enables adaptation to oncogene ablation in pancreatic cancer	33
	Expression of Hh ligands and GLI transcription factors are anti-correlated and predict survival outcomes in PDA	34
	GLI expression and activity correlates with a mesenchymal cell state and the basal-like subtype of PDA	43
	GLI2 is required for maintenance of the basal-like state	47

GLI2 induction is sufficient to drive a classical to basal-like subtype switch in PDA cells	53
GLI2 mediates basal-like subtype switching in response to oncogenic KRAS ^{G12D} ablation	59
Acquired resistance and tumor relapse following KRAS* ablation is mediated by GLI2	60
The secreted ligand Osteopontin (OPN) promotes basal-like subtype conversion downstream of GLI2	68
Loss of OPN in basal-like cells suppresses <i>in vivo</i> tumor growth	69
Methods	82
Chapter 3 Mechanisms of cell plasticity: implications for pancreatic cancer subtypes and treatment options	93
References	100

List of Figures:

Chapter 1

Figure 1.1	Step-wise progression of pancreatic ductal adenocarcinoma (PDA)	4
Figure 1.2	Identification of PDA subtypes	14
Figure 1.3	EMT and subtype switching promote plasticity and aggressive disease in PDA	19
Figure 1.4	Hedgehog signaling in PDA	31

Chapter 2

Figure 2.1	Expression and activity of GLI proteins is anti-correlated with Hh ligand levels in PDA	35
Figure 2.2	GLI proteins are expressed in basal-like PDA	39
Figure 2.3	Cox proportional hazards regression models for predictors of overall survival and progression-free survival.	41
Figure 2.4	GLI expression and activity correlates with EMT and the basal-like subtype of PDA	45
Figure 2.5	GLI2 is required to maintain the basal-like state in PDA	49
Figure 2.6	GLI2 knockout results in loss of basal-like identity in PDA	51
Figure 2.7	GLI2 is sufficient to drive basal-like subtype switching	55
Figure 2.8	GLI proteins promote the basal-like phenotype	57
Figure 2.9	GLI2-mediated basal-like subtype switching rescues viability of PDA cells following KRAS ^{G12D} ablation	62

Figure 2.10	GLI2 is upregulated in response to KRAS ^{G12D} ablation	64
Figure 2.11	GLI2 is necessary and sufficient to promote bypass of KRAS ^{G12D} -mediated oncogene addiction	66
Figure 2.12	OPN is a downstream effector of GLI2 that promotes a basal-like subtype switch	71
Figure 2.13	Secreted OPN promotes the basal-like subtype of PDA downstream of GLI2	73
Figure 2.14	OPN loss impairs growth of basal-like PDA	75

List of Tables:

Chapter 2

Table 2.1	Human and mouse primer sequences used in this study	77
Table 2.2	Classical and basal-like gene signatures	80

CHAPTER 1

Introduction

PANCREATIC DUCTAL ADENOCARCINOMA

Pancreatic ductal adenocarcinoma (PDA) is projected to become the second leading cause of cancer-related deaths by 2030 (Rahib et al. 2014), and has a 5-year survival rate of <10%. Although significant strides have been made in understanding disease development and progression, patient prognosis remains poor. Thus, a substantial unmet need exists to better understand the molecular drivers and underlying biology of this disease.

Disease development and progression

PDA arises from normal pancreatic epithelium and can originate from both acinar and ductal cells in the exocrine pancreas (Habbe et al. 2008; Gidekel Friedlander et al. 2009; Kopp et al. 2012; Bailey et al. 2016a). Step-wise progression to PDA occurs via acinar-to-ductal metaplasia (ADM), leading to the generation of precursor lesions known as pancreatic intraepithelial neoplasia (PanIN) (Hruban et al. 2006; Sipos et al. 2009; Kopp et al. 2012; Ying et al. 2016) (**Figure 1.1 A**). Less common macroscopic precursor lesions such as intraductal papillary mucinous neoplasm (IPMN) and mucinous cystic neoplasm (MCN) are cystic lesions with variable malignant potential (Hruban et al. 2004; Ying et al. 2016; Collisson et al. 2019). PanINs represent the most common microscopic precursor lesion and are labeled as PanIN1-3 based on histological features and increasing grade (Hruban et al. 2004; Sipos et al. 2009). PanIN1 are considered low-grade dysplasia, while PanIN2 lesions typically display loss of cell polarity, increased nuclear crowding, cell enlargement, hyperchromasia and frequent papillary formation

(Hruban et al. 2004; Sipos et al. 2009). High-grade PanIN3 represent advanced lesions with severe nuclear atypia, luminal necrosis and epithelial cell budding into ductal lumen (Hruban et al. 2004; Sipos et al. 2009). PanIN3 are almost exclusively found in patients with PDA while low-grade lesions can be found in normal pancreas or in patients with chronic pancreatitis (Ying et al. 2016). Microscopic PanINs are currently below the detectable size threshold to screen for using standard imaging techniques, thus the identification of screening modalities to effectively detect pre-malignant disease represents a key area of research that could have a significant impact in reducing mortality rates in PDA (Ying et al. 2016; Collisson et al. 2019).

Figure 1.1

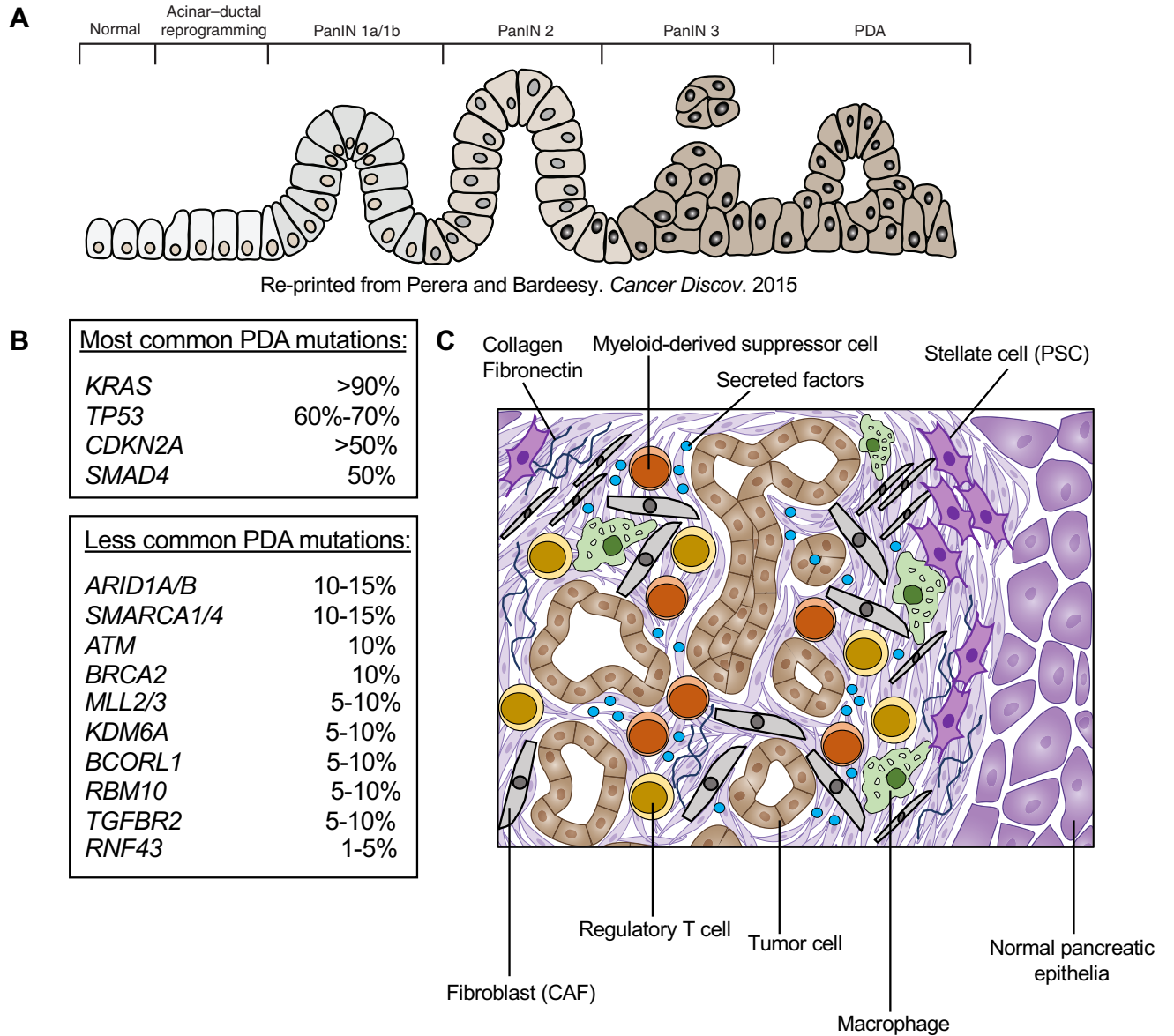


Figure 1.1. Step-wise progression of pancreatic ductal adenocarcinoma (PDA)

(A) Schematic showing the step-wise progression of PDA from normal pancreatic epithelia to acinar-ductal metaplasia (ADM), pancreatic intraepithelial neoplasia (PanIN) and frank metastatic adenocarcinoma. Figure re-printed from Perera et al. 2015 (Perera and Bardeesy 2015). (B) Common (top) and less common (bottom) genetic mutations that occur over the course of PDA progression and their associated frequencies. (C) Schematic depicting the overall composition of a PDA tumor to include various stromal cell types, secreted factors and a collagen/fibronectin rich extra-cellular matrix. Figure adapted from Kottakis et al. 2015 (Kottakis and Bardeesy 2015).

Genetic alterations in pancreatic cancer

Activating mutations in the *KRAS* oncogene occur in ~95% of PDA precursor lesions, highlighting the dependency of PDA development on this genetic alteration. During the progression of PDA, common inactivating mutations or deletions occur in tumor suppressor genes *TP53*, *CDKN2A* and *SMAD4* in ~50-70% of cases (Jones et al. 2008; Biankin et al. 2012; Ryan et al. 2014; Waddell et al. 2015; Witkiewicz et al. 2015) (**Figure 1.1 B**). Additional recurrent genetic alterations in *KDM6A*, *BCORL1*, *RBM10*, *MLL3*, *ARID1A*, *TGFBR2*, *RNF43*, *ATM*, *SMARCA4* and others have also been identified, however, the prevalence of these mutations drops to less than 10% (Ryan et al. 2014; Ying et al. 2016; Collisson et al. 2019). Interestingly, despite their low prevalence, these additional mutations converge on specific pathways that include NOTCH, Hedgehog, beta-catenin, axon guidance, chromatin remodeling, and DNA damage response pathways (Ryan et al. 2014; Ying et al. 2016; Collisson et al. 2019), illustrating potential opportunities for therapeutic intervention. Thus, a lack of actionable targets due to a relatively homogenous mutational landscape is a key characteristic of PDA. Therefore, successful future therapies will likely encompass combined targeting of the aforementioned signaling pathways or other aspects of the disease (i.e. such as stromal components - see below). Targeting oncogenic *KRAS* represents the most straightforward approach to treating this disease, however 'drugging' RAS has proven notoriously difficult. Nevertheless, recent studies have made exciting progress in this regard, bringing *KRAS* targeted therapy closer to entering the clinic.

Targeting mutant KRAS

Despite its central importance in PDA, attempts to target mutant KRAS therapeutically have been largely unsuccessful. However, the recent development of *KRAS*^{G12C} inhibitors has renewed interest in drugging mutant KRAS in a diverse array of tumors that harbor this mutation (Ostrem et al. 2013; Patricelli et al. 2016; Janes et al. 2018; Lou et al. 2019). Although *KRAS*^{G12D} and *KRAS*^{G12V} represent the most common *KRAS* mutations in PDA (Witkiewicz et al. 2015; Cancer Genome Atlas Research 2017), the small fraction of tumors harboring the *KRAS*^{G12C} allele would likely show exquisite sensitivity to G12C specific inhibitors. Similar to other targeted therapies, it is not improbable that resistance to *KRAS*^{G12C} inhibitors would eventually emerge. Although the G12C allele represents a minority of cases in PDA, identifying potential resistance mechanisms for this group could inform combinatorial regimens that co-suppress pathways that become upregulated in response to KRAS inhibition. Indeed, a recent study uncovered a diverse array of unique vulnerabilities once KRAS is inhibited, termed “collateral dependencies”, providing a framework to design combination therapies to enhance drug response (Lou et al. 2019).

Stromal contributions to disease pathogenesis

An additional characteristic of PDA is the dense stromal cell content that is commonly associated with this disease and in some cases can comprise up to 70% of the bulk tumor mass (Lafaro and Melstrom 2019). This stromal infiltrate is comprised of pancreatic stellate cells (PSCs), cancer associated fibroblasts (CAFs) and immune cells (**Figure 1.1 C**). Together, PDA stromal components create a rich microenvironment

comprised of cytokines, growth factors and other molecular cues whose contribution to tumorigenesis and progression are incompletely understood. For example, a novel role for PSC-derived CAFs was recently described as a source of secreted lipids such as lysophosphatidylcholines (LPS), which sustain PDA cell growth (Auciello et al. 2019). Simultaneously, the dense stromal infiltrate can impede the penetration and growth of blood vessels, thereby blocking effective delivery of chemotherapy or other targeted agents to the tumor, and thus can act as a physical barrier to therapy (Ryan et al. 2014; Ying et al. 2016; Lafaro and Melstrom 2019; Whittle and Hingorani 2019). The pro- or anti-tumorigenic function of each cell type present in PDA stroma remains under investigation and can potentially be leveraged in combinatorial therapeutic strategies. For example, depletion of stromal components can enhance delivery of chemotherapy through the elimination of hyaluronic acid, which was shown to cause a decrease in interstitial fluid pressure, increased vascularity and improved drug delivery (Provenzano et al. 2012). Similarly, activation of the vitamin D receptor with a vitamin D analog repressed the activated state of cancer-associated PSCs and impaired the secretion of pro-tumorigenic factors, leading to overall reduced fibrosis and inflammation and increased sensitivity to chemotherapy *in vivo* (Sherman et al. 2014). While this and other studies support a pro-tumorigenic role for the stroma, certain stromal components can also restrain PDA progression thereby having an anti-tumorigenic role (Lee et al. 2014; Ozdemir et al. 2014; Rhim et al. 2014). For example, targeting the stroma with Smoothed inhibitors was initially thought to inhibit pro-growth Hedgehog signaling in CAFs and therefore enhance drug delivery to tumor cells and improve patient outcomes (Olive et al. 2009). However, several clinical trials in PDA patients demonstrated that

Smoothened inhibition either had no clinical benefit or enhanced tumor progression (Olive et al. 2009; Catenacci et al. 2015). These studies highlight the complexity of PDA stroma and emphasize the need for detailed experimentation that investigates the role of each stromal component and the vast signaling interactions that occur between the tumor cells and microenvironment.

IDENTIFICATION OF PANCREATIC CANCER SUBTYPES

Transcriptional profiling revolutionizes subtype identification in cancer

Despite ample studies illuminating the potential clinical utility of targeting mutations occurring in individual genes, few examples exist demonstrating successful adaptation into clinical practice. Thus, new methodologies are needed to further understand the molecular underpinnings of PDA that go beyond genetics. Transcriptional profiling of lymphoma and breast cancer has been utilized to successfully establish consensus molecular subtypes that can inform the deployment of anti-cancer therapies in these cancers (Alizadeh et al. 2000; Perou et al. 2000; Sorlie et al. 2001). Importantly, these molecular subtypes correlated with specific histological features and clinical outcomes and marked the advent of a new mode of “personalized therapy” for cancer patients. For example, diffuse large B-cell lymphoma (DLBCL) was found to exist in two broad subtypes largely reflecting the differentiation status of the cancer cells. Patients with the well-differentiated or low-grade ‘germinal centre B-like’ subtype displayed dramatically better survival outcomes in response to chemotherapy compared to those with the poorly-differentiated high-grade ‘activated’ subtype (Alizadeh et al. 2000). Similarly, the original

classification of breast tumors revealed the presence of luminal and basal subtypes (Perou et al. 2000), which subsequently has expanded to include the five distinct subtypes that correlate with patient prognosis and response to therapy (Sorlie et al. 2001; Sorlie et al. 2003; Parker et al. 2009; Sotiriou and Pusztai 2009). These include the HER2-positive, luminal A, luminal B, claudin-low, and basal-like subgroups. Comparable to DLBCL, the basal-like subtype of breast cancer represents the most aggressive variant with the shortest overall survival and worst prognosis (Parker et al. 2009; Sotiriou and Pusztai 2009; Perou 2010). Basal-like and HER2-positive breast tumors are also histologically distinct from their luminal counterparts in that they are often high-grade and poorly-differentiated with high levels of proliferative marker Ki-67 (Sorlie et al. 2001; Sorlie et al. 2003; Parker et al. 2009; Perou 2010). Development of monoclonal antibodies, such as Trastuzumab (Herceptin), which target the HER2 receptor, for treatment of HER2 positive breast tumors have shown a profound improvement in survival in this patient population (Lambertini et al. 2017). Similarly, estrogen receptor-positive breast tumors, which are usually identified as either luminal A or B, have been successfully treated with the antiestrogen compound Tamoxifen for several decades (Jordan 2003). Conversely, the basal-like subgroup largely encompasses “triple-negative” breast tumors, which lack expression of HER2, estrogen and progesterone receptors, representing a subgroup where effective therapies are still lacking (Perou 2010). Colorectal cancer has also been subjected to expression profiling and the following six subtypes were originally identified: chromosomal-unstable (CIN)-immune down, deficient mismatch repair (dMMR), KRAS-mutant, cancer stem cell (CSC), CIN-Wnt up, and CIN-normal (Marisa et al. 2013). Although mutations in *KRAS*, *TP53* and *BRAF* occur at ~40%, ~50% and ~10% in this

cancer, respectively, subtypes were largely not associated with these genetic alterations (with the exception of the KRAS-mutant subtype) (Marisa et al. 2013). Rather, subtypes differed based on unique chromosomal arrangements, altered DNA damage repair pathways, and differing degrees of differentiation, stemness and Wnt signaling, with the CSC subtype displaying the worst prognosis (Marisa et al. 2013). A related study identified the following six subtypes: goblet-like, enterocyte, stem-like, inflammatory, cetuximab-sensitive transit-amplifying (CS-TA) and cetuximab-resistant transit-amplifying (CR-TA) (Sadanandam et al. 2013). Similar to Marisa et al. stemness and Wnt signaling played a defining role in delineating subtype identity, where the stem-like subtype represented the most aggressive variant with the worst disease-free survival while TA and goblet-like subtypes showed the best prognosis (Sadanandam et al. 2013). Importantly, the authors found that a subset of TA tumors responded to EGFR inhibitor cetuximab while the remaining tumors were more sensitive to cMET inhibition, further delineating this group into two distinct subtypes (Sadanandam et al. 2013). Additionally, TA and goblet-like subtypes demonstrated significantly better disease-free survival after surgical resection relative to the other subtypes with no added benefit in receiving chemoradiotherapy, suggesting that patients with these tumors may be spared from receiving chemotherapy if presenting with localized disease (Sadanandam et al. 2013). Furthermore, the authors were able to identify stem-like tumors as being significantly more responsive to FOLFIRI chemotherapy compared to the other subtypes (Sadanandam et al. 2013). Thus, transcriptional subtyping of a remarkably heterogenous disease such as colorectal cancer has identified appropriate treatment courses for specific patient groups, independent of genetic mutations. Collectively, these studies

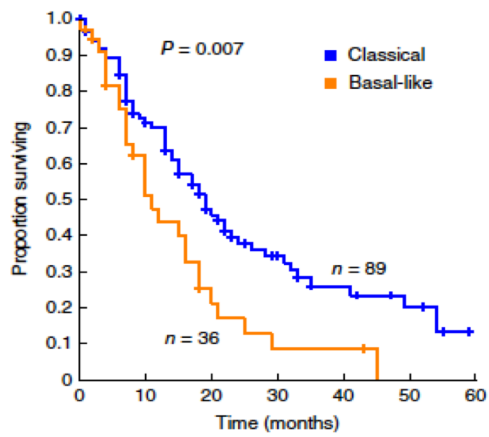
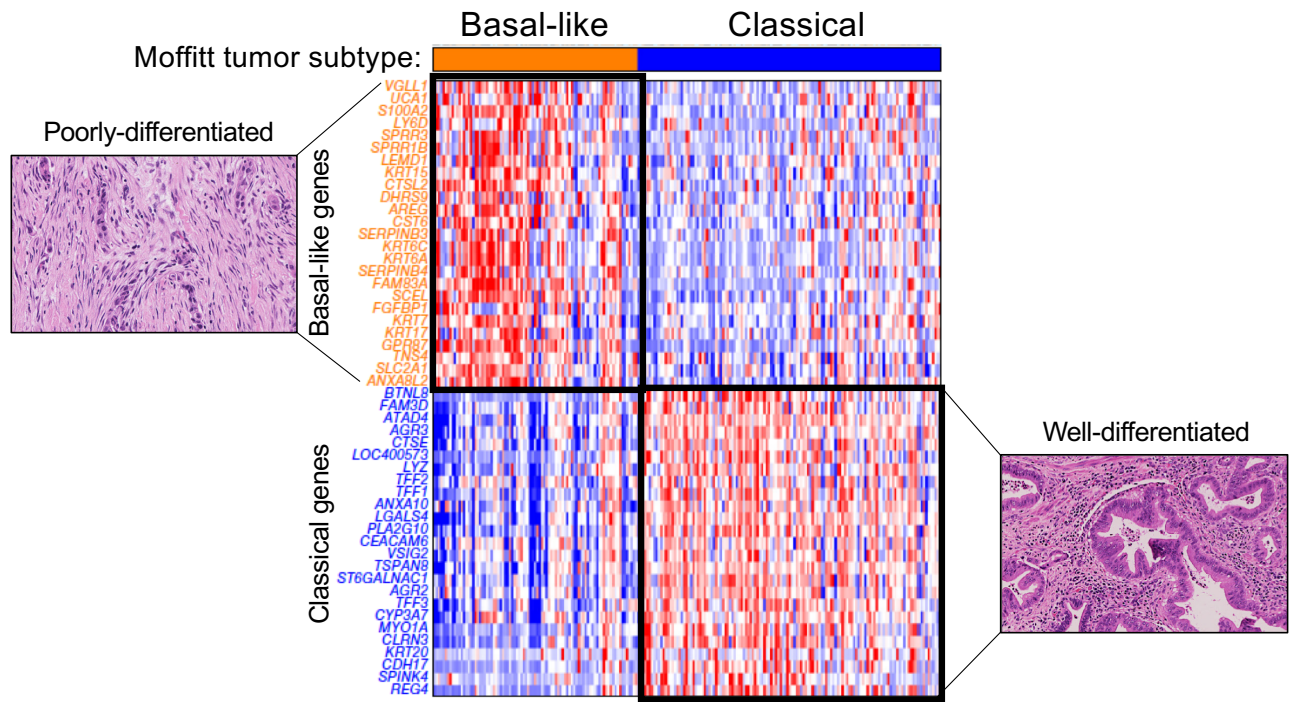
highlight the importance of utilizing genetic and transcriptomic classifications to establish distinct subtypes of cancer and create a framework for defining molecular signatures that can stratify tumors that do not harbor obvious genetic heterogeneity – such as PDA and other cancers (De Sousa et al. 2013; Marisa et al. 2013; Sadanandam et al. 2013; Cancer Genome Atlas Research 2014; Damrauer et al. 2014).

Pancreatic cancer subtypes

Despite progress in this area, the difficulty of capturing high purity patient PDA samples due to stromal cell contamination has made it difficult to sub classify this disease. Recent advances using laser capture microdissection and improved computation analysis have allowed several groups to successfully identify subtypes of pancreatic cancer with distinct molecular features (Collisson et al. 2011; Moffitt et al. 2015; Bailey et al. 2016b; Collisson et al. 2019) (**Figure 1.2**). Although these studies differ in methodology and resulting taxonomies, two broad groups emerge as bona-fide molecular subtypes of PDA – one that represents a well-differentiated, progenitor-like subset with better overall survival (classical) while the other represents a poorly-differentiated, mesenchymal-like subset that correlates with markedly worse prognosis (basal-like) (Moffitt et al. 2015; Cancer Genome Atlas Research 2017; Aung et al. 2018). Indeed, a study conducted by The Cancer Genome Atlas (TCGA) reproduced each classification scheme identified by Collisson, Moffitt and Bailey and found that tumors emerge as either basal-like or classical in samples enriched for high epithelial cell purity (Cancer Genome Atlas Research 2017). Classical PDA is enriched for expression of epithelial differentiation genes, whereas basal-like PDA is characterized by laminin and basal keratin gene expression, stem cell

and epithelial-to-mesenchymal transition (EMT) markers, analogous to the basal subtypes previously defined in bladder and breast cancers (Perou et al. 2000; Sorlie et al. 2001; Parker et al. 2009; Curtis et al. 2012; Cancer Genome Atlas Research 2014; Damrauer et al. 2014). Furthermore, these subtypes are preserved in different experimental models of PDA including organoids (Boj et al. 2015; Huang et al. 2015; Seino et al. 2018; Tiriach et al. 2018) and cell line cultures (Collisson et al. 2011; Moffitt et al. 2015; Martinelli et al. 2017), providing an important opportunity to identify key factors responsible for establishing and maintaining subtype specificity and how these programs integrate with pathways known to be deregulated in PDA.

Figure 1.2



Re-printed from Moffitt et al. *Nat Genetics*. 2015

Figure 1.2. Identification of PDA subtypes

Two consensus molecular subtypes have been identified in PDA according to the Collisson, Moffitt, Bailey transcriptomic signatures. The heatmap and Kaplan-Meier survival analysis are re-printed from Moffitt et al. 2015. The basal-like subtype (left) exhibits poorly-differentiated histology, is associated with proliferative, invasive and inflammatory signatures with high enrichment for genes associated with EMT, and displays overall worse survival outcomes in patients, while the classical subtype (right) is associated with well-differentiated histology, an epithelial/progenitor-like gene signature and overall better survival outcomes. Hematoxylin and eosin stained images are adapted from Kalimuthu et al. 2019.

Few studies have aimed to define master regulators of subtype identity in PDA. However, several have uncovered aspects of phenotypic heterogeneity and plasticity that are relevant to our work. For example, GATA6 was identified as being enriched in the classical subtype and shown to be important for inhibiting de-differentiation, EMT and metastasis in human PDA cell lines (Martinelli et al. 2017). Importantly, this study showed that GATA6 status was predictive of response to treatment in that patients with GATA6 high tumors responded better to 5-FU/leucovorin treatment compared to those with GATA6 low tumors (Martinelli et al. 2017). Others have identified SMARCB1, a SWI/SNF chromatin remodeling factor, in a genetically engineered mouse (GEM) model of PDA as a gatekeeper for an epithelial cell state (Genovese et al. 2017). Additionally, studies aimed at studying the role of EMT regulator ZEB1 in PDA pathogenesis observed significant heterogeneity in GEM models of PDA in regard to epithelial and mesenchymal phenotypes, with ZEB1 depleted tumors found to exist solely in an epithelial-locked state (Krebs et al. 2017). These tumors were unable to metastasize and were enriched for the classical subtype gene signature (Krebs et al. 2017). More recently, loss of KDM6A, a histone demethylase and member of the COMPASS-like epigenetic complex, was found to frequently occur in basal-like/squamous PDA, where activated super enhancers normally silenced by KDM6A activate TP63, ZEB1, and MYC driven transcriptional programs (Andricovich et al. 2018). Interestingly, KDM6A loss sensitized PDA cells to bromodomain inhibitors, highlighting a potential vulnerability of the basal-like/squamous subtype. Consistent with these findings, TP63 (Δ Np63 isoform) was confirmed to be an important regulator of the basal-like/squamous subtype in loss-and gain-of-function experiments, emphasizing the significance in further understanding and identifying

master regulators of phenotypic heterogeneity and subtype identity in PDA (Somerville et al. 2018). Although these studies lay the groundwork for identifying regulators of subtype identity, future work will be necessary to determine how we can leverage this knowledge to better design targeted therapies in patients.

EMT CONTRIBUTES TO TUMOR CELL PLASTICITY AND SUBTYPE CONVERSION

EMT promotes cancer cell plasticity

The ability of a cell to undergo a change in cell state is an important contributor to tumor cell plasticity and heterogeneity and provides a potential explanation for treatment failure and resistance (Polyak and Weinberg 2009; Singh and Settleman 2010; Nieto 2013; Kemper et al. 2014). The best described example of cellular plasticity and the ability to dynamically interconvert between states is the process of EMT and MET, where epithelial cells lose their differentiated characteristics (cell-cell contacts, planar and apical-basal polarity, lack of motility) and acquire mesenchymal features (loss of cell-cell contacts, increased motility and invasiveness), and vice versa (Yang and Weinberg 2008; Thiery et al. 2009) (**Figure 1.3**). Originally described as a phenomenon limited to *in vitro* cell culture, its relevance to physiological settings such as embryogenesis and tumorigenesis has since been demonstrated (Yang and Weinberg 2008; Thiery et al. 2009; Nieto 2013). Specifically, EMT has been shown to contribute to invasion, metastatic dissemination and resistance to therapy in cancer, while MET has been shown to be important for the formation and out-growth of distant metastasis following cell seeding (Polyak and Weinberg 2009; Singh and Settleman 2010). In addition to these two states,

recent work has highlighted that tumor cells can exist along a continuum of EMT with intermediate states conferring different levels of phenotypic plasticity and invasive properties (Jordan et al. 2011; Huang et al. 2013; Aiello et al. 2018) (**Figure 1.3**). For example, in a GEM model of PDA, a “partial-EMT” was seen in carcinoma cells that lost plasma membrane-associated E-cadherin yet retained high levels of transcript and protein (Aiello et al. 2018). Cells that had undergone partial-EMT and to a lesser extent those that had undergone a “complete-EMT” retained the ability to re-localize E-cadherin to the plasma membrane, demonstrating that inherent plasticity allows PDA cells to switch EMT subtypes (Aiello et al. 2018). Furthermore, differences in EMT subtype was shown to affect migration capacity where tumor cells that underwent a partial-EMT invaded as multi-cell clusters that retained cell-cell contacts while tumor cells that underwent a complete-EMT invaded as single cells that disseminated from the primary cell mass (Aiello et al. 2018). In agreement, an independent GEM model demonstrated PDA cells with different degrees of epithelial plasticity preferentially metastasized to different sites, where p120-catenin and E-cadherin positive PDA cells were prone to seed the liver in contrast to lung metastasis which favored negative expression of p120-catenin and E-cadherin (Reichert et al. 2018). Together, these studies suggest that EMT is an important contributor to phenotypic plasticity of carcinoma cells, which can impact critical steps of PDA pathogenesis including metastasis.

Figure 1.3

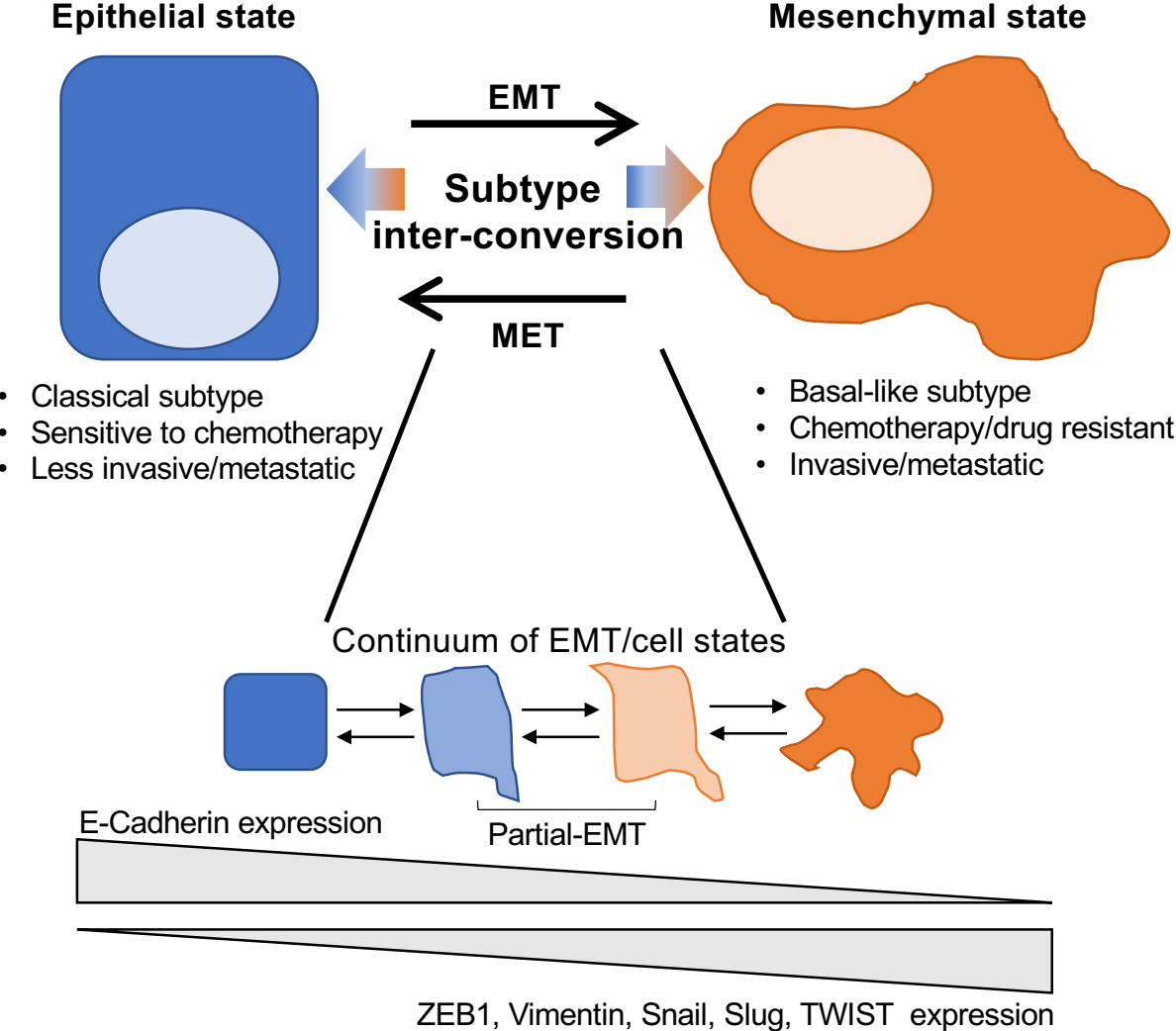


Figure 1.3. EMT and subtype switching promote plasticity and aggressive disease in PDA

Schematic depicting EMT and subtype switching between epithelial and mesenchymal phenotypes. An epithelial-like state is broadly associated with the classical subtype of PDA and the equivalent in other tumor types, is reported to be more sensitive to specific chemotherapy regimens and is less metastatic. A mesenchymal state is associated with the basal-like subtype of PDA and other cancers and exhibits *de novo* and acquired resistance to chemotherapy and targeted inhibitors while being particularly invasive and metastatic. A continuum of EMT and cell states is becoming more appreciated as a contributor to cancer cell plasticity and therapy resistance.

The role of EMT in basal-like pancreatic cancer

Aggressive subtypes of many cancers, such as the basal-like subtype in breast and bladder cancer, often display features of EMT (Perou et al. 2000; Sorlie et al. 2001; Parker et al. 2009; Curtis et al. 2012; Cancer Genome Atlas Research 2014; Damrauer et al. 2014). Indeed, these particular tumors have a higher incidence of metastasis, are more refractory to therapy, and have higher expression of EMT markers such as ZEB1, TWIST1, and SNAI1/2. Similarly, in PDA, basal-like patient tumors and patient-derived organoids have higher expression of TWIST1 and ZEB1 and are enriched for EMT by gene set enrichment analysis (GSEA) compared to classical tumors, suggesting that the underlying aggressive phenotype observed in basal-like cancers is due at least in part to the inherent plasticity that exists in mesenchymal cells (Collisson et al. 2011; Krebs et al. 2017; Tiriach et al. 2018). The basal-like subtype of PDA was similarly shown to be associated with significantly higher rates of metastasis. Specifically, every patient with a basal-like tumor exhibited widespread metastatic PDA, whereas patients who had classical tumors were associated with both localized disease and metastatic cases (Aung et al. 2018). Additionally, partial response to chemotherapy was observed in 34% (13/38) of patients with classical tumors while only 8% (1/12) of patients with basal-like tumors experienced benefit, providing further evidence that the basal-like variant is especially aggressive and refractory to first line chemotherapy (Aung et al. 2018). A study that generated PDA patient-derived organoids with the aim of performing therapeutic profiling revealed that longitudinal generation of PDA organoid cultures from the lung metastasis of a patient who initially responded to gemcitabine, paclitaxel, 5-FU, and oxaliplatin, but eventually succumbed to disease, acquired amplification of the *KRAS* allele, gained

resistance to the aforementioned therapies, and switched to the basal-like subtype (Tiriác et al. 2018). This patient acquired resistance to all commonly used chemotherapeutics for PDA, highlighting a common issue encountered in the clinic, and the need to uncover new vulnerabilities in refractory cases.

Although EMT has been implicated in tumorigenesis, progression and metastasis, its true role in PDA development is yet to be fully understood. For example, EMT and stem cell features (defined as the ability to self-renew, proliferate and differentiate) have been linked to ZEB1-mediated repression of epithelial promoting and stemness-inhibiting microRNAs. This dual regulation by ZEB1 was shown to be crucial in promoting PDA metastasis (Wellner et al. 2009). Strikingly, ZEB1-mediated EMT was also shown to contribute to early dissemination of pancreatic cells harboring the *KRAS*^{G12D} oncogenic mutation in a lineage-tracing GEM model of PDA (Rhim et al. 2012). This study challenges the paradigm of metastasis occurring as a late event in PDA pathogenesis since dissemination of pancreatic cells occurred before the development of the primary tumor and were associated with EMT and maintained a mesenchymal and stem cell-like phenotype (Rhim et al. 2012). Importantly, the authors also found that the EMT status of transformed cells is not a stable property and that MET can also spontaneously occur *in vivo* (Rhim et al. 2012). These findings support a role for EMT and a stem cell program in the early dissemination and metastasis of PDA cells *in vivo* (Rhim et al. 2012), however, the molecular mechanisms and specific transcription factors important for maintaining a mesenchymal state or promoting EMT to MET plasticity are yet to be fully defined. Context-specific roles for traditionally described EMT transcription factors such as SNAI1/2, TWIST1/2 and ZEB1/2 are important to consider in PDA. For example, in a

GEM model of PDA, ablation of *SNAI1* or *TWIST1* was found to have no effect on the rate of metastasis, leading to the conclusion that PDA cells can metastasize without activating an EMT program (Zheng et al. 2015). If correct, this finding represents a major shift in how we understand malignant progression of PDA cells. However, significant caveats exist in this study including how the authors confirm attenuation of EMT following genetic ablation of EMT factors, and the assumption that *SNAI1* or *TWIST1* alone are the relevant master regulators of EMT during the development of metastatic disease. In response to this study, Aiello and colleagues show that the methods used by Zheng et al. to classify cells as having undergone EMT are incomplete (Aiello et al. 2017). The authors show that α -SMA (the primary EMT distinguisher used by Zheng et al.) is an unreliable marker. Thus, the true effect of *SNAI1* and *TWIST1* deletion on EMT is still unclear. In contrast to this study, *ZEB1* knockout using an autochthonous PDA GEM model used in Zheng et al. strongly inhibited mesenchymal cell state, formation of precursor lesions, invasion and metastasis during tumor progression. This study suggests that *ZEB1*-driven EMT is important for PDA pathogenesis and metastatic progression (Krebs et al. 2017). Overall, the exact contributions of EMT to PDA initiation, maintenance and dissemination remain highly contested. Moreover, whether alternative regulators of EMT exist in PDA that can compensate for loss of classical EMT factors such as *TWIST1* and *SNAI1* have not been explored. Finally, the molecular mechanisms of how EMT and epithelial plasticity contribute to defining subtypes is an open area of research, on which our study provides much needed clarity.

Contributions of EMT to drug resistance in cancer

The contribution of EMT to dissemination and metastasis is becoming widely accepted, however, its role in promoting drug resistance and relapse requires further investigation. EMT has been broadly associated with drug resistance. For example, in lung cancer, an epithelial rather than a mesenchymal gene signature was associated with sensitivity to EGFR inhibition (Yauch et al. 2005). In clinical trials, non-small cell lung cancer (NSCLC) patients with high expression of E-cadherin in tumors were found to be more responsive to EGFR inhibition than tumors with low E-cadherin expression, suggesting that mesenchymal-like NSCLC cells are inherently refractory to EGFR therapy through *de novo* mechanisms (Thomson et al. 2005). Since these initial findings, others have similarly found that restoring E-cadherin expression through the co-treatment of a HDAC inhibitor or silencing of *ZEB1* reverts the EMT phenotype and re-sensitizes lung cancer cell lines to EGFR inhibition (Witta et al. 2006; Yoshida et al. 2016). Furthermore, an EMT gene signature was identified as being predictive of resistance to EGFR and PI3K inhibition *in vitro* and in patient samples (Uramoto et al. 2010; Byers et al. 2013). Similar parallels have been observed in head and neck squamous cell carcinoma, urothelial carcinoma, colorectal cancer and other tumor types (Frederick et al. 2007; Black et al. 2008; Dallas et al. 2009; Shibue and Weinberg 2017). Future work will require a deeper understanding of the intricate mechanisms that potentiate *de novo* drug resistance caused by EMT.

SUBTYPE SWITCHING UNDERLIES FEATURES OF AGGRESSIVE DISEASE

The ability of a cell to undergo a broad phenotypic switch has been demonstrated as critical “escape route” in evading growth arrest or cell death in response to therapy (Kemper et al. 2014). One example of this phenomenon is the rare but consistent observation that EGFR mutant NSCLC adenocarcinoma transforms to histologically distinct small-cell lung cancer (SCLC) as an acquired resistance mechanism to EGFR inhibition (~14% of acquired resistance cases) (Sequist et al. 2011; Yu et al. 2013; Oser et al. 2015). Treatment strategies for NSCLC and SCLC differ substantially, thus their identification is an important step in deciding a relevant course of action. NSCLC adenocarcinomas have a high prevalence of activating *KRAS* and *EGFR* mutations, *ALK* translocations, are commonly localized peripherally, and believed to originate from alveolar type II cells (Oser et al. 2015). SCLC are characterized by high frequency of *TP53* and *RB1* loss of function mutations and are thought to arise from neuroendocrine cells within the distal part of the conduction airways and are therefore positive for neuroendocrine markers synaptophysin, chromogranin and NCAM by immunohistochemical staining (Oser et al. 2015). Genomic sequencing of repeat biopsy samples revealed that 100% of patients with EGFR-mutant adenocarcinoma that transformed to SCLC harbored *RB1* loss, suggesting this genetic alteration is a required event leading to transformation from NSCLC adenocarcinoma to SCLC (Yu et al. 2013). Additionally, each transformed SCLC tumor retained the original EGFR-activating mutation and occasionally acquired additional mutations such as in *PIK3CA* (Sequist et al. 2011). Despite retaining the original EGFR mutation upon transformation to SCLC, these tumors express low-levels of EGFR protein, which is thought to contribute to their

resistance to EGFR inhibitor treatment (Oser et al. 2015). This observed plasticity between adenocarcinoma and SCLC and their ability to switch histologies has called into question whether a shared cell of origin exists between these two subsets of lung cancer and highlights that the overall mechanistic understanding of how this switch occurs is unknown. For example, it is undetermined whether a small percentage of NSCLC harboring *RB1* loss preexists in the original tumor and is able to expand upon drug treatment, or if this mutation is acquired later to promote an active switch to the SCLC phenotype. Additionally, in melanoma cells, an “invasive” signature was associated with low levels of MITF, a master transcriptional regulator of melanocyte development and differentiation, and *de novo* resistance to BRAF^{V600E} or MEK inhibition (Konieczkowski et al. 2014). Moreover, melanoma cells were shown to adapt to BRAF^{V600E} or MEK inhibition in an acquired resistance setting by switching to an invasive phenotype, which was also associated with loss of MITF expression (Zipser et al. 2011). Collectively, these studies demonstrate that inherent plasticity and the ability to undergo a change in cell state is an important contributor to therapy resistance in various tumor settings.

Phenotypic switching as a resistance mechanism to oncogenic *KRAS* inhibition is an important issue to address in PDA given the near universal occurrence of activating *KRAS* mutations and the ongoing development of clinically useful inhibitors. A study aimed at identifying a “KRAS Addiction” signature identified lung and pancreatic cell lines that either do or do not require *KRAS* to maintain viability (Singh et al. 2009). Those that were more reliant upon *KRAS* expression were associated with a well-differentiated epithelial phenotype and expressed high levels of E-cadherin whereas *KRAS*-“independent” cells expressed readily detectable levels of Vimentin, indicating strong

association between KRAS-dependency and EMT (Singh et al. 2009). Interestingly, altering EMT status based on treatment with TGF β 1 to induce EMT and RNAi depletion of *ZEB1* to promote MET was shown to either reverse or promote KRAS dependency, respectively (Singh et al. 2009). These findings suggest that KRAS dependency is not a stable feature of cancer cells, and that changes in cell phenotype can dictate the degree to which cancer cells are oncogene addicted. However, it is unclear whether this observed phenomenon is applicable *in vivo* since GEM models of PDA demonstrate that tumors are highly dependent on the presence of oncogenic KRAS. Indeed, in a GEM model of PDA where the expression of mutant *KRAS* is under the control of a Tet-inducible promoter, removal of doxycycline leads to rapid loss of KRAS expression and complete tumor regression, demonstrating oncogenic KRAS addiction *in vivo* (Ying et al. 2012; Kapoor et al. 2014). However, most tumors escaped from doxycycline-induced KRAS silencing and tumor relapse was evident after 9-47 weeks (Kapoor et al. 2014). Relapsed tumors exhibited poorly-differentiated or sarcomatoid features and incidence of lung and liver metastasis increased (Kapoor et al. 2014). Interestingly, half of relapsed tumors re-expressed KRAS expression whereas the remaining tumors did not and were designated as KRAS-independent (Kapoor et al. 2014). KRAS-independent tumors were found to cluster with the quasi-mesenchymal subtype identified by Collisson et al. whereas the KRAS-expressing relapsed tumors clustered with the classical subtype (Kapoor et al. 2014). The transcriptional co-activator YAP1 was found to be genomically amplified in three of the KRAS-independent tumors and was shown to effectively substitute for oncogenic KRAS in maintaining survival and viability, representing a novel bypass mechanism to KRAS ablation (Kapoor et al. 2014). In related work, Shao et al. aimed to

identify genes that functionally substitute for oncogenic RAS in a human colon cancer cell line. YAP1 was similarly identified as well as a transcriptional program involving EMT, suggesting that cancer cells co-opt transcriptional programs that involve phenotypically switching to a mesenchymal state as a common acquired resistance mechanism to oncogenic KRAS loss (Shao et al. 2014). Together, these studies raise the intriguing possibility that other transcriptional regulators may be responsible in promoting phenotypic switching as a survival mechanism in response to oncogene inhibition in PDA and in other tumor types.

THE ROLE OF HEDGEHOG SIGNALING IN PANCREATIC CANCER

The Hedgehog (Hh) pathway is activated in PDA and has been found to play important and complex roles in PDA pathogenesis (**Figure 1.4**) (Morris et al. 2010). Whereas the developing and normal adult pancreas lack expression of Hh pathway ligands, the Sonic Hedgehog (SHH) and Indian Hedgehog (IHH) ligands are prominently induced in the pancreatic epithelium upon injury and throughout PDA development, from early precursor PanIN to invasive disease (Berman et al. 2003; Thayer et al. 2003; Prasad et al. 2005; Nolan-Stevaux et al. 2009) (**Figure 1.4 A**). The neoplastic cells and stromal fibroblasts also express the Hh receptor Smoothed (SMO) and the Glioma associated oncogene homology (GLI) transcription factors – GLI1 and GLI2, which mediate Hh signaling downstream of SMO, and GLI3 which functions as a transcriptional repressor (Hui and Angers 2011; Robbins et al. 2012). While *SMO* deletion in the pancreatic epithelium has no effect on mutant KRAS-driven PDA in GEM models, studies from our

group and others reveal a surprising role for SHH in restraining cancer growth (Lee et al. 2014; Mathew et al. 2014; Rhim et al. 2014; Liu et al. 2016) (**Figure 1.4 B,C**). By contrast, several lines of evidence indicate that activation of GLI transcription factors in the pancreatic epithelium is required for oncogenesis in PDA (Dennler et al. 2007; Ji et al. 2007; Nolan-Stevaux et al. 2009; Rajurkar et al. 2012; Xu et al. 2012). First, pancreas-specific transgenic over-expression of the *Gli3* repressor attenuates PDA progression (Rajurkar et al. 2012). Second, forced *Gli2* over-expression cooperates with oncogenic *Kras* to promote aggressive poorly differentiated tumors (Pasca di Magliano et al. 2006). While much emphasis has been placed on ligand-mediated activation of Hh signaling in stromal cells within PDA, the tumor cell-autonomous roles of GLI proteins have remained unclear (**Figure 1.4 C**). In other cancer settings GLI proteins have been implicated in cell cycle progression, activation of pro-survival programs and a cancer-associated EMT (Yoon et al. 2002; Alexaki et al. 2010; Das et al. 2013; Han et al. 2015; Neelakantan et al. 2017). Therefore, we explored a novel role for GLI transcription factors in regulating cell state and plasticity in PDA. Given the incomplete understanding of the specific contributions of Hedgehog signaling components, we reasoned that there may be context-specific roles for Hh ligands and GLI transcription factors in PDA pathogenesis. Specifically, we hypothesize that GLI proteins function to promote aggressive tumorigenic behavior and poorly-differentiated disease through the regulation of basal-like subtype identity, while Hh ligand acts to restrain aggressive PDA growth and instead promotes a well-differentiated classical subtype state. In Chapter 2, I present work that demonstrates a crucial role for GLI2 in functioning as a master regulator of the basal-like subtype of PDA and determine a mechanism for how this process occurs. We uncover a novel

signaling axis that encompasses GLI2-dependent secretion of pro-inflammatory ligand Osteopontin (OPN), which further acts to establish a basal-like identity. Moreover, we hypothesize that GLI2 can functionally substitute for oncogenic KRAS signaling in PDA and show that a GLI2-mediated phenotypic switch to a basal-like state contributes to acquired resistance to KRAS ablation. Overall, these data identify GLI2 as a Hh-independent, cell autonomous driver of an aggressive variant of PDA and illuminate the complex role of tumor heterogeneity, plasticity and differential regulation of Hh pathway components in PDA tumorigenesis.

Figure 1.4

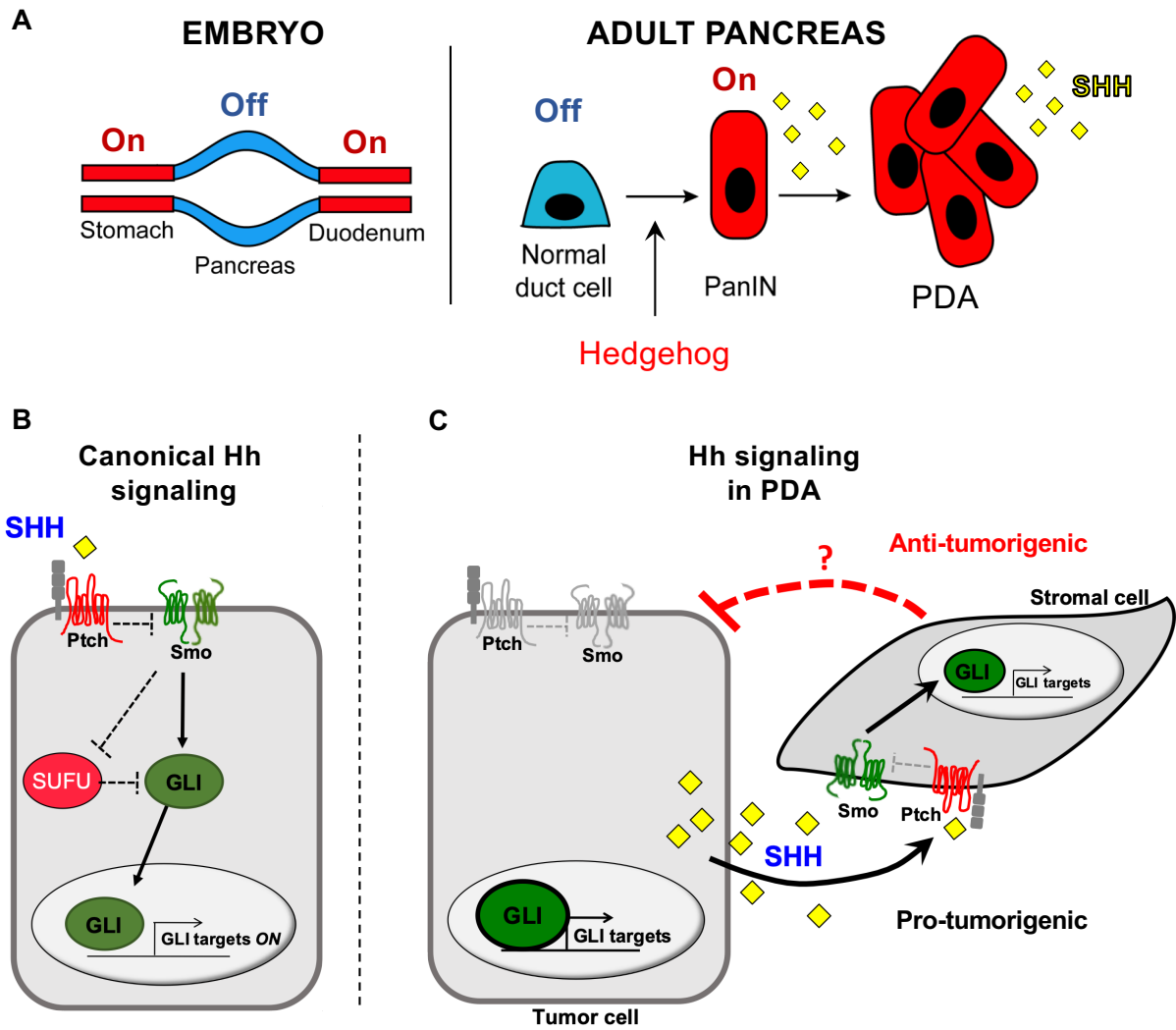


Figure 1.4. Hedgehog signaling in PDA

(A) Hedgehog signaling is absent in the developing (left - blue) and normal adult pancreas (right - blue). Upon transformation to PanIN, SHH ligand is induced and is secreted by neoplastic cells. (B) Diagram illustrating the canonical Hedgehog signaling pathway where SHH ligand binds to transmembrane receptor PTCH, alleviating SMO and leading to stabilization and nuclear translocation of the GLI family of transcription factors. (C) Schematic summarizing the more complicated roles of Hh signaling components in PDA. Tumor cells retain the ability to express GLI transcription factors independent of upstream SHH ligand binding. SHH secreted by tumor cells acts in a paracrine manner on Hh-responsive stromal cells, which act to restrain tumor growth through mechanisms that are incompletely understood.

CHAPTER 2

**GLI2-OPN mediated subtype switching enables adaptation
to oncogene ablation in pancreatic cancer**

Results:

Expression of Hh ligands and GLI transcription factors are anti-correlated and predict survival outcomes in PDA.

To explore the relationship between the Hh pathway components in PDA we first determined the expression levels of SHH and GLI family transcription factors (GLI1, GLI2, GLI3) in a panel of 14 human PDA cell lines using validated antibodies (**Figure 2.2 A,B**). We found that all PDA cell lines expressed Hh pathway proteins to varying degrees. GLI1 and GLI3 expression were restricted to two and one cell line respectively, while GLI2 was readily detectable in 10/14 lines. Moreover, high levels of SHH were observed in 7/14 cell lines, while the remainder showed low or undetectable levels of expression (**Figure 2.1 A**). No significant differences in the level of the SMO receptor were observed across the panel. Notably, cell lines expressing the highest levels of GLI2 (KP4, MiaPaca and Panc0327 cells) displayed the lowest levels of SHH expression (**Figure 2.1 A**; asterisk). Conversely, GLI expression was uniformly low in lines with high levels of SHH. Accordingly, GLI responsive luciferase reporter assay (Sasaki et al. 1997) demonstrated that GLI transcriptional activity was inversely correlated with SHH expression and positively correlated with GLI expression (**Figure 2.1 B,C**), such that all SHH^{hi} cell lines lacked basal reporter activity (**Figures 2.1 B**), whereas the GLI^{hi} KP4, MiaPaca and Panc0327 lines exhibited the highest levels of activity (**Figure 2.1 B,C**). Luciferase activity was specific to GLI proteins as shRNA mediated knockdown of GLI2 or treating cells with GANT61 inhibitor, which blocks GLI binding to DNA (Lauth et al. 2007), suppressed GLI-driven luciferase activity (**Figure 2.2 C,D**).

Figure 2.1

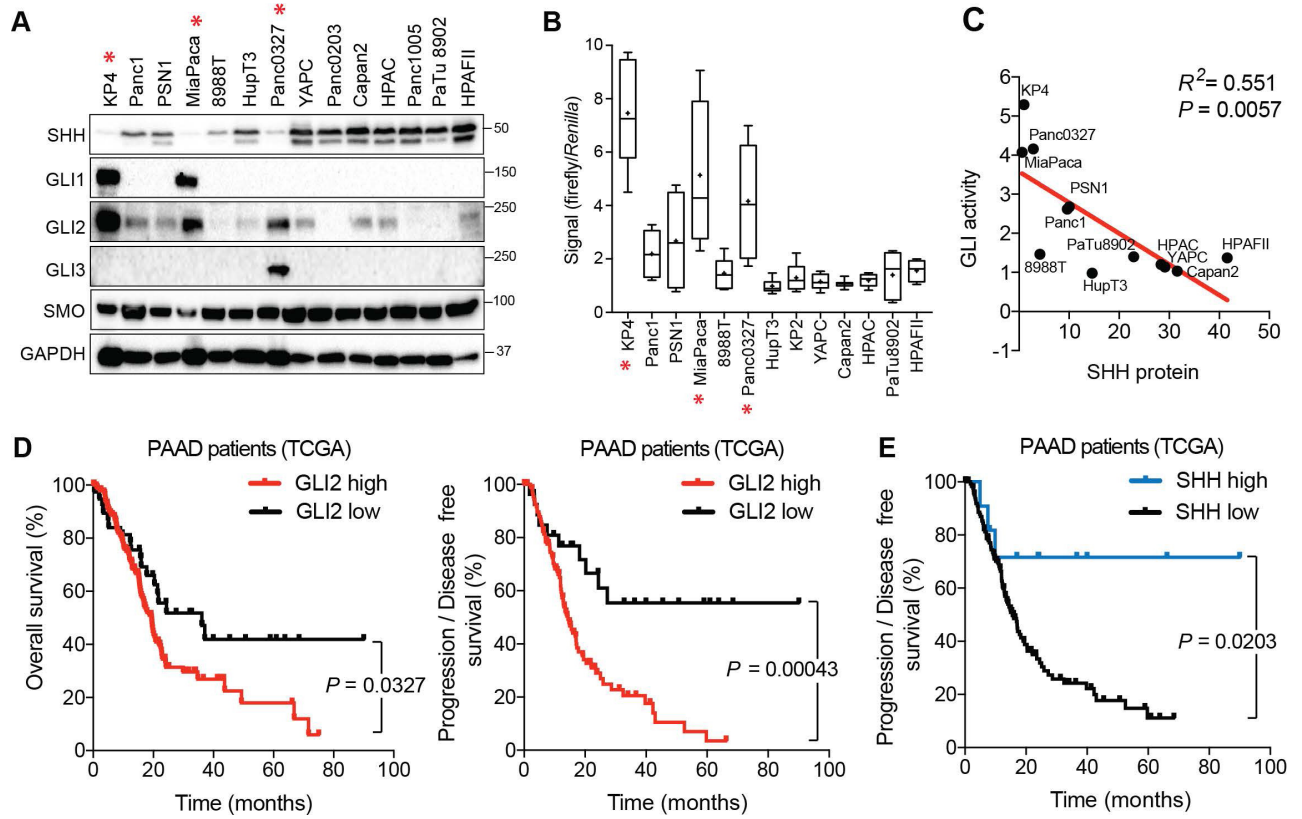


Figure 2.1. Expression and activity of GLI proteins is anti-correlated with Hh ligand levels in PDA

(A) Immunoblots showing expression of the indicated proteins in 14 human PDA cell lines. Cell lines denoted with an asterisk represent GLI^{hi}/Hh^{lo} lines. (B) The indicated cell lines were transfected with the 8 x 3'Gli-binding site luciferase plasmid and luciferase activity was measured 48hrs post transfection. For each box-and-whisker plot, center asterisk indicates the mean of $n = 3$ experiments with a total of 10 independently transfected cultures for each cell line. (C) GLI activity as measured by GLI luciferase assay (B) is anti-correlated with SHH protein levels (A). Linear regression line is shown in red along with corresponding statistics. (D) High expression of *GLI2* predicts shorter overall (left; GLI2 high $n = 147$, GLI2 low $n = 38$) and disease-free (right; GLI2 high $n = 114$, GLI2 low $n = 27$) survival while high *SHH* expression predicts extended disease-free survival (SHH high $n = 11$, SHH low $n = 130$) for patients with PDA from The Cancer Genome Atlas (TCGA). Data from 186 patients. *P* value calculated by Log-rank test.

The anti-correlation between *GLI2* and *SHH* was further corroborated by analyzing RNA-sequencing (RNA-seq) data of resected PDA specimens from The Cancer Genome Atlas (TCGA) study (Cancer Genome Atlas Research 2017). Samples were binned into two groups based on whether *GLI2* expression levels were higher or lower than the mean mRNA expression within the sample set (see Methods for details). Consistent with the cell line data, tumors expressing high levels of *GLI2* mRNA had significantly lower expression of *SHH* and *IHH* (**Figure 2.2 E**). Importantly, given that stromal cells also express *GLI2*, we confirmed that high *GLI2* status was independent of stromal cell content. Of the 51 PDA tumors characterized as *GLI2* high, a relatively even distribution between high purity (>33% tumor/stromal cell content; n = 23) and low purity (<33% tumor/stromal cell content; n = 27) samples was observed (see Methods for details), indicating that *GLI2* expression in stromal cells is an unlikely confounding factor in determining tumor cell *GLI2* status in this patient cohort. These findings indicate that PDA cell lines and tumors segregate into GLI^{hi}/Hh^{lo} and GLI^{lo}/Hh^{hi} subgroups, independent of tumor cell purity, further supporting an inverse relationship between expression of Hh ligands and *GLI* transcription factors in PDA. Notably, high expression levels of *GLI2* in primary PDA tumors correlated with shortened overall and disease-free survival (**Figure 2.1 D**). In contrast, high *SHH* expression levels were associated with longer disease-free survival (**Figure 2.1 E**). *GLI2* or *SHH* high versus low expression level was not correlated with clinical variables such as age, sex, T stage, N stage, or M stage, although as expected from our data there was a correlation between high *SHH* and low *GLI2* expression and vice-versa (**Figure 2.2 F,G**). A multivariate analysis of the hazard attributable to *SHH* or *GLI2* status demonstrated that no other variables explained the

relationship between SHH or GLI2 and overall or progression free survival (**Figure 2.3**). Collectively, our data point to an unexpected dichotomy among PDA tumors and cell lines with respect to Hh pathway circuitry, with high GLI transcriptional activity dissociated from canonical ligand-dependent signaling and associated with worse patient outcomes. Given these findings we sought to determine the functions of GLI2 – the main transcriptional activator amongst the GLI family of proteins (Hui and Angers 2011), - in PDA and examine how its increased activity may promote a more aggressive tumor phenotype.

Figure 2.2

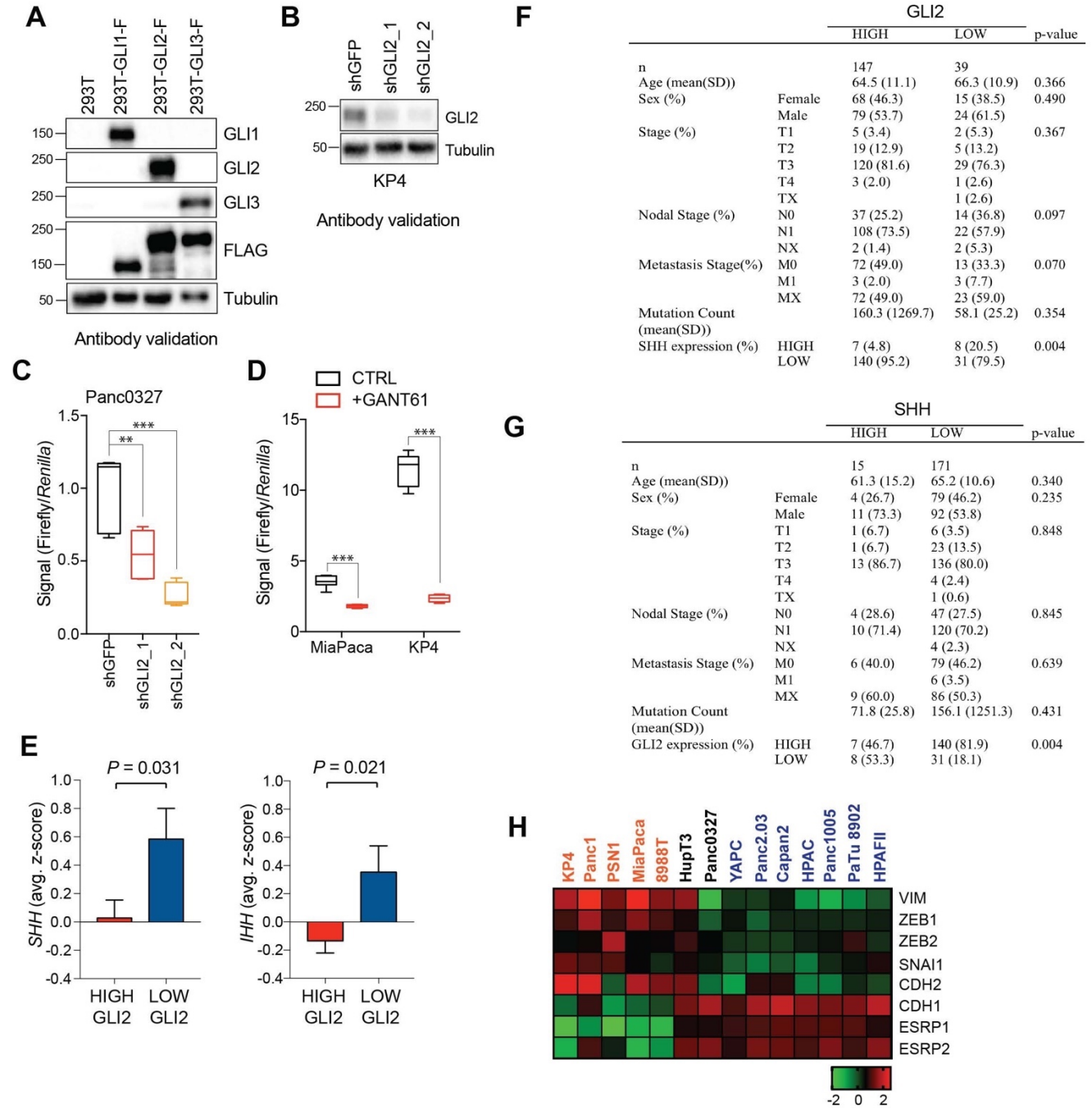


Figure 2.2. GLI proteins are expressed in basal-like PDA

(A) Lysates from 293T cells transiently transfected with Flag tagged GLI constructs were probed with GLI specific antibodies as indicated. (B) Immunoblot showing loss of the GLI2 specific band following knockdown of GLI2 with two distinct shRNA constructs in KP4 cells. (C,D) GLI luciferase activity in Panc0327 cells following shRNA mediated knockdown of *GLI2* (C) and in MiaPaca and KP4 cells following treatment with 5 μ M GANT61 for 3 days (D). *P* values were calculated by two-tailed unpaired *t* test. **P* < 0.05; ***P* < 0.01; ****P* < 0.001. (E) Comparison of *SHH* (left) and *IHH* (right) mRNA expression in RNA-seq data from TCGA PDA tumors binned into *GLI2* high (n = 51) and *GLI2* low (n = 41) groups. (F,G) Demographic and clinical information stratified by GLI2 (high: z > -1) (F), and stratified by SHH (high: z > 2) (G). (H) mRNA expression of epithelial to mesenchymal transition (EMT) markers as indicated.

Figure 2.3

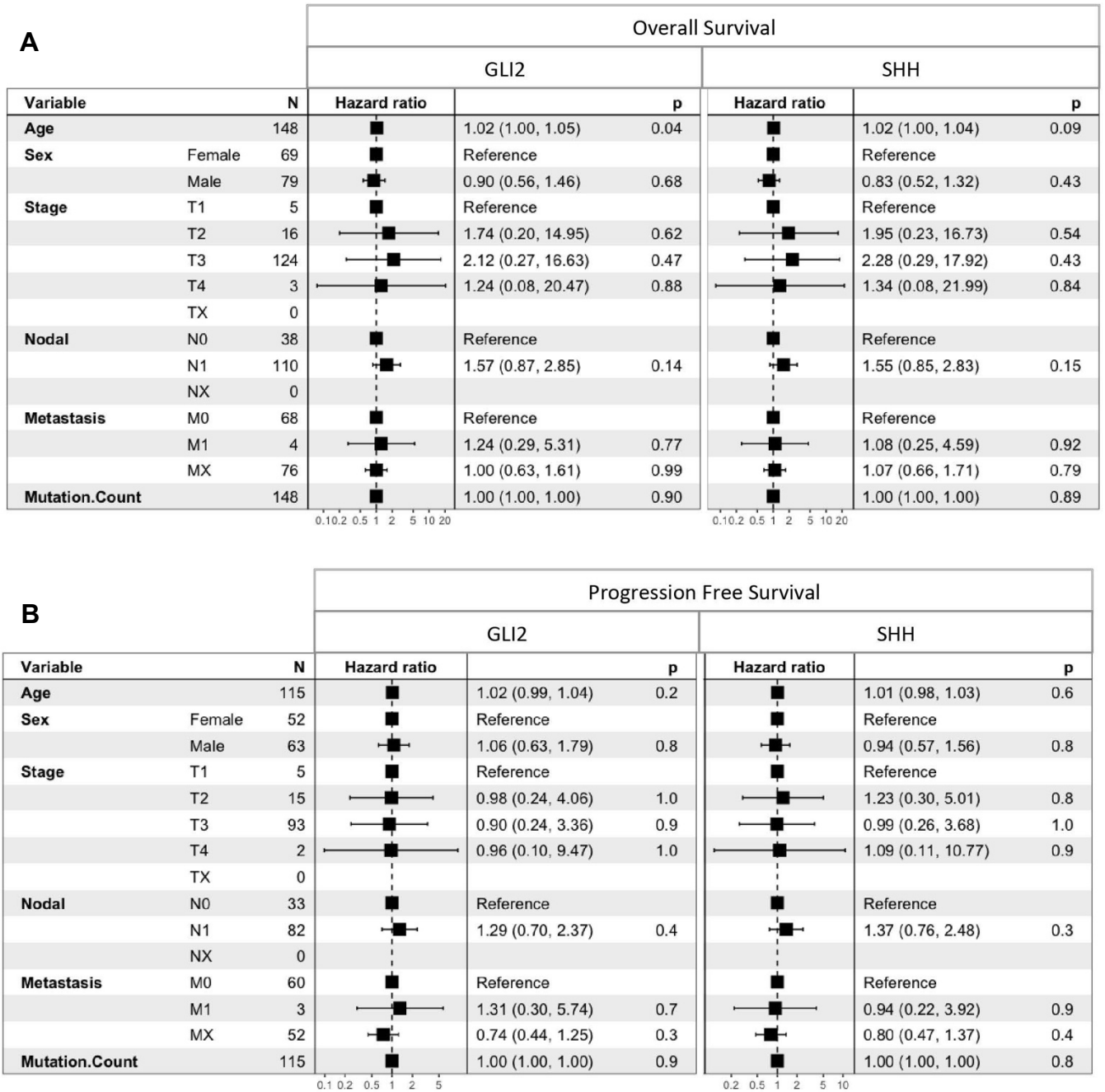


Figure 2.3. Cox proportional hazards regression models for predictors of overall survival and progression-free survival

(A) Cox regression model for overall survival stratified by GLI2 and SHH expression reveals age at diagnosis as a significant predictor of overall survival in GLI2 high samples while no covariates are significant predictors of overall survival in SHH high samples (B) Cox regression model for progression free survival stratified by GLI2 high and SHH high reveals no covariates as significant predictors. Differences in sample sizes (n) attributed to missing clinical data.

GLI expression and activity correlates with a mesenchymal cell state and the basal-like subtype of PDA.

We sought to determine the relationship between GLI expression and EMT in PDA, given the role of this program in cancer aggressiveness. Reexamination of our panel of 14 PDA cell lines by immunoblot (**Figure 2.4 A**) and qRT-PCR (**Figure 2.2 H**) for mesenchymal markers - ZEB1, ZEB2, Vimentin (VIM), SNAI1, SNAI2, N-Cadherin (CDH2) - and epithelial markers – E-Cadherin (CDH1), Epithelial splicing regulatory protein 1 and 2 (ESRP1, ESRP2) – enabled classification into EMT low and EMT high groups. Notably, whereas none of the GLI^{lo}/Hh^{hi} cell lines showed an EMT signature, most of the GLI^{hi}/Hh^{lo} cell lines were in the EMT high group, with the exceptions, HupT3 and Panc0327, displaying an intermediate phenotype (**Figure 2.4 A; Figure 2.1 B,C**). To assess whether GLI activity correlates with EMT status more broadly, we used a published EMT score generated from a meta-analysis of 18 independent gene expression studies of EMT (Groger et al. 2012). This signature assigned 38 human PDA cell lines as EMT high or low (Groger et al. 2012; Viswanathan et al. 2017), and we found that GLI activity (see **Figure 2.1 B**) correlated positively with EMT in our PDA cell line panel (**Figure 2.4 B**), while SHH expression correlated negatively (**Figure 2.4 C**). Intermediate cell lines, Panc0327 and HupT3 clustered together with the mesenchymal and epithelial-like cohort, respectively (**Figure 2.4 B**). Together these findings indicate that GLI^{hi} status correlates with a mesenchymal cell state in PDA.

EMT and poorly differentiated histopathology are features of basal-like PDA, prompting us to examine the relationship between GLI/Hh and subtype identity. To assay classical and basal-like status in PDA cell lines, we used concordant gene signatures

based on the Collisson, Moffitt and Bailey studies (Collisson et al. 2011; Moffitt et al. 2015; Bailey et al. 2016b; Cancer Genome Atlas Research 2017) (See Methods and **Table 2.2**). As expected, PDA cell lines with elevated levels of epithelial marker expression ($GLI^{\text{lo}}/Hh^{\text{hi}}$ lines) closely correlated with enrichment of the classical gene program (Collisson et al. 2011; Aung et al. 2018) (**Figure 2.4 A,D**). We next analyzed GLI status in 149 TCGA PDA samples pre-classified as classical or basal-like using the Collisson, Moffitt and Bailey signatures (Cancer Genome Atlas Research 2017). Strikingly, *GLI2* mRNA expression was enriched in the basal-like tumors, (**Figure 2.4 E left**), whereas high *SHH* and *IHH* expression correlated with the classical subtype (**Figure 2.4 E middle, right**). Collectively these data demonstrate that GLI-high status is a hallmark of the basal-like, EMT-high state that portends poor patient prognosis (**Figure 2.4 F**).

Figure 2.4

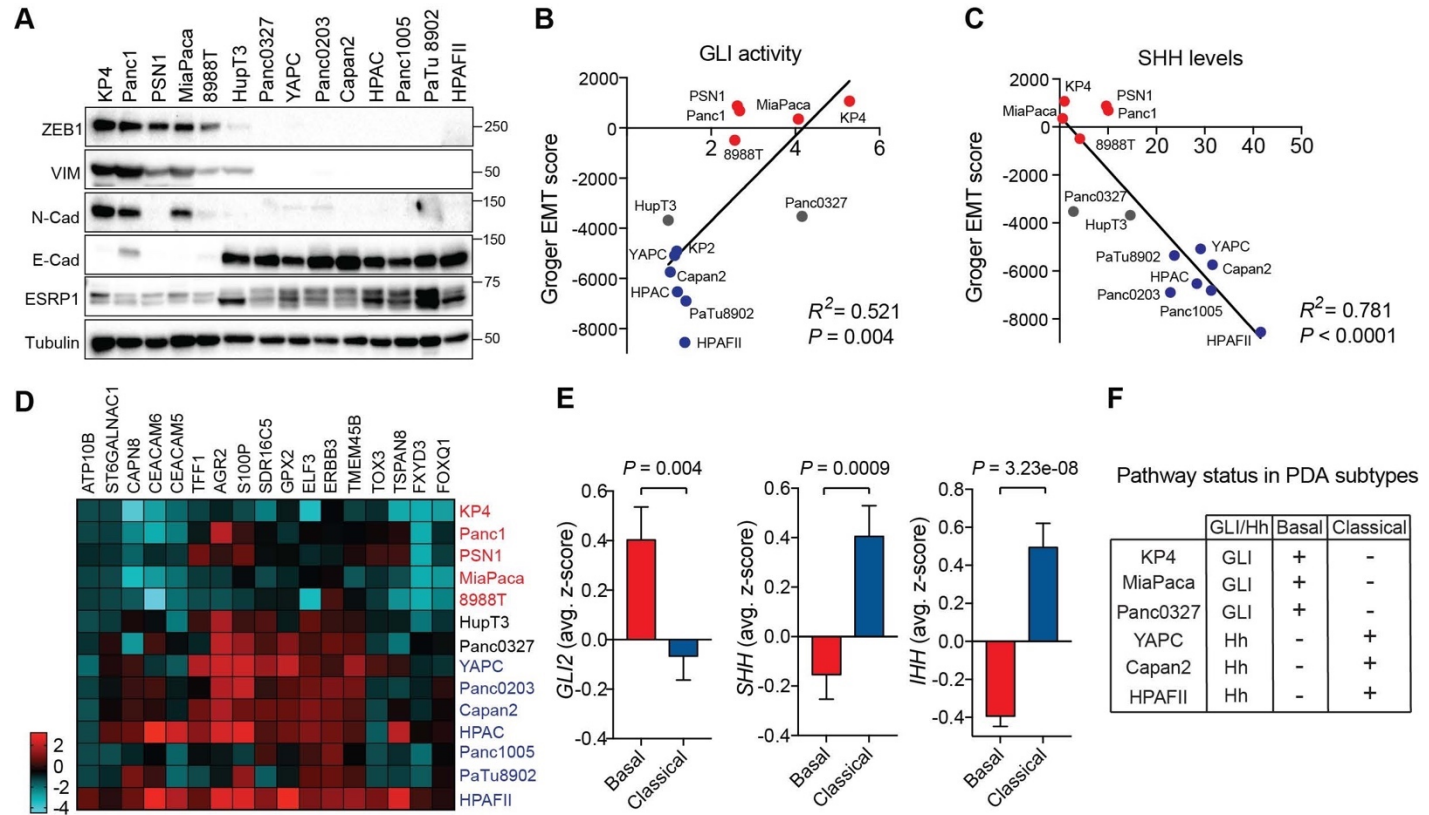


Figure 2.4. GLI expression and activity correlates with EMT and the basal-like subtype of PDA

(A) Human PDA cell lines segregate into two groups based on protein expression of EMT associated markers as indicated. Mesenchymal markers (ZEB1, VIM, N-Cadherin), epithelial markers (E-Cadherin, ESRP1). (B,C) GLI activity (B) as measured by GLI luciferase assay and SHH protein levels (see Fig. 1) (C) correlated to EMT score. Linear regression line is shown in red along with corresponding statistics. Epithelial cell lines are indicated in blue, and mesenchymal cell lines are indicated in red. Intermediate lines are indicated in grey. (D) mRNA expression of the classical subtype gene set (see methods) across 14 human PDA cell lines. Epithelial cell lines (blue) express higher levels of the classical gene program. (E) Expression of Hh pathway components correlates with PDA subtypes. *GLI2* mRNA expression is higher in TCGA PDA samples (n = 149) classified as basal-like (n = 65), while *SHH* and *IHH* expression is higher in samples classified as classical (n = 84). Bar represents average normalized z-score. (F) Table outlining the relationship between GLI and Hh expression to PDA subtypes in PDA human cell lines.

GLI2 is required for maintenance of the basal-like state

To test whether GLI function is necessary to sustain the basal-like phenotype, we suppressed GLI2 levels via siRNA or shRNA mediated knockdown or CRISPR-Cas9 mediated knockout in basal-like cell lines, KP4 and Panc0327. Loss of GLI2 led to a decrease in basal-like markers (KRT5, KRT14) and SOX2 and induction of epithelial markers (**Figure 2.5 A; Figure 2.6 A**). Accordingly, expression of the basal-like signature and EMT associated genes were also significantly reduced following GLI2 knockdown (KP4) (**Figure 2.5 B,C**) or knockout (Panc0327) (**Figure 2.6 B,C**).

Similarly, GLI2 knockout in KP4 and Panc0327 cells (GLI2^{KO}) resulted in a clear switch towards a more epithelial like morphology in 2D monolayer culture (**Figure 2.5 D**) and 3D matrigel growth (KP4; **Figure 2.6 D**). Moreover, immunofluorescence staining of GLI2 knockdown and GLI2^{KO} in KP4 and Panc0327 cells, respectively, showed a prominent nuclear relocalization of ESRP1 relative to Cas9 control cells, where ESRP1 was predominantly cytoplasmic (**Figure 2.5 E; Figure 2.6 E**). We next determined whether loss of the basal-like state compromises tumor growth. KP4 GLI2^{KO} cells showed a modest difference in *in vitro* growth rate (**Figure 2.5 F**) however GLI2^{KO} tumor xenografts displayed significantly reduced *in vivo* growth relative to Cas9 control tumors (**Figure 2.5 G**). Importantly, slow growing KP4 GLI2^{KO} tumors displayed reduced expression of the basal-like marker S100A2 (**Figure 2.5 H**, top row) and increased expression of the classical marker GATA6 (**Figure 2.5 H**, bottom row), suggesting that GLI2-dependent maintenance of a basal-like state is important for facilitating rapid *in vivo* tumor growth.

Collectively these data indicate that GLI2 is required to drive a common program that couples EMT and the basal-like subtype of PDA and that a significant level of cellular plasticity exists within PDA molecular subtypes.

Figure 2.5

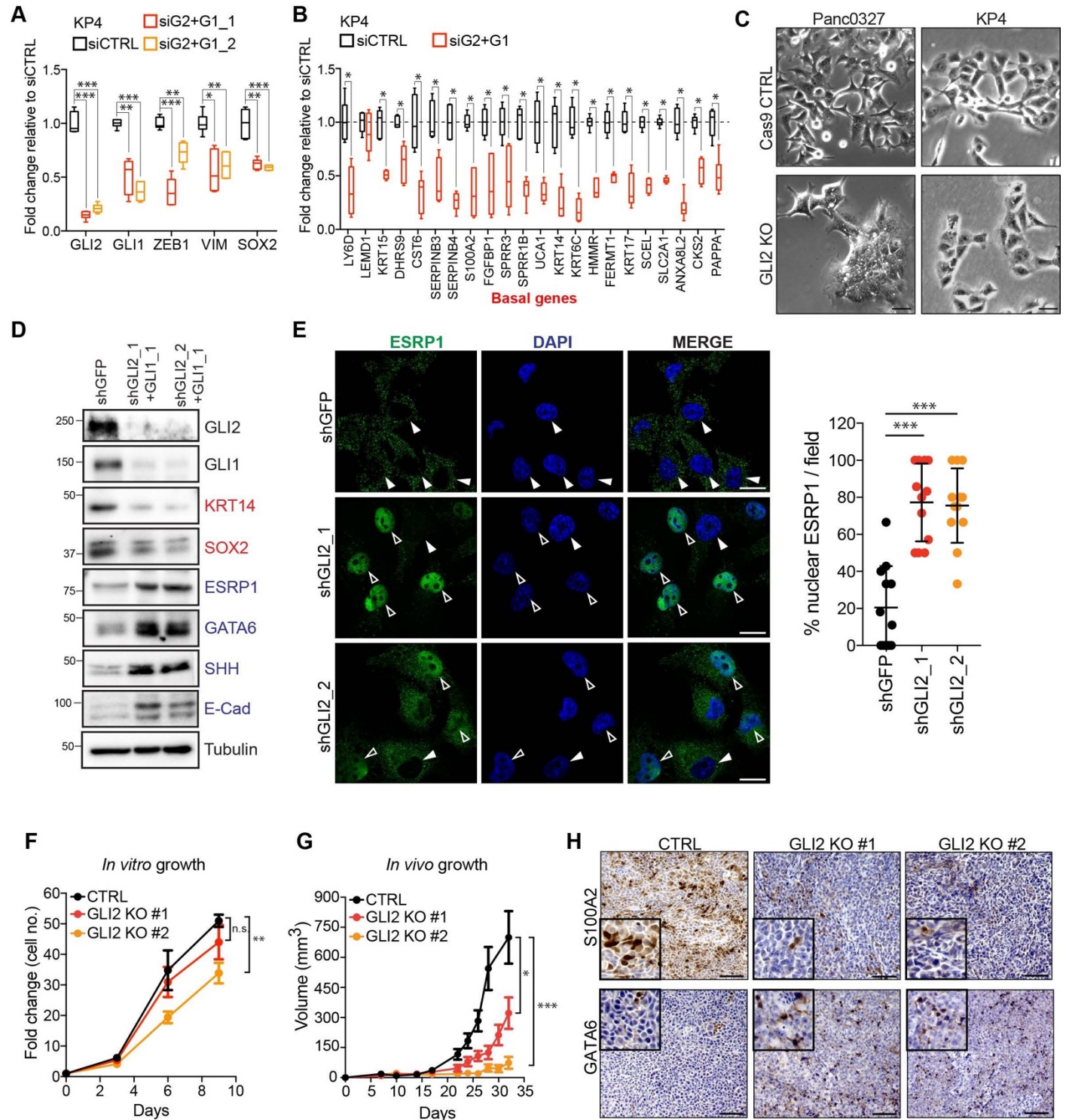


Figure 2.5. GLI2 is required to maintain the basal-like state in PDA

(A,B) Graph shows the effect of siRNA mediated GLI2 and GLI1 combined knockdown on EMT associated gene expression (A) and basal-like subtype gene expression (B) determined by qRT-PCR, displayed as fold change normalized to a scrambled siRNA control in KP4 cells (n = 2). (C) Brightfield images of Panc0327 and KP4 cells grown in 2D monolayer show loss of a mesenchymal phenotype upon GLI2 knockout (GLI2 KO) compared to Cas9 control cells (CTRL). Scale bar, 100µm. (D) Immunoblot shows the effect of shRNA mediated GLI2 and GLI1 combined knockdown on expression of the indicated proteins in KP4 cells. (E) Immunofluorescence staining (left) and quantification (right) of percentage ESRP1 nuclear localization in KP4 control (shGFP) and shRNA mediated GLI2 knockdown cells. Data represent 10 fields from 2 independent experiments. Solid arrowheads indicate absence of nuclear ESRP1; open arrowheads indicate nuclear ESRP1. Scale bar, 50µm. (F) Quantification of *in vitro* growth rate of KP4 Cas9 CTRL and GLI2 KO cells. (G) Quantification of *in vivo* growth of KP4 CTRL and GLI2 KO subcutaneous xenografts. Error bars represent s.e.m. (H) Immunohistochemistry of KP4 xenografts show downregulation of basal-like marker S100A2 (top) and upregulation of GATA6 (bottom) in GLI2 KO cells compared to CTRL, consistent with loss of the basal-like state. Scale bars, 200µm. *P* values were calculated by two-tailed unpaired *t* test. n.s. = not significant; **P* < 0.05; ***P* < 0.01; ****P* < 0.001.

Figure 2.6

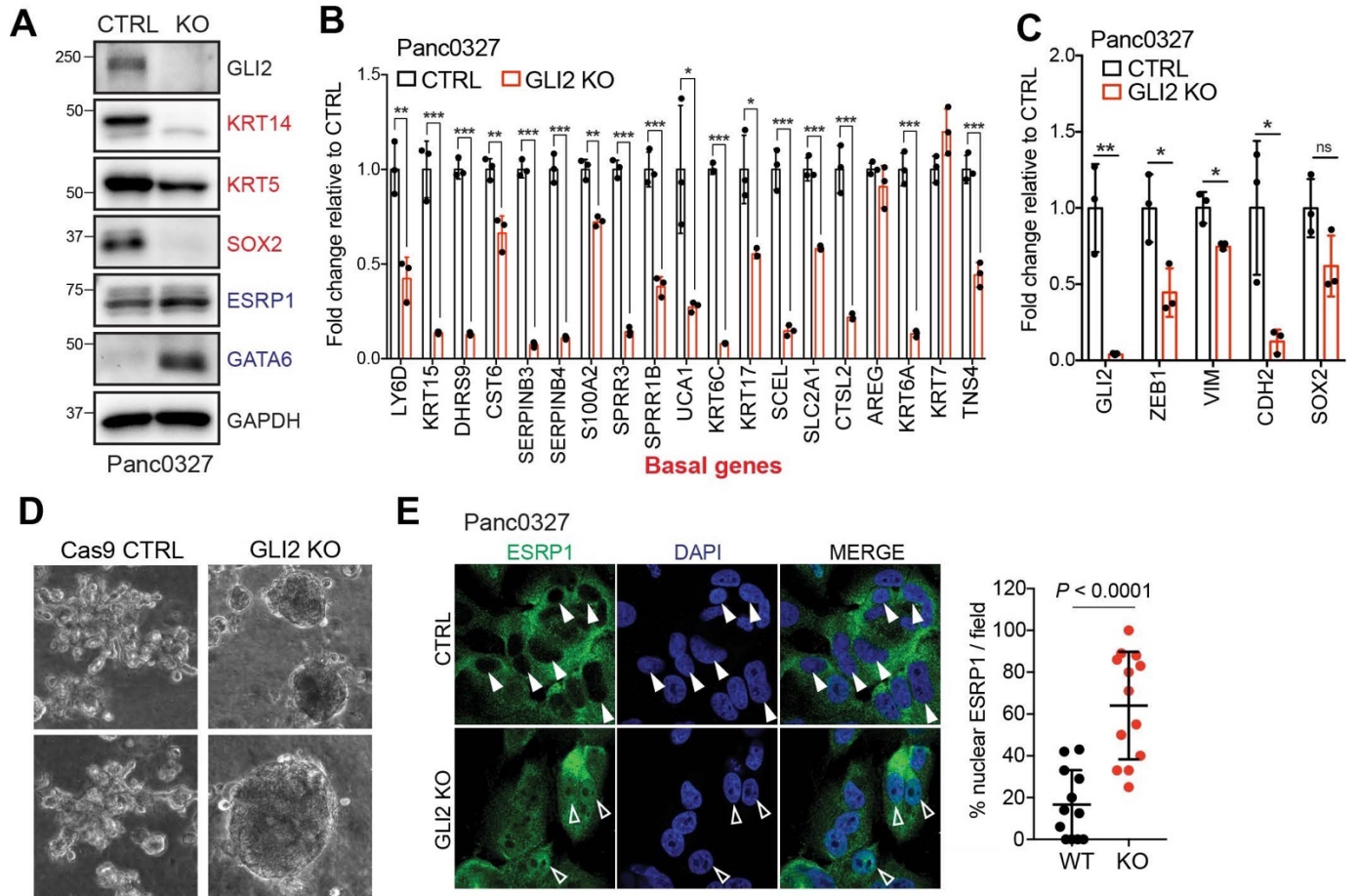


Figure 2.6. GLI2 knockout results in loss of basal-like identity in PDA

(A) Immunoblot shows the effect of GLI2 knockout (KO) in Panc0327 cells on protein expression of the indicated markers. (B,C) Graph shows the effect of CRISPR-Cas9 mediated GLI2 knockout (GLI2 KO) in Panc0327 cells on mRNA expression of the basal-like subtype genes (B) and EMT markers (C) determined by qRT-PCR, displayed as fold change normalized to Cas9 control (CTRL) cells. (D) Images show the effect of GLI2 KO in KP4 cells grown in 3D matrigel culture. Note the change from a mesenchymal to an epithelial phenotype. (E) Immunofluorescence staining (left) and quantification (right) of percentage ESRP1 nuclear localization in Panc0327 Cas9 control (CTRL) and GLI2 KO cells. Data represent 10 fields from 2 independent experiments. Solid arrowheads indicate absence of nuclear ESRP1; open arrowheads indicate nuclear ESRP1. Scale bar, 50µm. *P* values were calculated by two-tailed unpaired *t* test. **P* < 0.05; ***P* < 0.01; ****P* < 0.001.

GLI2 induction is sufficient to drive a classical to basal-like subtype switch in PDA cells.

To determine whether GLI proteins have functional roles in driving subtype specification, we engineered classical subtype PDA cell lines (YAPC, HPAFII) to stably overexpress GLI2 (**Figure 2.7 A; Figure 2.8 A**). Luciferase assays revealed that ectopic GLI2 expression in YAPC cells resulted in comparable GLI transcriptional activity to what is observed in the basal-like cell lines (**Figure 2.8 B vs Figure 2.1 B**). Strikingly, GLI2 overexpression strongly induced the mesenchymal markers ZEB1, VIM and basal-like marker KRT14 in YAPC cells and led to downregulation of epithelial markers E-Cadherin and ESRP1, and the transcription factor GATA6 - a putative regulator of the classical subtype of PDA (Collisson et al. 2011; Martinelli et al. 2017) and SHH in YAPC and HPAFII cells (**Figure 2.7 A; Figure 2.8 A**). Consistent with a switch towards a mesenchymal-like cell state, YAPC- and HPAFII-GLI2 cells showed a significant change in cell morphology compared to control cells expressing empty vector (EV) (**Figure 2.7 B and Figure 2.8 C**), characterized by a more elongated, less compact morphology when grown as monolayer cultures or as 3D matrigel cultures (**Figure 2.7 B**). Together, these data indicate that GLI2 can promote an EMT-like switch in classical PDA cells.

We next engineered YAPC and HPAFII cells to express GLI2 in a doxycycline (Dox)-inducible manner (iGLI2 cells), to study the downstream gene programs controlled by GLI2 with further resolution (**Figure 2.7 C**). We performed RNA-seq analysis of YAPC-iGLI2 cells compared to EV control cells (YAPC-iEV) following 6 days of Dox treatment. Gene set enrichment analysis (GSEA) using the Cancer Hallmarks database indicated that “Epithelial_Mesenchymal_Transition” was the most statistically significant program

activated by GLI2 (**Figure 2.7 D**). We further validated that Dox inducible activation of GLI2 in YAPC cells led to an increase in EMT markers, consistent with our results with stable GLI2 over-expression (**Figure 2.8 D**). In keeping with the relationship between EMT and the basal-like subtype, qPCR analysis indicated that Dox treatment of iGLI2 cells for 3 days resulted in a significant increase in basal-like subtype genes and a corresponding decrease in a subset of classical genes in both YAPC- and HPAFII-iGLI2 cells (**Figure 2.7 E**). In addition, the expression levels of stemness associated markers *SOX2* and *CD44* increased (**Figure 2.7 F**), while *SHH* and *GATA6* showed a significant decrease upon GLI2 induction and basal-like subtype switching in YAPC cells (**Figure 2.7 G**). Similarly, forced expression of a constitutively active GLI2 lacking the N-terminal repressor domain (Pasca di Magliano et al. 2006) (Δ N-GLI2) also lead to a decrease in *SHH* and *GATA6* levels in YAPC cells (**Figure 2.8 E**). Thus, GLI2-mediated conversion from a classical to a basal-like state also incorporates loss of SHH, which is in support of our observed inverse correlation between GLI proteins and Hh ligand expression in cell lines and patient tumors.

Figure 2.7

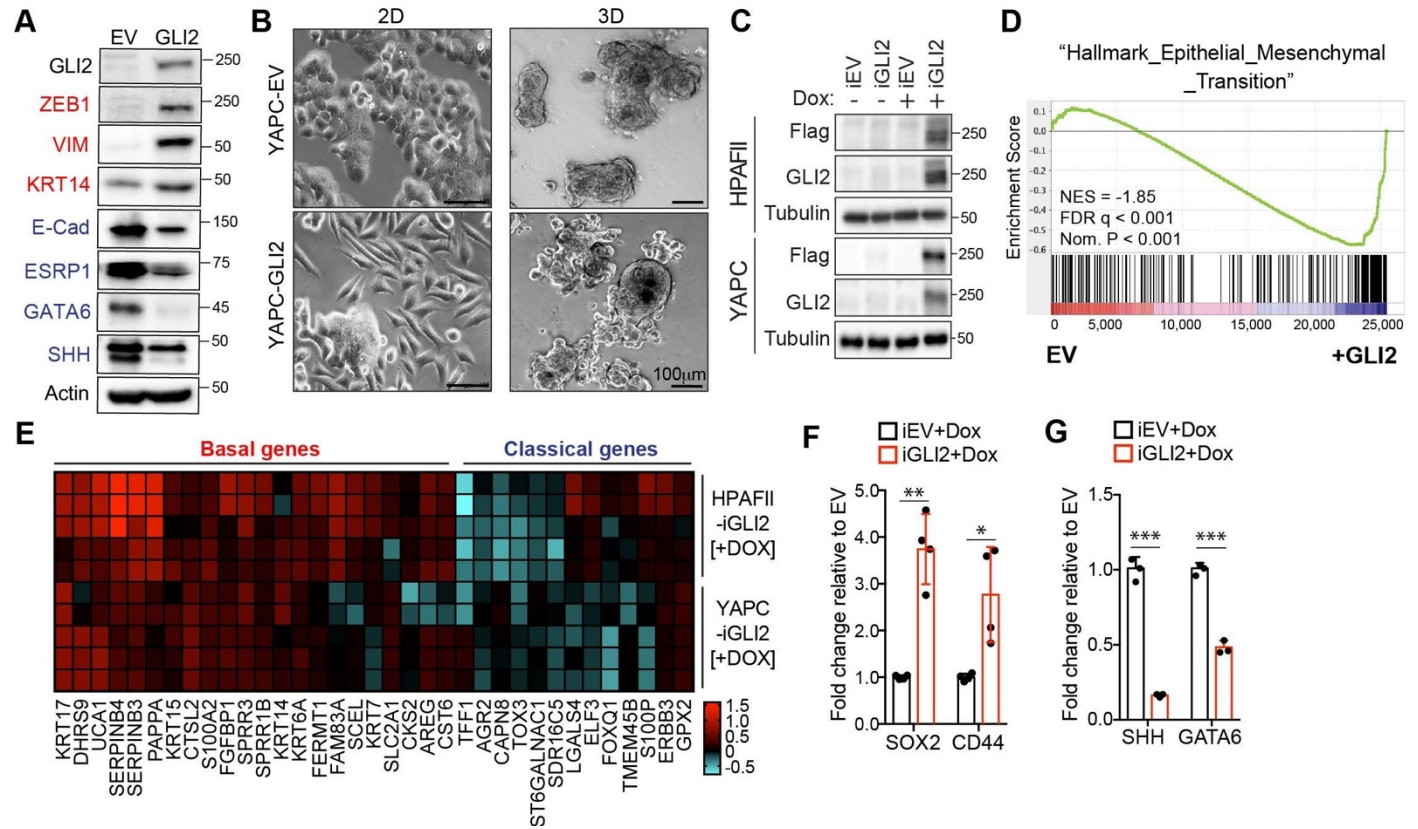


Figure 2.7 GLI2 is sufficient to drive basal-like subtype switching

(A) Immunoblot shows expression of the indicated proteins in YAPC cells stably expressing empty vector (EV) or Flag tagged GLI2 (GLI2). (B) Images show the effect of stable expression of Flag tagged GLI2 in YAPC cells on morphology when grown in 2D (left) and as 3D spheroids (right). Note the switch to a mesenchymal phenotype in the GLI2 expressing cells. Scale bars, 100 μ m. (C) Immunoblot shows GLI2 induction in HPAFII- and YAPC-iGLI2 cells following treatment with Dox. (D) Gene set enrichment analysis (GSEA) of RNA-sequencing data shows significant enrichment of the “Hallmarks_Epithelial_Mesenchymal_Transition” gene set in YAPC-iGLI2 cells treated with 1 μ g/ml Dox for 6 days to induce expression of GLI2, compared to identically treated YAPC-iEV control cells, (n = 3). (E) Heatmap shows expression of basal-like (red) and classical (blue) subtype associated genes determined by qRT-PCR following 1 μ g/ml Dox treatment of replicate HPAFII-iGLI2 (top) and YAPC-iGLI2 (bottom) cells for 3 days. Values from n = 5 replicates per cell are normalized to gene expression in identically treated iEV control cells and log₁₀ transformed. (F,G) Graph shows the effect of GLI2 induction in YAPC-iGLI2 cells treated with 1 μ g/mL Dox for 3 days on SOX2 and CD44 (F) and SHH and GATA6 (G) mRNA expression, displayed as fold change normalized to identically treated iEV control cells, (data represent n = 3 experiments). P values were calculated by two-tailed unpaired t test. *P < 0.05; **P < 0.01; ***P < 0.001.

Figure 2.8

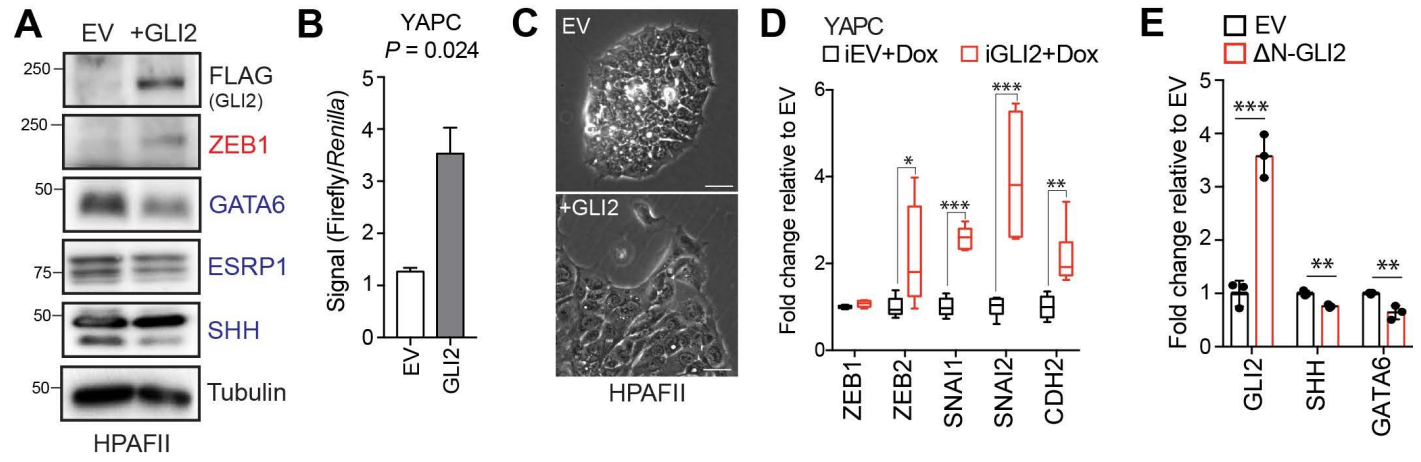


Figure 2.8. GLI proteins promote the basal-like phenotype

(A) Immunoblot of HPAFII cells stably expressing empty vector (EV) or Flag tagged GLI2 (+GLI2). (B) Luciferase assay measuring GLI activity in YAPC cells ectopically expressing EV or Flag tagged GLI2 (GLI2). (C) Effect of ectopic GLI2 expression on morphology of HPAFII cells relative to EV control cells. (D) Graph shows mRNA levels of the indicated genes following Dox induced expression of GLI2 in YAPC-iGLI2 cells after 3 days. Values represent fold change normalized to identically treated iEV control cells, (n = 3). (E) Effect of stable over-expression of Δ N-GLI2 in YAPC cells on *GLI2*, *SHH* and *GATA6* mRNA levels, displayed as fold change normalized to EV control cells. *P* values were calculated by two-tailed unpaired *t* test. * *P* < 0.05, ** *P* < 0.01, *** *P* < 0.001.

GLI2 mediates basal-like subtype switching in response to oncogenic KRAS^{G12D} ablation.

Recent studies have shown that PDA tumor cells can survive in the absence of oncogenic KRAS (referred to hereafter as KRAS^{*}) signaling by activating alternative mechanisms that maintain their growth (Singh et al. 2009; Kapoor et al. 2014; Kemper et al. 2014; Shao et al. 2014). These circuits often restore critical functions of KRAS^{*}, such as tumor cell proliferation and evasion of apoptosis, thereby enabling cancer cells to escape KRAS^{*} withdrawal. Moreover, basal-like PDA cell lines have been shown to harbor reduced dependency on KRAS^{*} for growth (Singh et al. 2009). Therefore, we hypothesized that GLI2-mediated basal-like subtype switching of classical PDA cells could likewise obviate KRAS^{*}-dependency. First, we measured GLI1 and GLI2 expression levels in response to oncogenic Kras^{*} extinction in cells derived from a murine PDA model driven by a Dox-inducible Kras^{*} allele [termed the iKRAS model (Ying et al. 2012)]. In this system, removal of Dox from the culture media led to a 50% reduction in *Kras* mRNA expression within 24 hrs and complete extinction by 72 hours (**Figure 2.10 A,B**). Interestingly, a reciprocal increase in *Gli2* and *Gli1* expression was evident within 24 hrs of Dox removal and persisted for at least 5 days (**Figure 2.9 A-C; Figure 2.10 A**). Moreover, there was a corresponding up-regulation of *Zeb1* and *Vim* mRNA and of basal-like subtype genes, consistent with induction of EMT and basal-like features (**Figure 2.10 C,D**). Similarly, shRNA-mediated knockdown of *KRAS* in the human PDA cell lines YAPC and HPAFII led to a concomitant increase in GLI expression, EMT markers (**Figure 2.9 D; Figure 2.10 E**) and basal-like subtype genes (**Figure 2.9 E**). Importantly, expression of the basal-like program was dependent on GLI2, as treatment of iKRAS4 cells with the

GLI inhibitor, GANT61 (5 μ M), suppressed basal-like gene induction in response to KRAS* ablation (**Figure 2.9 F**). Thus, upon KRAS* suppression, upregulation of GLI expression is responsible for induction of the basal-like gene program.

Acquired resistance and tumor relapse following KRAS* ablation is mediated by GLI2.

To test whether GLI2 induction is required to sustain growth of tumor cells following suppression of KRAS*, we stably overexpressed Flag-tagged mouse GLI2 in iKRAS cell lines (iKRAS-GLI2) prior to Dox withdrawal (**Figure 2.11 A**). Consistent with our findings in human PDA cell lines following ectopic expression of GLI2, murine iKRAS-GLI2 cells similarly displayed an increase in expression of basal (KRT5, KRT14) and EMT markers and SOX2 (**Figure 2.11 B**). In the presence of Dox (KRAS* on), iKRAS-GLI2 cells had a growth advantage over control cells (**Figure 2.9 G**, quantified in graph; '+ Dox'). Upon Dox withdrawal (KRAS* off), control cells (iKRAS-EV) failed to form colonies after 6 days while iKRAS-GLI2 cells were able to form colonies within the same time frame (**Figure 2.9 G**, quantified in graph; '- Dox'; **Figure 2.11 C**). This phenotype was recapitulated in 3D spheroid culture, where ectopic GLI2 expression rescued growth of iKRAS cells by 2.5 fold following Dox withdrawal (**Figure 2.11 D**). Similarly, human YAPC-GLI2 PDA cells were capable of sustained growth as 3D spheroids following shRNA-mediated knockdown of KRAS* relative to YAPC-EV cells (**Figure 2.9 H,I**; **Figure 2.11 E**). Thus, activation of GLI2 in PDA cells accelerates the emergence of clones that grow in the absence of KRAS*.

Sustained KRAS* pathway suppression in the iKRAS model was shown to induce significant tumor regression, however this was often followed by rapid tumor re-growth (Kapoor et al. 2014; Shao et al. 2014). Relapsed tumors retain KRAS* pathway suppression (**Figure 2.9 J**) and a subset harbor genomic amplification of the Hippo pathway transcriptional coactivator, YAP1 (Kapoor et al. 2014), which we have confirmed in 3 of 7 “Escaper” tumor cells lines (**Figure 2.9 J**; cell lines denoted as EY1-3). Interestingly, several Escaper cell lines do not harbor YAP1 amplification, suggesting that additional mechanisms may exist which mediate bypass of KRAS* extinction. Strikingly, we find that GLI2 is upregulated in 6/7 Escaper cell lines, including 4/7 lacking YAP1 induction. These results suggest that PDA cells co-opt several bypass mechanisms to circumvent KRAS* inactivation, including YAP1 and GLI2 upregulation, which may functionally compensate for KRAS* loss.

To further test the role of GLI2 in tumor relapse following KRAS* suppression, we grew independently derived iKRAS cell lines (iKRAS1 and iKRAS4) in the presence or absence of Dox for 15-18 days following shRNA mediated knockdown of *Gli2* (**Figure 2.11 F**). In the presence of Dox, loss of GLI2 did not have a significant effect on spheroid growth compared to shGFP control cells (**Figure 2.9 K** top row, **L**; **Figure 2.11 G** top row, **H**). However, the eventual emergence of resistant colonies in the absence of Dox was suppressed in shGLI2 cells compared with shGFP control (**Figure 2.9 K** bottom row, **M** arrowheads; **Figure 2.11 G**, bottom row, arrowheads and **I**). Thus, GLI2-mediated basal-like subtype switching can rescue viability upon KRAS* suppression, whereas its loss exacerbates the growth deficits caused by KRAS* loss.

Figure 2.9

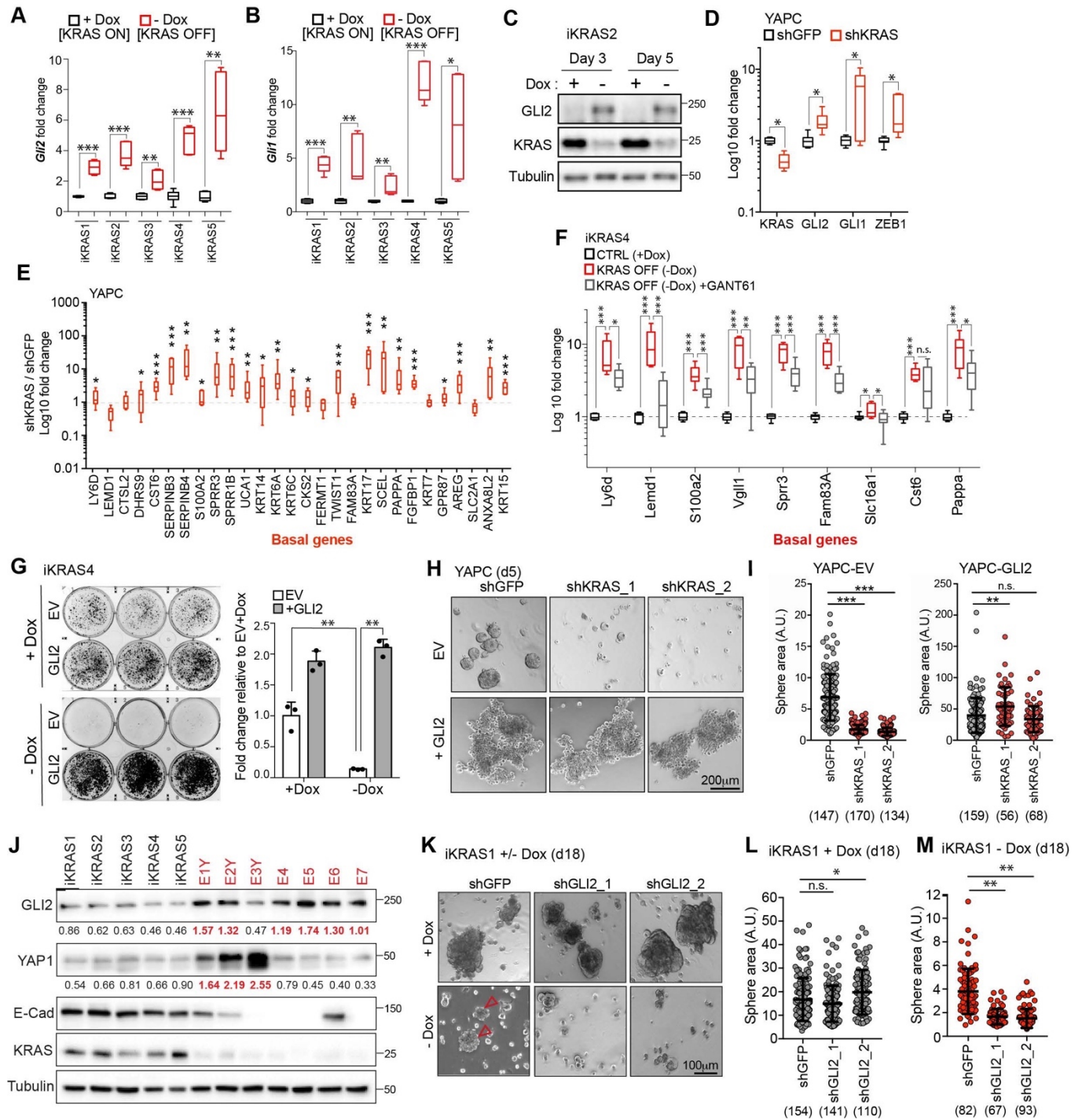


Figure 2.9. GLI2-mediated basal-like subtype switching rescues viability of PDA cells following KRAS^{G12D} ablation

(A,B) Effect of Dox depletion for 3 days on levels of *Gli2* (A) and *Gli1* (B) mRNA as measured by qRT-PCR in the indicated iKRAS cell lines, (n = 3). (C) Immunoblot shows expression of GLI2 and KRAS in iKRAS2 cells + Dox and – Dox for 3 and 5 days. (D,E) Effect of shRNA mediated knockdown of *KRAS* on *GLI2*, *GLI1*, *ZEB1* mRNA levels (D) and basal-like gene expression (E) as measured by qRT-PCR in YAPC cells. (n = 3). (F) Fold change in the basal-like gene signature in iKRAS4 cells following Dox removal (red plot) for 3 days or Dox removal in conjunction with 5 μ M GANT61 treatment (grey plot). qRT-PCR measurement of the indicated genes in both conditions are normalized to the + Dox control condition (black plot) (n = 3). (G) Colony forming ability of iKRAS4 cells stably expressing empty vector (EV) or Flag tagged mGLI2 (GLI2) grown in the presence (top) or absence (bottom) of Dox for 6 days, followed by staining with crystal violet. Graph shows the fold change in growth relative to the EV + Dox setting. Results shown are representative of n = 3 experiments. (H,I) Images (H) show the effect of stable expression of EV (top) or Flag tagged GLI2 (bottom) on YAPC sphere formation 5 days post shRNA-mediated knockdown of *KRAS* compared to control cells (shGFP). Quantification of sphere area for each condition is shown (I). Number of spheres measured per condition is indicated in parenthesis. Scale bar, 200 μ m. (J) Immunoblots show expression of the indicated proteins in iKRAS (black) and Escaper (red) cell lines. Numerical values indicate levels of GLI2 and YAP1 normalized to Tubulin. Escaper cell lines denoted with ‘Y’ harbor genomic amplification of *Yap1*. (K-M) Images (K) show the effect of shRNA-mediated knockdown of *Gli2* using two separate hairpins on iKRAS1 sphere formation when grown in the presence (top) or absence (bottom) of Dox for 18 days. Quantification of sphere area in the presence (L) and absence (M) of Dox is shown. Number of spheres measured per condition is indicated in parenthesis. Arrowheads indicate growth of KRAS^{G12D} independent spheroids. Scale bar, 100 μ m. *P* values were calculated by two-tailed unpaired *t* test. n.s. = not significant, **P* < 0.05; ***P* < 0.01; ****P* < 0.001.

Figure 2.10

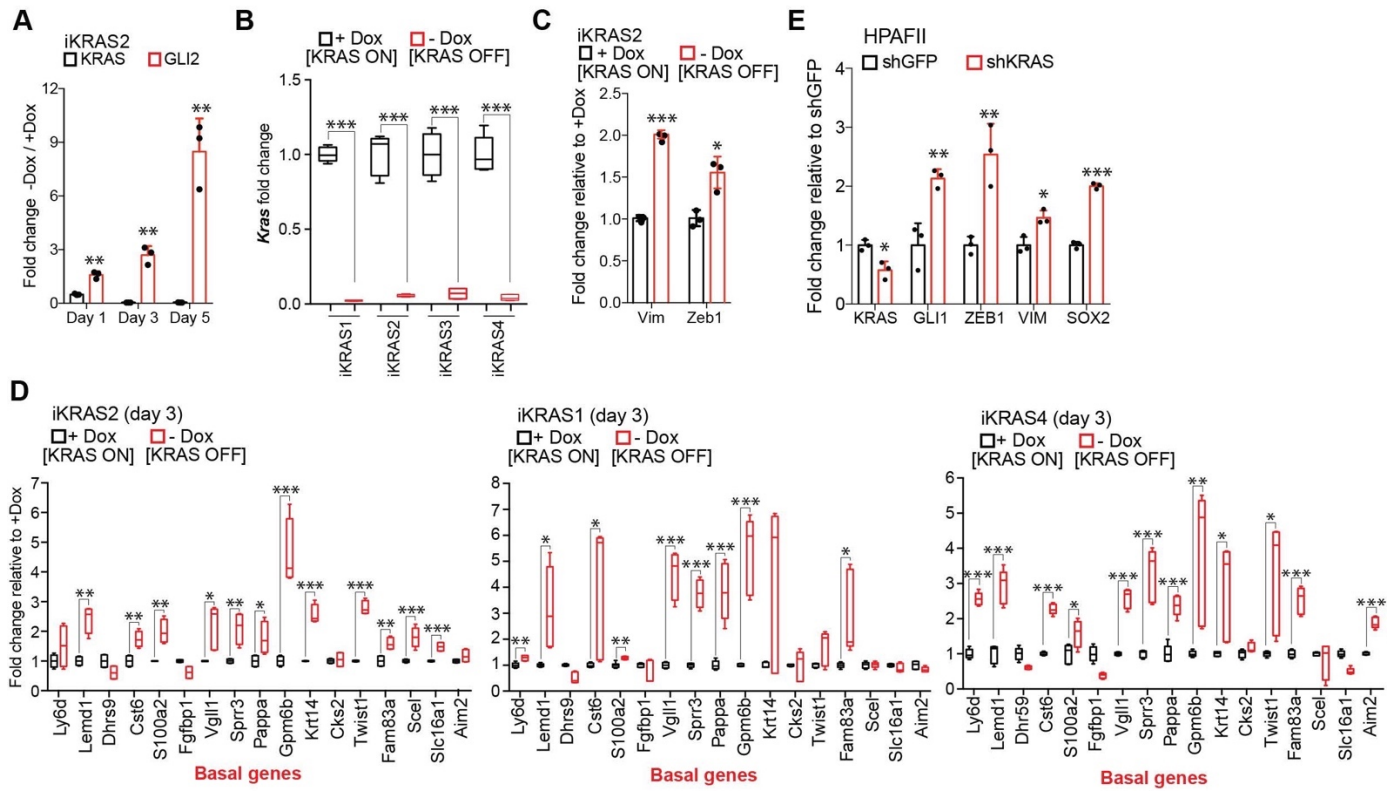


Figure 2.10. GLI2 is upregulated in response to KRAS^{G12D} ablation

(A) Graph shows effect of Dox withdrawal for 1, 3 and 5 days on *Kras* and *Gli2* mRNA expression in iKRAS2 cells as measured by qRT-PCR. Results are representative of n = 3 experiments. (B) Graph shows the effect of Dox depletion for 3 days on mRNA expression of *Kras* in iKRAS cell lines as measured by qRT-PCR. (C) Graph shows the effect of Dox depletion for 5 days on *Vim* and *Zeb1* mRNA expression in iKRAS2 cells as measured by qRT-PCR. Results are representative of n = 3 experiments. (D) Effect of Dox depletion for 3 days on mRNA expression of basal-like genes in the indicated iKRAS cell lines as measured by qRT-PCR. Results are shown as fold change relative to the +Dox condition. Significantly upregulated genes are indicated for each iKRAS cell line. (E) Effect of shRNA mediated knockdown of *KRAS* on the indicated genes as measured by qRT-PCR in HPAFII cells. *P* values were calculated by two-tailed unpaired *t* test. **P* < 0.05; ***P* < 0.01; ****P* < 0.001; # *P* < 0.001.

Figure 2.11

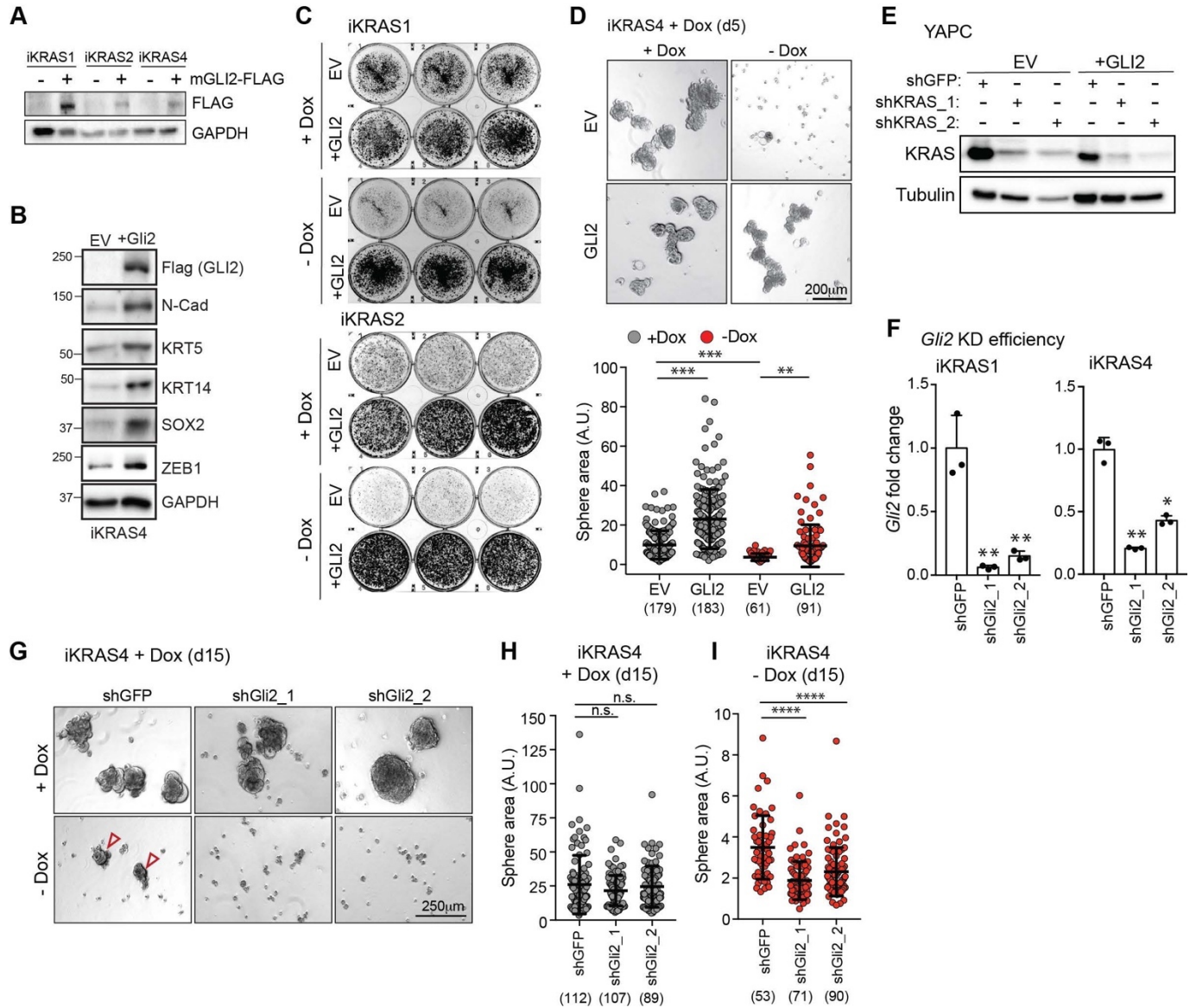


Figure 2.11. GLI2 is necessary and sufficient to promote bypass of KRAS^{G12D}-mediated oncogene addiction

(A) Immunoblot shows expression of Flag in iKRAS cells stably expressing empty vector or Flag tagged mouse GLI2 (mGLI2-FLAG). (B) Immunoblot shows the effect of ectopically expressing empty vector (EV) or Flag tagged mGli2 (+Gli2) in iKRAS4 cells on indicated EMT markers. (C) Colony forming ability of iKRAS1 and iKRAS2 cells stably expressing EV or mGLI2-FLAG (+GLI2) grown in the presence (top) or absence (bottom) of Dox for 6 days, followed by staining with crystal violet. (D) Images (top) show the effect of stable expression of EV or mGLI2-FLAG on iKRAS4 sphere formation when grown in the presence (left) or absence (right) of Dox for 5 days. Quantification of sphere area for each condition is shown (below). Number of spheres measured per condition is indicated in parenthesis. Scale bars, 200 μ m. (E) Immunoblot shows shRNA mediated knockdown efficiency of KRAS in YAPC-EV and YAPC-GLI2 cells. (F) qRT-PCR measuring *Gli2* transcript in iKRAS1 (left) and iKRAS4 (right) cells following infection with shRNA targeting mouse *Gli2*. (G) Images show the effect of shRNA-mediated knockdown of *Gli2* on iKRAS4 sphere formation in the presence (top) or absence (bottom) of 1 μ g/ml Dox for 15 days. Arrowheads indicate growth of KRAS^{G12D} independent spheroids. Scale bars, 250 μ m. (H, I) Quantification of sphere area shown in 'G'. Area of spheres grown in the presence (H) or absence (I) of Dox following infection with shGFP control hairpin or sh*Gli2* in iKRAS4 cells. Number of spheres measured is indicated in parenthesis. *P* values were calculated by two-tailed unpaired *t* test. n.s. = not significant, **P* < 0.05; ***P* < 0.01; *** *P* < 0.001; **** *P* < 0.0001.

The secreted ligand Osteopontin (OPN) promotes basal-like subtype conversion downstream of GLI2.

We next interrogated candidate downstream GLI2 targets that may drive subtype interconversion. Among the most upregulated transcripts expressed in YAPC-iGLI2 cells following GLI2 induction were genes encoding secreted factors including Secreted Phosphoprotein 1 (SPP1) encoding Osteopontin (OPN), fibroblast growth factor 19 (FGF19) and SPOCK2 [SPARC (Osteonectin)] and the basal-like gene S100A2 (**Figure 2.12 A**). OPN is a secreted glycosylated phosphoprotein classified as a member of the ‘small integrin-binding ligand N-linked glycoproteins’ (SIBLINGs) and has been associated with tumorigenesis and metastasis of several tumor types (Yoon et al. 2002; Rangaswami et al. 2006; Das et al. 2009; Pietras et al. 2014; Ahmed et al. 2016; Zhao et al. 2018). We confirmed upregulation of secreted OPN in YAPC-iGLI2 (**Figure 2.13 A**) and in a second cell line, HPAFII-iGLI2 (**Figure 2.12 B,C**) 3 days post induction of GLI2. Similarly, ectopic expression of Δ N-GLI2 in YAPC cells also led to an increase in *SPP1* expression (**Figure 2.13 B**). Consistent with direct regulation of *SPP1* transcription, chromatin immuno-precipitation of GLI2 showed binding to a GLI consensus element found upstream of the human *SPP1* transcriptional start site (**Figure 2.12 D**) (Kijewska et al. 2017).

Expression of *SPP1* is significantly increased in YAPC cells during basal-like subtype switching in response to KRAS* suppression (**Figure 2.12 E**), suggesting that OPN induction is a hallmark of the basal-like cell state in PDA. Accordingly, we found that GLI2-high basal-like cell lines expressed the highest levels of *SPP1* mRNA (**Figure 2.13 C**) and OPN protein levels in addition to higher levels of OPN receptors, CD44 and

integrin beta 3, as well as integrin alpha 5 (**Figure 2.12 F**) (Weber et al. 1996; Rangaswami et al. 2006; Zhao et al. 2018), compared to classical subtype cells. Moreover, knockdown of GLI2 alone or in combination with GLI1 led to a significant decrease in *SPP1* transcript (**Figure 2.12 G,H; Figure 2.13 D**) and secreted protein (**Figure 2.13 E**), establishing GLI transcription factors as endogenous regulators of *SPP1* expression.

We next tested whether treatment of classical subtype PDA cells with exogenous OPN is sufficient to induce a basal-like subtype switch. Exposure of Capan2 cells to recombinant OPN led to a significant increase in expression of basal-like genes, and a decrease in a subset of classical genes (**Figure 2.12 I**). A similar induction of basal-like genes was also observed in YAPC cells treated with exogenous OPN (**Figure 2.13 F**). To assess whether OPN promotes a basal-like program downstream of GLI2, we determined the ability of exogenous OPN to rescue basal gene expression upon GLI2 knockdown in basal-like cells. shRNA mediated GLI2 knockdown in Panc0327 cells led to a decrease in 13 basal-like genes, of which 12 were significantly rescued following co-treatment with recombinant OPN (**Figure 2.12 J**).

Loss of OPN in basal-like cells suppresses *in vivo* tumor growth.

To test the role of the GLI-OPN axis in tumorigenesis, we first generated an OPN-deleted KP4 line via CRISPR-mediated gene editing (**Figure 2.14 A**). OPN-deleted KP4 cells displayed a decrease in basal-like markers KRT14 (**Figure 2.14 B**) and a concomitant increase in classical-associated markers, E-cadherin and GATA6 (**Figure**

2.14 B, C), along with a switch towards a more epithelial like morphology on monolayer culture (**Figure 2.14 D**).

Similar to $GLI2^{KO}$ cells, $SPP1^{KO}$ cells did not show a significant growth defect *in vitro* relative to Cas9 controls cells (**Figure 2.14 E**). However $SPP1^{KO}$ cells displayed a dramatic defect in growth as tumor xenografts in mice (**Figure 2.14 F,G**). Similarly, $SPP1^{KO}$ cells were significantly impaired in their ability to form metastatic tumors in the lungs of recipient mice following tail vein injection, whereas Cas9 control cells gave rise to widespread metastatic disease (**Figure 2.14 H,I**). Accordingly, the reduced overall tumor burden of mice injected with $SPP1^{KO}$ cells led to their prolonged survival relative to the control cohort (**Figure 2.14 J**). These data indicate that OPN, downstream of $GLI2$, is a major growth regulator of basal-like tumors. Consistent with this notion, high expression levels of $SPP1$ mRNA in basal-like tumors correlated with shortened overall survival of PDA patients (**Figure 2.14 K**).

Collectively, our findings support a key role for a GLI - OPN axis in promoting and maintaining a basal-like phenotype that is key for PDA tumorigenesis, and highlight the importance of $GLI2$ -dependent, dynamic inter-conversion between subtypes in enabling adaptation to cellular stress, such as following loss of oncogenic $KRAS$ (**Figure 2.14 L**).

Figure 2.12

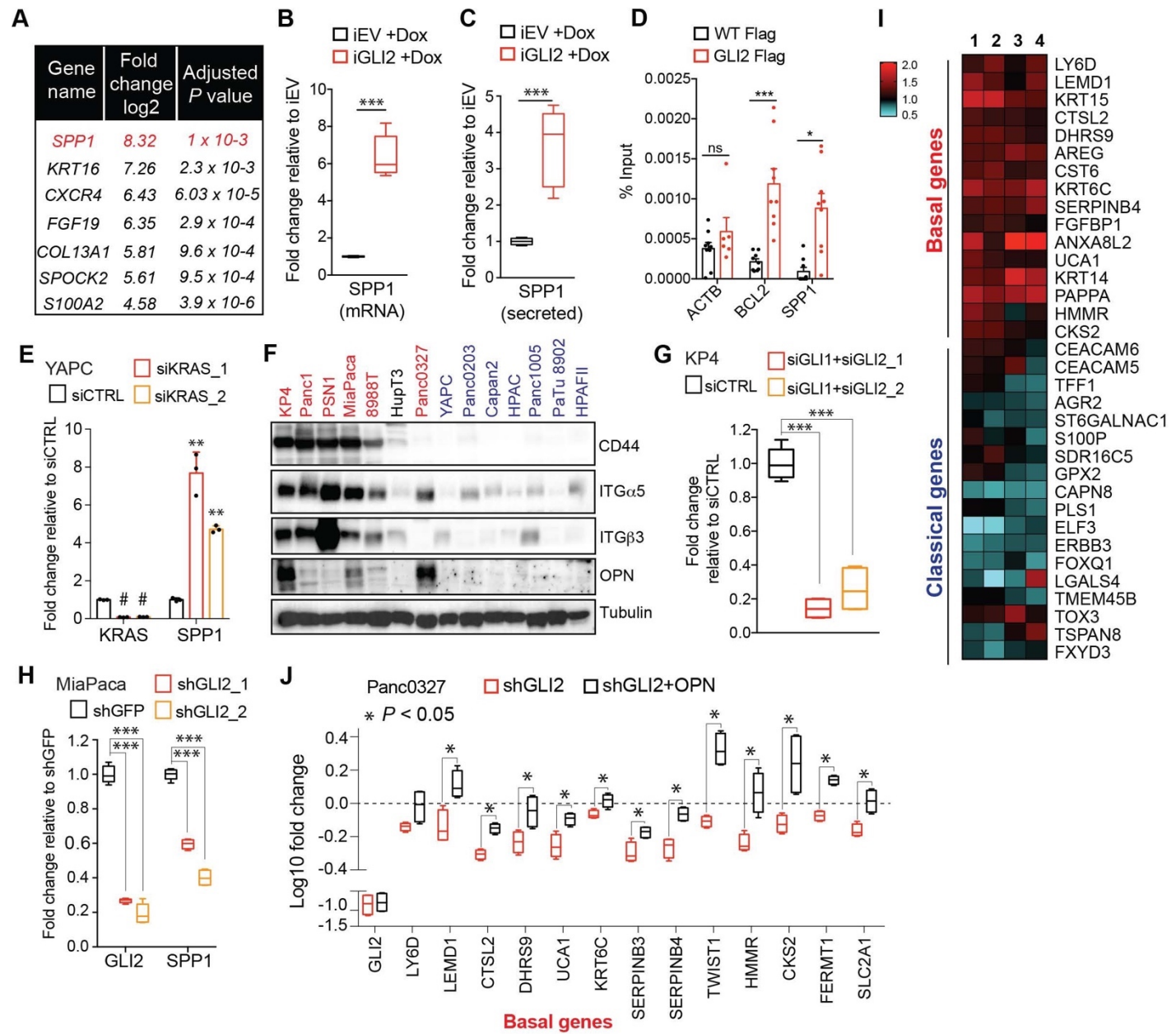


Figure 2.12. OPN is a downstream effector of GLI2 that promotes a basal-like subtype switch

(A) Top altered genes identified via RNA-sequencing analysis of YAPC-iGLI2 cells + Dox relative to YAPC-iEV + Dox, (n = 3). (B,C) Graph shows the relative fold change in human *SPP1* mRNA (B) and secreted protein (OPN) in the conditioned media as measured by ELISA (C) of HPAFII-iGLI2 cells treated with 1µg/mL Dox for 3 days normalized to identically treated HPAFII-iEV. (D) Chromatin immunoprecipitation of Flag-tagged GLI2 in 293T cells shows enrichment of binding to the *BCL2* and *SPP1* promoter relative to WT control cells (n=3). Error bars indicate s.e.m. (E) Effect of siRNA mediated knockdown of *KRAS* in YAPC cells on *SPP1* mRNA expression as measured by qRT-PCR. (F) Western blot of OPN receptors, CD44, integrin alpha 5 and integrin beta 3 in basal-like (red) and classical (blue) PDA cell lines. (G,H) Effect of *GLI2* knockdown in KP4 (G) and MiaPaca (H) cells, on mRNA expression of the indicated genes. (I) Heatmap shows the effect of treating Capan2 cells with 1µg/mL recombinant human OPN for 3 days on expression of the basal-like and classical subtype genes as measured by qRT-PCR (n = 4). Values are normalized to no treatment and log₂ transformed. (J) Effect of shRNA mediated knockdown of *GLI2* alone (red) or in conjunction with 1µg/mL OPN treatment (black) on expression of basal genes in Panc0327 cells. Values are normalized to no treatment and log₁₀ transformed. *P* values were calculated by two-tailed unpaired *t* test. **P* < 0.05; ***P* < 0.01; ****P* < 0.001.

Figure 2.13

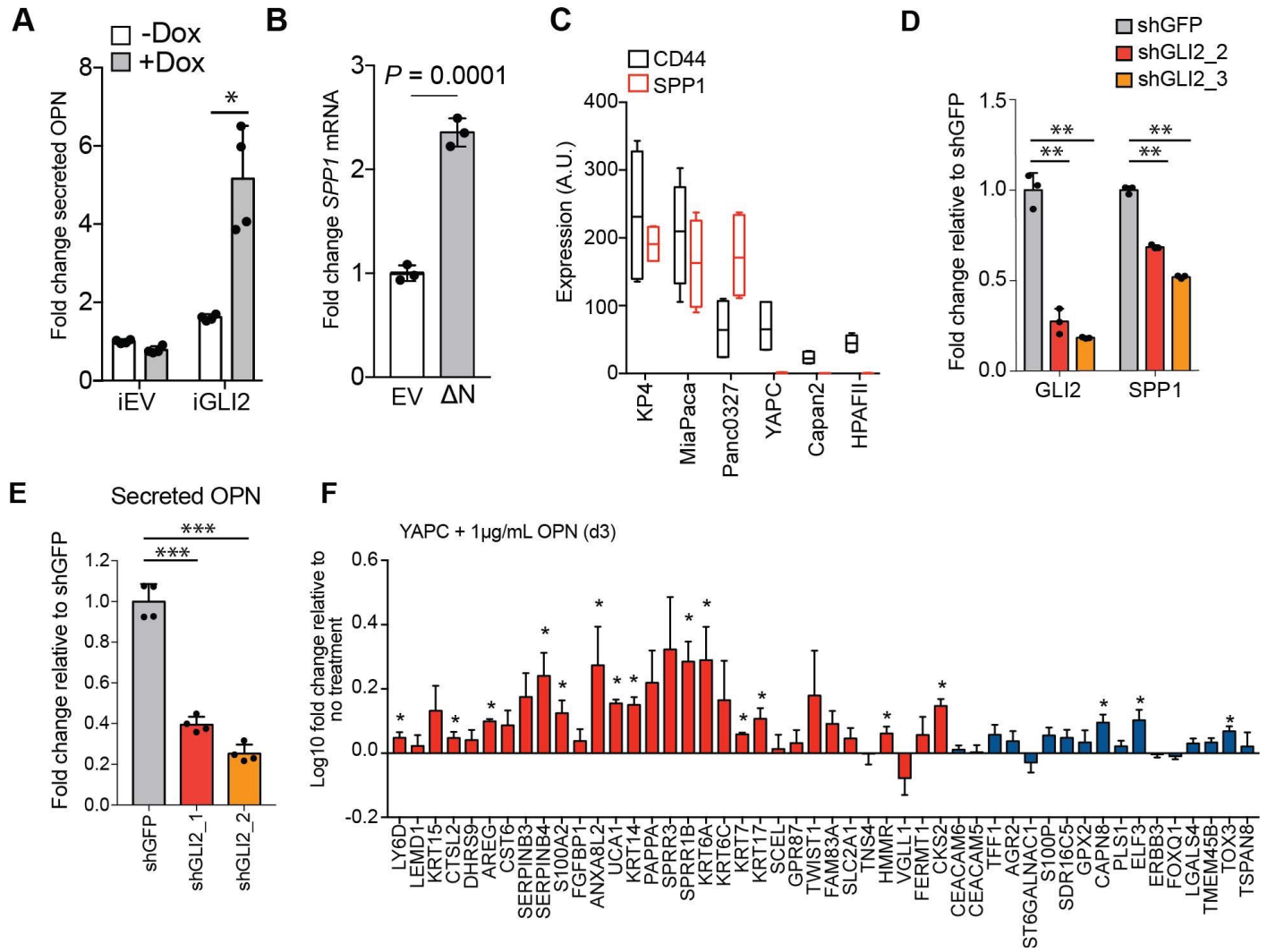


Figure 2.13. Secreted OPN promotes the basal-like subtype of PDA downstream of GLI2

(A) Graph shows the relative fold change in human OPN in the conditioned media of YAPC-iEV and -iGLI2 cells treated with 1µg/mL Dox for 3 days as measured by ELISA. All values are normalized to OPN levels in YAPC-iEV grown in the absence of Dox. (B) Graph shows relative fold change in *SPP1* mRNA levels following transient expression of Δ N-GLI2 (Δ N) in YAPC cells. (C) Graph represents mRNA levels of *SPP1* and *CD44* in the indicated human PDA cell lines as measured by qRT-PCR. (D,E) Effect of shRNA mediated knockdown of *GLI2* with two distinct hairpins on the mRNA expression of the indicated genes (D) and secreted OPN as measured by ELISA (E) in Panc0327 cells. (F) Expression of basal-like and classical subtype genes as measured by qRT-PCR following treatment of YAPC cells with 1µg/mL recombinant human OPN for 3 days. Values are normalized to no treatment and log10 transformed. Error bars are plotted as s.e.m. *P* values were calculated by two-tailed unpaired *t* test. **P* < 0.05; ***P* < 0.01; ****P* < 0.001.

Figure 2.14

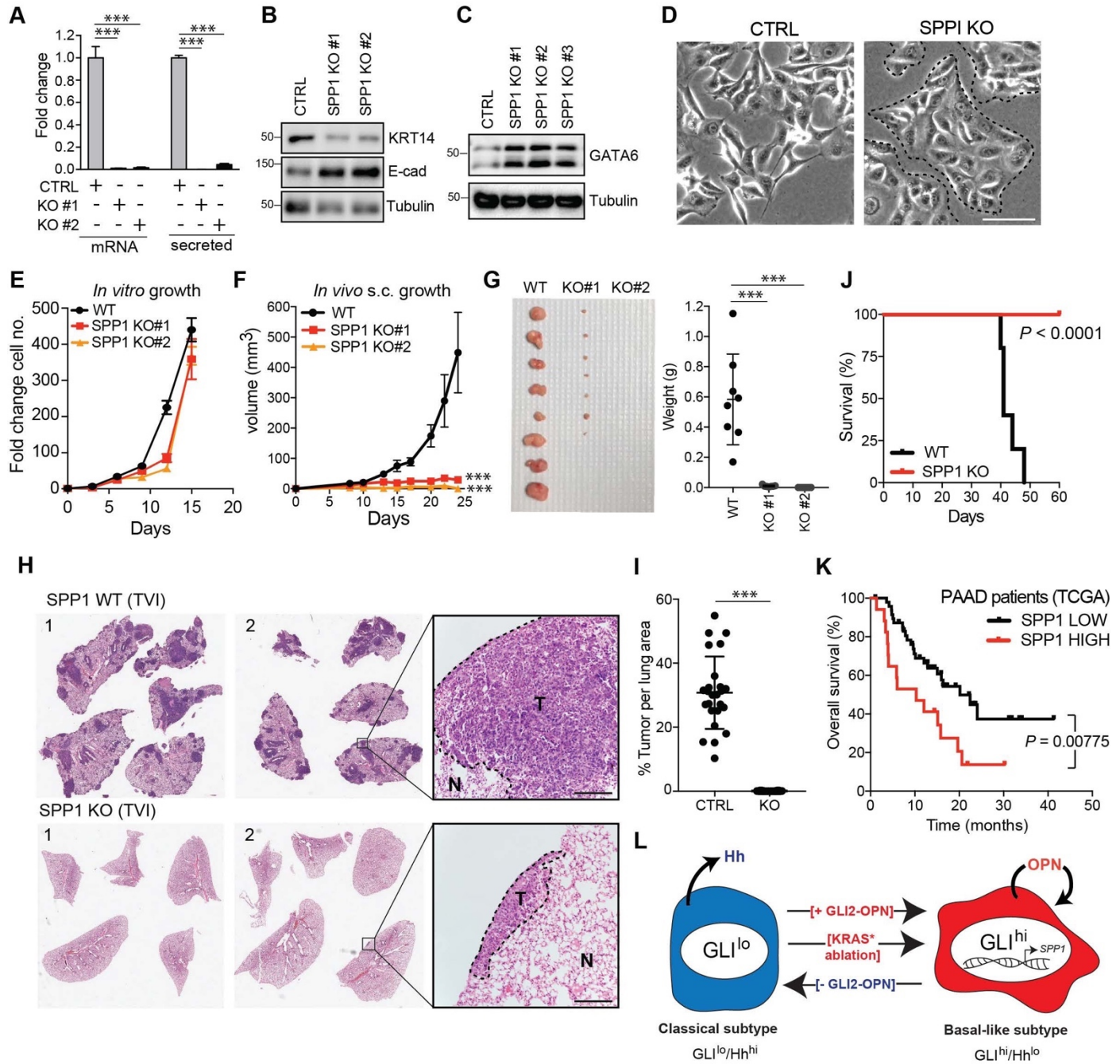


Figure 2.14. OPN loss impairs growth of basal-like PDA

(A) CRISPR-Cas9 mediated knockout of *SPP1* in KP4 cells leads to a decrease in mRNA expression and secreted Osteopontin in two independent clones. (B,C) Immunoblot of KRT14 and E-cadherin (B) and GATA6 (C) levels following KO of *SPP1* in KP4 cells. (D) Brightfield images of KP4 cell morphology when grown in 2D monolayer following KO of *SPP1*. Note the switch to a more epithelial phenotype in the KO cells. Scale bars, 100 μ m. (E) *In vitro* growth rate of KP4 control versus *SPP1* KO cell lines. Error bars represent s.e.m. (F) Growth rate of control and *SPP1* KO KP4 cells following subcutaneous injection into the flank of NOD/SCID mice. Error bars represent s.e.m. (G) Relative size of control and *SPP1* KO KP4 xenografts resected at day 25 (left) and comparative tumor weight (graph at right). (H) Representative H&E stained sections of lungs at endpoint following tail vein injection (TVI) of 2×10^6 KP4 control cells (WT; top) or *SPP1* KO (bottom) into NOD/SCID mice. Scale bars, 400 μ m. (I) Quantification of metastatic tumor burden in the lungs as a percentage of total lung area per mouse (n=5 CTRL; n=10 *SPP1* KO). (J) Kaplan-Meier graph depicting survival of NOD/SCID mice following TVI of KP4 WT (black) or *SPP1* KO cells (red). (K) High expression of *SPP1* in basal-like PDA patient tumors from The Cancer Genome Atlas (TCGA) predicts shorter overall survival (*SPP1* high n = 17, *SPP1* low n = 48). Data from 65 patients. (L) Model depicting a classical to basal-like switch mediated by a GLI2-OPN signaling axis in response to *KRAS*^{G12D} ablation. The classical and basal-like subtypes are marked by GLI^{lo}/Hh^{hi} and GLI^{hi}/Hh^{lo} expression, respectively. *P* value calculated by Log-rank test and by two-tailed unpaired *t* test. **P* < 0.05; ***P* < 0.01; ****P* < 0.001.

Table 2.1 Human and mouse primer sequences used in this study

Human Primers		
Gene	FWD (5' to 3')	REV (5' to 3')
18S	GCTTGCGTTGATTAAGTCCC	GCCTCACTAAACCATCCAATC
GLI2	TCAAGGAAGATCTGGACAGG	TGTGCTCGTTGTTGATGTG
GLI1	AGCGTGAGCCTGAATCTGTG	CAGCATGTA CTGGGCTTTGAA
SHH	CTACGAGTCCAAGGCACATATC	CAGGTCCTTCACCAGCTTG
SPP1	CTCCATTGACTCGAACGACTC	CAGGTCTGCGAAACTTCTTAGAT
CD44	CTGCCGCTTTGCAGGTGTA	CATTGTGGGCAAGGTGCTATT
VIM	AGTCCACTGAGTACCGGAGAC	CATTTACGCATCTGGCGTTC
ZEB1	GATGATGAATGCGAGTCAGATGC	ACAGCAGTGTCTTGTGTTGT
ZEB2	ATGACCTGCCACCTGGA ACTC	GCGGTA CTTGATGTGCTCCTTC
SNA11	TCGGAAGCCTAACTACAGCGA	AGATGAGCATTGGCAGCGAG
CDH2	TCAGGCGTCTGTAGAGGCTT	ATGCACATCCTTCGATAAGACTG
CDH1	ATTTTTCCCTCGACACCCGAT	TCCCAGGCGTAGACCAAGA
ESRP1	ACTAAAATAGACGTCGAAAGCC	GCCCATCAGTACAGAGACAG
ESRP2	ATGCAGCATCCAAGCACCT	CTGTCTCCAGTCCTAAACCCT
SOX2	GCCGAGTGGAACTTTTGTGCG	GGCAGCGTGTACTTATCCTTCT
CD24	CGCGGTGCGACTGGAAT	AAAGAAAAGTCCGCGCCTC
KRAS	ACAGAGAGTGGAGGATGCTTT	TTTCACACAGCCAGGAGTCTT
WNT7A	CTGTGGCTGCGACAAAGAGAA	GCCGTGGCACTTACATTCC
GATA6	CTCAGTTCCTACGCTTCGCAT	GTCGAGGTCAGTGAACAGCA
Classical genes:		
ATP10B	AAGAGCAGACCTATGTGCAGA	GCATATCCCATTGGGGTCAGAG
ST6GALNAC1	AGAAAGGTCTCTACAGTCCCTG	TGTGTGTTGAGGGCATTGTTC
CAPN8	CTCAAGGCATCATCTGGAAGC	ACCCTGACAAATGTCTGTGCG
CEACAM6	TCAATGGGACGTTCCAGCAAT	CACTCCAATCGTGATGCCGA
CEACAM5	AAGAAATGACGCAAGAGCCTATG	CCCGAAAGGTAAGACGAGTCTG
TFF1	CCCCGTGAAAGACAGAATTGT	GGTGTGTCGTA AACAGCAG
AGR2	GTCAGCATTCTTGCTCCTTGT	GGGTCGAGAGTCCTTTGTGTC
S100P	AAGGATGCCGTGGATAAATTGC	ACACGATGAACTCACTGAAGTC
SDR16C5	TATACCTGCGATTGCAGCCAA	CGATTCCGGCATTGTTGATTAGG
GPX2	GAATGGGCAGAACGAGCATC	CCGGCCCTATGAGGAACTTC
ELF3	GGCCGATGACTTGGTACTGAC	GCTTGCGTCTGTA CTTGTCTTC
ERBB3	GACCCAGGTCTACGATGGGAA	GTGAGCTGAGTCAAGCGGAG
TMEM45B	GCTTCCAGGGAGTTTCTTCT	CTTCCGCGTGTGGCTAAAGTA
TOX3	ATTCCACCAATCACGCCTCC	GGATCGCTGAGGGCTTGAAA
TSPAN8	ACTTCTTGTCTGGCTATGTGG	CACAGCAACGTAGGAGCTAGA
FXYD3	GGCTTAAGAGGCCCGAGTTT	TGCATTTTGC ACTCATGACGA
FOXQ1	CACGCAGCAAGCCATATACG	CGTTGAGCGAAAGGTTGTGG
LGALS4	CGACGCTGCCTTACTACCAG	CCAACCACAAAGTTCACGAAGA
PLS1	ACAAGAGGGAAGGGATTACTGC	AGATGCTTACAGTCAGGGTCATT
Basal-like genes:		
LY6D	CCAGCAACTGCAAGCATTC	CACAGTCCTTCTTCACCAGATT

Gene	FWD (5' to 3')	REV (5' to 3')
LEMD1	ATTGCAGAACCAACTTGAGAAGC	CGCGCAGTAGTCTCTCTCTT
KRT15	TCTGCTAGGTTTGTCTCTTCAGG	CCAGGGCACGTACCTTGTC
CTSL2	CGTGACGCCAGTGAAGAATCA	CGCTCAGTGAGACAAGTTTCC
DHRS9	CTGTGGACTCGTAAAGGAAAAC	GCAGCGATTACATGAAATCCCT
AREG	GAGCCGACTATGACTACTCAGA	TCACTTTCCGTCTTGTTTTGGG
CST6	TACTTCCTGACGATGGAGATGG	GAGTTCTGCCAGGGAACCAC
SERPINB4	CTGGGTGGAAAGTCAAACGAA	TGTCGTATCATTGCCAATAGTCC
SERPINB3	CGCGGTCTCGTGCTATCTG	ATCCGAATCCTACTACAGCGG
S100A2	ATGAGTGGGAATGGCAAGAG	CTCCCAGGGTGAGGATTTATATG
FGFBP1	GGAAACAAGTTGCCCGGAATC	AATAGAGTGGAGCTGACTAGCTT
SPRR3	CCAGCAGAAGCAGACCTTTAC	TCCTTGGTTGTGGGAACAAATA
SPRR1B	TCCCCTATCCCATTCTGCGT	AGCAGCTGAAAACCTAGCTCTGG
UCA1	GCCAGCCTCAGCTTAATCCA	CCCTGTTGCTAAGCCGATGA
KRT14	GTGGGTGGAGATGTCAATGT	CATCCTTGCGGTTCTTCTCT
KRT6A	TCTCACTGTTGGTAAAGCCAG	CTGGCTGAGTTGGCACTGAA
KRT6C	GGGTTTCAGTGCCAACTCAG	CCAGGCCATATAAGCTGCGG
PAPPA	ACAAAGACCCACGCTACTTTTT	CATGAACTGCCCATCATAGGTG
HMMR	AGAACCAACTCAAGCAACAGG	AGGAGACGCCACTTGTTAATTC
CKS2	TTCGACGAACACTACGAGTACC	GGACACCAAGTCTCCTCCAC
FERMT1	GGTGAGGTTGCGAGTCAGC	CCAGACGGCTTTAACAAGGAA
TWIST1	GTCCGCAGTCTTACGAGGAG	GCTTGAGGGTCTGAATCTTGCT
FAM83A	GGAGATGTGTGACAAAGTCCAG	CCAGCGAATTTCTGCTGCTG
KRT17	GCCGCATCCTCAACGAGAT	CGCGGTTCAAGTTCCTCTGTC
SCEL	TCGGTACAGTTCTGATGACACT	AACATGGACATGCTCCTATTGG
KRT7	CATGCAGGATGTGGTGGAGG	CCGTCTCATTGAGGGTCTCTG
GPR87	GCCAGGAAAGAACCACCC	GATCCACACTGCTAAACCATTCA
SLC2A1	ATTGGCTCCGGTATCGTCAAC	GCTCAGATAGGACATCCAGGGTA
ANXA8L2	AAAGCCATGAAGGGGATCGG	GTTACAGCACAAGTGACCCTG
TNS4	AGCCAGGGGCTTTTGTATAA	AGACGACTCGATGAGGAAGTG
VGLL1	TCAGAGTGAAGGTGTGATGCT	GCACGGTTTGTGACAGGACT
Mouse primers		
18S	GTAACCCGTTGAACCCATT	CCATCCAATCGGTAGTAGCG
Gli2	CAACGCCTACTCTCCAGAC	GAGCCTTGATGTACTGTACCAC
Gli1	CTACTCGGGGTTCAATGATGC	TGTGGAGTTGGGGCTAGACAT
Vim	CGTCCACACGCACCTACAG	GGGGGATGAGGAATAGAGGCT
Zeb1	ACCGCCGTCATTTATCCTGAG	CATCTGGTGTCCGTTTTTCATCA
Kras	CAAGAGCGCCTTGACGATACA	CCAAGAGACAGGTTTCTCCATC
Basal-like genes:		
Ly6d	GCCTGGGCACTTCGATGTC	TGAGTTTGCACACTCTTTCCTC
Lemd1	GACTATGAGTTGCACAAGCATCT	TCTTCTCGTAGGTCTTCTGGTG
Dhrs9	ATGCTGTTTTGGTTGTTGGCT	GTTCTGGCTGCTAAGTTTCCA
Cst6	GAAGTTGTCACCCACCGACC	TTTGGTGTCTCGGAAGTAGTAGA
S100a2	ACGCCAGTCAAGAGGACGA	CCCCACATAGCTCAGCAGC
Fgfbp1	TGGCTACTCAGGCGTTCTCA	CGTCAGAGATTTAGATGTCTGCTG
Spr3	GAACAGCATCAAGTGAAGCAAC	CTGGAATCTTGGTGTCTTCTGG

Gene	FWD (5' to 3')	REV (5' to 3')
Krt14	AGCGGCAAGAGTGAGATTTCT	CCTCCAGGTTATTCTCCAGGG
Pappa	GGATGGGTCATGGGCATTCA	GAAAAAGTAGCGTGGATCTCTGT
Cks2	TCGATGAGCACTACGAGTACC	CCATCCTAGACTCTGTTGGACAC
Twist1	GGACAAGCTGAGCAAGATTCA	CGGAGAAGGCGTAGCTGAG
Fam83a	ATGAGTCGGTCAAGGCATGTG	TGAGGACAGGAAGTCTACCTCT
Scel	GACAACAGGGTTTTTCAGGACG	TACCGGCTAATTGTGGCTTTT
Vgl1	TGTCTGGATACCTGAAAGCAGT	GGCCTCTTGAGGTTACGCA
Gpm6b	CAGGCACCGTGGCAATTCT	GTTGGATCACTTCACTCAGCAA
Slc16a1	GAGGTGGAGCTGACGAGGT	CATGGACACGAAGAGCACCC
Aim2	GTCACCAGTTCCTCAGTTGTG	CACCTCCATTGTCCCTGTTTTAT
shRNA sequences:		
HUMAN:		
KRAS	TRCN0000010369	CAGTTGAGACCTTCTAATTGG
KRAS	TRCN0000033263	GACGAATATGATCCAACAATA
GLI2	TRCN0000033329	CCGCTTCAGATGACAGATGTT
GLI2	TRCN0000033332	GCTCTACTACTACGGCCAGAT
MOUSE:		
Gli2	TRCN0000226034	TCGACCTACAACGCATGATTCC
Gli2	TRCN0000226035	TGTGGAGGACTGCCTACATAT
Gli2	TRCN0000219066	TATGTTTACCCGCTCCTATTT

Table 2.2 Classical and basal-like gene signatures

List of genes associated with the classical and basal-like gene signatures and their expression in the corresponding Moffitt, Collisson, and Bailey signatures

Classical signature genes			
Gene	Moffitt	Collisson	Bailey
ATP10B		X	X
ST6GALNAC1	X	X	X
CAPN8		X	X
CEACAM6	X	X	X
CEACAM5		X	
TFF1	X	X	X
AGR2	X	X	X
S100P		X	
SDR16C5		X	
GPX2		X	X
ELF3		X	
ERBB3		X	X
TMEM45B		X	
TOX3		X	X
TSPAN8	X	X	X
FXVD3		X	
FOXQ1		X	
LGALS4	X	X	X
PLS1		X	X
Basal-like signature genes			
Gene	Moffitt	Collisson	Bailey
LY6D	X		X
LEMD1	X		
KRT15	X		
CTSL2	X		
DHRS9	X		
AREG	X		
CST6	X		X
SERPINB4	X		
SERPINB3	X		
S100A2	X	X	X
FGFBP1	X		
SPRR3	X		X
SPRR1B	X		X
Gene	Moffitt	Collisson	Bailey
UCA1	X		

KRT14		X	X
KRT6A	X		X
KRT6C	X		X
PAPPA		X	
HMMR		X	
CKS2		X	
FERMT1		X	
TWIST1		X	X
FAM83A	X		X
KRT17	X		X
SCEL	X		
KRT7	X		
GPR87	X		X
SLC2A1	X		
ANXA8L2	X		
TNS4	X		X

Methods:

Antibodies and reagents

Antibodies against GLI2 H-300 (sc-28674) and GAPDH (sc-32233) were purchased from Santa Cruz Biotechnology; GLI3 (AF3690) from R&D Systems; SHH (ab53281), SMO (ab38686) and S100A2 (ab109494) from Abcam; GLI2 (18989-1-AP), KRAS (12063-1-AP), Tubulin (66031-1-Ig), E-Cadherin (20874-1-AP), and ESRP1 (21045-1-AP) from Proteintech; GLI1 (2534), FLAG (2368), ZEB1 (3396), Vimentin (5741), YAP1 (4912), N-Cadherin (4061), GATA6 (5851) from Cell Signaling Technology; Keratin 14 (905304) and Keratin 5 (905504) from BioLegend; Peroxidase goat anti-rabbit (PI-1000), horse anti-goat (PI-9500), and horse anti-mouse IgG (PI-2000) antibodies from Vector Labs. Keratinocyte SFM and supplements, RPM1, DMEM, DMEM F12 (1:1), fetal bovine serum (FBS) were purchased from Corning; tet system approved FBS from Clontech. Silencer select siRNA sequences against human GLI2, GLI1 and KRAS were purchased from Ambion.

Cell culture

Cell lines were obtained from the American Type Culture Collection (ATCC). Mouse PDA Dox-inducible iKRAS lines were gifts from Haoqiang Ying and Alec Kimmelman. Human PDA cell lines and HPDE cells were cultured as previously described (Perera et al. 2015) and iKRAS mouse cell lines were cultured as previously described (Kapoor et al. 2014). All cell lines were confirmed negative for mycoplasma contamination on a routine basis using MycoAlert Detection Kit (LT07-418) from Lonza. Colony formation was assessed

following plating of 3,000 cells per well, which were fixed with 4% paraformaldehyde and stained with 0.1% crystal violet after six days of growth. Cells grown in 3-dimensional culture were plated at 10,000-30,000 cells per well in 24-well plates onto Matrigel (354234; Corning) as previously described (Lee et al. 2007) and imaged using a Zeiss Axio Vert.A1 inverted confocal microscope after nine days. Alternatively, cells were plated at 20,000 cells per well in 24-well on ultra-low-attachment plates (Corning) in DMEM F12 supplemented with 1X B27 (17504044; Life Technologies), 20ng/mL EGF (GF144; EMD Millipore) and 20ng/mL bFGF (13256029; Life Technologies) and imaged after 5-18 days with 200 μ L fresh media added every five days.

Constructs

cDNA encoding C-terminal 3xFlag tagged human GLI1, GLI2, GLI3 and GLI2 Δ N were purchased from Addgene (#84922, 84920, 84921, 17649 respectively) and cloned into pMSCV retroviral vector or pRetroX-Tight-Pur doxycycline-inducible vector (generously provided by Dr. Nabeel Bardeesy; Massachusetts General Hospital). Mouse Gli2 was generously provided by Dr. Ryan Corcoran (Massachusetts General Hospital). Gli-luciferase and *Renilla* reporters were gifts from Dr. Jeremy Reiter (UCSF).

Lentiviral-mediated knockdown

All shRNA were obtained from Sigma Aldrich in the pLKO vector and sequences are listed in Supplemental table S2. HEK293T cells were transfected with lentiviral or retroviral plasmids and packaging constructs using X-tremeGENE transfection (6365787001; Sigma Aldrich) reagent according to the manufacturer's instructions and as previously

described (Perera et al. 2015). Cells were infected with virus-containing media using Polybrene reagent (TR-1003-G; EMD Millipore) according to the manufacturer's instructions, and selected for 48 hrs in 2 μ g/mL of puromycin or blasticidin.

Luciferase reporter assay

Cells were plated at 100,000 cells per well in 12-well or 24-well plates and co-transfected with Gli-luciferase and *Renilla* luciferase plasmids using Lipofectamine 2000 (11668019; Life Technologies) according to the manufacturer's instructions. Cells were lysed and assayed for activity using the Dual-Luciferase Assay kit (E1960; Promega) 48hrs post transfection.

ELISA and exogenous ligand treatments

Secreted OPN in the supernatant of cultured cells was measured using the Human Osteopontin Quantikine ELISA kit (DOST00; R&D systems) according to manufacturers protocol. For experiments where exogenous ligand was added, recombinant human OPN (1433-OP-050/CF; R&D Systems) was added at 1 μ g/mL and cells assayed 2-3 days later.

Drug treatment

Cells were treated with 5 μ M of GANT61 (3191/10; R&D Systems) for 3-5 days prior to collection of RNA or protein lysates. Alternatively, iKRAS cells were plated at 150,000 cells with or without Dox (1 μ g/mL) in the presence or absence of 5 μ M GANT61 and RNA was collected 72hrs post plating.

Immunoblotting

Cells were lysed in ice-cold lysis buffer (150 mM NaCl, 20 mM Tris [pH 7.5], 1mM EDTA, 1mM EGTA, 1% Triton X-100, 2.5 mM sodium pyrophosphate, 1mM β -glycerophosphate, 1 mM sodium vanadate, and one tablet of Pierce Protease Inhibitor Tablets, EDTA Free [Fisher Scientific-A32965] per 10 mL). Samples were clarified by sonication and centrifugation. Protein content was measured using Pierce™ BCA Protein Assay Kit (Life Technologies-23227), and 15-50 μ g protein was resolved on 8%-15% protein gels using SDS-PAGE and transferred onto PVDF membranes (EMD Millipore-IPVH00010). Membranes were blocked in 5% non-fat dry milk (VWR-89406056) made up in Tris-buffered saline with 0.2% Tween 20 (TBS-T) prior to incubation with primary antibody overnight at 4°C in either 5% non-fat dry milk or 5% bovine serum albumin (BSA, Sigma Aldrich-A4503). Membranes were washed in TBS-T and developed after 45-minute incubation in species-specific horseradish peroxidase-conjugated secondary antibody and visualized using supersignal west pico chemiluminescent substrate (Fisher Scientific-34080), and imaged using the ChemiDoc™ XRS+ System (Biorad).

Immunofluorescence

Cells were plated on fibronectin-coated glass cover-slips at 100,000–300,000 cells per coverslip. Twelve-to-sixteen hours later, the slides were rinsed with PBS once and fixed for 15 min with 4% paraformaldehyde at room temperature prior to permeabilization with 0.1% Saponin for 5 min. Slides were incubated with primary antibody in 5% normal goat serum overnight at 4 degC, rinsed four times with PBS, and incubated with secondary antibodies produced in goat (diluted 1:400 in 5% normal goat serum) for 45min at room

temperature in the dark. Slides were mounted on glass slides using Vectashield (Vector Laboratories) and imaged on a Zeiss Laser Scanning Microscope (LSM) 710. Images were processed using ImageJ.

RNA isolation and quantitative RT-PCR

Total cellular RNA was extracted using the PureLink™ RNA Mini Kit (12183025; Thermo Fisher). Reverse transcription was performed using the iScript™ Reverse Transcription Supermix (1708841; Bio-Rad) followed by quantitative RT-PCR with iTaq™ Universal SYBR Green Supermix (1725122; Bio-Rad) using the CFX384 Touch™ Real Time PCR Detection System (BioRad). Results are presented as the mean of at least 3 technical replicates and are representative of at least n = 3 biological replicates. Primer sequences are listed in Supplemental table S2.

Generation of GLI2 and SPP1 knockout cell lines using CRISPR/Cas9

GLI2 and SPP1 knockouts in KP4 cells were generated using the RNP-electroporation method as previously described (Liang et al. 2015). One million KP4 cells were used per electroporation using the Amaxa 4D Nucleofector kit (V4XC-9064, Lonza). Guide RNA and Cas9 complexes were formed using 160µM crRNA annealed to 160µM tracrRNA (Dharmacon) and incubated with 40µM Cas9 protein (purchased from University of California, Berkeley). Cutting efficiency was assessed 48 hours post electroporation using PCR and sanger sequencing. GLI2 and SPP1 knockout was confirmed using quantitative RT-PCR, immunoblotting and ELISA after clonal expansion of single cells.

Guide RNA sequences 5'-3':

GLI2 exon 2 – TTTGGCTTCTTGCTTCTCGG

SPP1 exon 2 – GTATGGCACAGGTGATGCCT

PCR primer sequences 5'-3':

GLI2 exon 2 FW – GTGAAGGAGTGAGCGAACATGC

GLI2 exon 2 RV – TCTTCGCCCTCCATAAACCCAG

SPP1 exon 2 FW – GCAAATTTCCCTTTCCCTTGCC

SPP1 exon 2 RV – ACTGTGCTTGGTACTGGCCTAG

Chromatin Immunoprecipitation

293T cells were transiently transfected with GLI2-Flag and fixed with 1% formaldehyde for 15 minutes and quenched with 125mM glycine for 5 minutes. Cells were washed with cold PBS and collected as 10^7 cell pellets. Cells were resuspended in 500 μ L cold L1 buffer (50mM Tris pH 8.0, 2mM EDTA, 0.1% NP-40, 10% glycerol, 1mM PMSF, 1x Pierce Protease Inhibitor) on ice for 5 min, centrifuged and resuspended in 450 μ L cold SDS buffer (50mM Tris pH 8.0, 10mM EDTA, 1% SDS, 1mM PMSF, 1x Pierce Protease Inhibitor). Chromatin was sheared for 10 cycles using the Bioruptor Pico to obtain fragments of 200-500 base pairs, and diluted 1:10 in cold CHIP buffer (0.5% NP-40, 5mM EDTA, 200mM NaCl, 50 μ M Tris pH 8.0, 1mM PMSF). Diluted chromatin was pre-cleared with 100 μ L washed Protein A Dynabeads (Invitrogen) at 4°C for 1 hr then immunoprecipitated with Flag antibody (CST, 14793) or negative control Rabbit IgG (CST, 2729) at 4°C overnight. Immunocomplexes were recovered using 50 μ L washed Protein A Dynabeads at 4°C for 2 hr. Beads were washed two times in following buffers: 800 μ L Wash buffer (0.1% SDS, 1% NP-40, 2mM EDTA, 500mM NaCl, 20mM Tris pH

8.0, 1mM PMSF), LiCl buffer (0.1% SDS, 1% NP-40, 2mM EDTA, 0.5M LiCl, 20mM Tris pH 8.0, 1mM PMSF) then TE buffer (1mM EDTA, 10mM Tris pH 8.0) for 5 min each all on ice. Complexes were eluted by resuspending beads in 100 μ L 2% SDS in TE buffer then de-crosslinked overnight with 5 μ L NaCl at 65°C. Recovered DNA was PCR purified and analyzed using qPCR. Primers were used to amplify a region that contains a GLI binding site in the *SPP1* promoter (-2324 to -2316) as reported in Kijewska et al. 2017. Primers targeting the *ACTB* promoter served as a negative control while primers targeting a known GLI binding site in the *BCL2* promoter (-957 to -949) served as a positive control (Regl et al. 2004).

ChIP qPCR primer sequences 5'-3':

ACTB promoter FW – ATGCAGCGATCAGTGGCGT

ACTB promoter RV – TCCAGCTTCTTGTCAACACCTC

BCL2 promoter FW – CCGGACGCGCCCTCCC

BCL2 promoter RV – GGTGCCTGTCCTCTTACTTCATTCTC

SPP1 promoter FW – CTGACAGAAAATCCTACTCAGAAAA

SPP1 promoter RV – AAAGTAGGAAATGGATGCTGCG

Subcutaneous and tail vein injections

For xenograft experiments, 4 million KP4 Cas9 control, GLI2^{KO}, or SPP1^{KO} cells were injected into the flank of *NOD.SCID-II2rg^{-/-}* (NSG) immunodeficient mice, and tumor volumes were measured using a caliper and calculated as tumor volume = $\frac{1}{2}$ (length x width²). For tail vein injections, 2 million cells were injected into the tail vein of NSG mice. End point criteria included poor body condition and weight loss. Sample sizes for *in vivo*

experiments were calculated using an online tool (<http://www.bu.edu/orcccommittees/iacuc/policies-and-guidelines/sample-size-calculations/>), taking into account variability of the assays and inter-individual differences within groups. In summary, we will use 8-10 mice per cohort (male and female) which provides statistical power of >0.8 ($\alpha=0.05$) to detect differences of approximately 50%, assuming a normal distribution.

Histology and immunostaining

Tissue samples were fixed overnight in 10% formalin, and then embedded in paraffin and sectioned (5 mm thickness) by the UCSF mouse histopathology core. Haematoxylin and eosin staining was performed using standard methods. Slides were baked at 60°C for an hour, deparaffinized in xylenes (three treatments, 5 min each), rehydrated sequentially in ethanol (5 min in 100%, 5 min in 90%, 5 min in 70%, 5 min in 50%, and 5 min in 30%), and washed for 5 min in water twice. For antigen unmasking, specimens were cooked in a 10 mM sodium citrate buffer (pH 6.0) for 10 min at 95°C using conventional pressure cooker, rinsed three times with PBS, incubated for 1 hr with 1% H₂O₂ at room temperature to block endogenous peroxidase activity, washed three times with PBS, and blocked with 2.5% goat serum in PBS for 1 hr. Primary antibodies were diluted in blocking solution as follows: anti-S100A2 (abcam, ab109494) 1:200; anti-GATA6 (CST, 5851) 1:500 and incubated with the tissue sections at 4°C overnight. Specimens were then washed three times for 5 min each in PBS and incubated with secondary anti-mouse/rabbit IgG (Vector Laboratories, MP-7500) for 1 hr at room temperature. Following 3 washes in PBS, slides were stained for peroxidase for 3 min with the DAB (di-aminebenzidine) substrate kit (SK-

4100, Vector Laboratories), washed with water and counterstained with hematoxylin. Stained slides were photographed with a KEYENCE BZ-X710 microscope.

RNAseq and GSEA

RNA sequencing data containing gene expression values from pancreatic ductal adenocarcinoma samples sequenced as part of the TCGA project was downloaded from the cBioPortal (<http://www.cbioportal.org/index.do>). The data are represented as z scores where zero represents the mean value of normalized and log transformed gene expression for samples diploid at that locus in the sample set, and a z score of one corresponding to expression one standard deviation above the mean. A subset of tumors corresponding to those with levels of *GLI2* expression that were high (z score > 0.5; n = 51) or low (z score < -0.5; n = 41) were then analyzed for their corresponding gene expression values of the ligands *IHH* or *SHH* (Figure 2.2 E). Assignment of PDA TCGA samples as classical or basal-like and extent of tumor cellularity was based on an independently published study (Cancer Genome Atlas Research 2017). Overall survival (OS) was defined as the time of surgery to the date of death from any cause. Disease-free survival (DFS) was defined as the date of surgery to the date of tumor recurrence at any site or to the date of last follow-up. Parameters for determining OS and DFS were defined as z score > -1 for *GLI2* high status, z score > 2 for *SHH* high status (Figure 2.1 D,E) and z score > 0.5 for *SPP1* high status (Figure 2.14 K). OS and DFS were analyzed using Kaplan–Meier and log-rank tests. Significance was determined as a *P* value < 0.05.

Data for the YAPC-iEV and YAPC-iGLI2 cells in Figure 2.5 D was processed using a standard RNA-seq pipeline that used Trimmomatic to clip and trim the reads, tophat2

to align the reads to hg19, and cuffdiff to calculate differential expression. GSEA (<http://www.broadinstitute.org/gsea/index.jsp>) of the expression data was used to assess enrichment of the epithelial-to-mesenchymal gene signature. The Moffitt (Moffitt et al. 2015) basal-like gene signature was used to assign basal-like status. For the classical signature a combination of genes from the Collisson classical (Collisson et al. 2011), Moffitt classical (Moffitt et al. 2015) and Bailey progenitor (Bailey et al. 2016b) signatures were used (See Table 2.2).

Image and statistical analysis

Image analysis, including densitometry and spheroid quantification was conducted using Image J software (NIH). Statistical analyses of results are expressed as mean +/- standard deviation unless otherwise indicated. For each box-and-whisker plot, center line is the median and whiskers represent the minimum and maximum values. Significance was analyzed using two-tailed Student's t-test and Log-rank (Mantel-Cox) test for survival data. A P value of less than 0.05 was considered statistically significant. Graphing and statistical analyses were performed with GraphPad Prism 7 software. All experiments were performed at least 3 times or in at least 2 separate cell lines. Data is displayed as either representative or the average of 2-4 independent biological replicates with at least 3 technical replicates per experiment.

Correlations between demographic and clinical factor variables and the genes of interest, GLI2 and SHH were performed. Correlations were stratified based on expression levels (previously defined with z score thresholds). Significance was analyzed using a Chi squared test for categorical variables (sex, TNM staging), Fisher's exact test for

dichotomous categorical variables (GLI2 and SHH expression), and a two-sample t-test for continuous variables (age and mutation count). A p-value < 0.05 was considered a statistically significant association.

Cox proportional hazards survival analysis regression models were used to identify demographic and clinical factors with significant predictive value for the outcomes of overall survival and progression free survival. Factors included in the analysis were age at diagnosis, sex, TNM staging, mutation count, and GLI2 and SHH expression levels previously defined based on z-scores. Unstratified models and models stratified based on GLI2 and SHH expression levels were performed. A p-value <.05 was considered a statistically significant association. Differences in sample sizes (n) attributed to missing clinical data. These analyses and figures were generated using R statistical software.

Acknowledgements:

We thank E Collisson, L Selleri, D Raleigh and R Zoncu for advice and helpful comments on the manuscript and F Kottakis and J Yano for bioinformatics and technical support, respectively. RMP is the Nadia's Gift Foundation Innovator of the Damon Runyon Cancer Research Foundation (DRR-46-17). This work is additionally supported by an NIH Director's New Innovator Award (1DP2CA216364) and Pancreatic Cancer Action Network Career Development Award to R Perera and a National Science Foundation Graduate Research Fellowship and an NIH F31 Ruth L Kirschstein National Research Service Award to C Adams.

CHAPTER 3

Mechanisms of cell plasticity: implications for pancreatic cancer subtypes and treatment options

DISCUSSION

While the clinical relevance of PDA subtypes is becoming increasingly appreciated, a mechanistic understanding of the molecular underpinnings of PDA subtype identity is lacking. Our findings establish a broad equivalence between basal-like and EMT-high, versus classical and EMT-low states of PDA. Moreover, we have identified a novel role for the GLI2 transcription factor as a central driver for promoting and maintaining the basal-like state in PDA. We found that high GLI2 status independently predicts shortened survival of PDA patients and correlates with the aggressive basal-like subtype of PDA. In contrast, high levels of Hh ligands correlate with longer patient survival and are associated with the classical subtype of PDA. These findings highlight a remarkable rewiring of the Hh signaling pathway in PDA, whereby expression of Hh ligands and GLI proteins trend towards mutual exclusivity and instead correlate with classical and basal-like subtypes, respectively (**Figure 2.14 L**).

Importantly, GLI2 is required for maintaining the basal-like state as GLI2 knockdown in tumor derived human and mouse PDA cell lines suppresses the basal-like program *in vitro*, attenuating expression of mesenchymal and stem cell markers. Conversely, forced expression of GLI2 in classical subtype cells was sufficient to induce a switch to a basal-like phenotype. Thus, GLI2 has critical functions in promoting and maintaining the basal-like phenotype and conferring enhanced plasticity to PDA cells by enabling interconversion between subtype states.

Mechanistically, our findings indicate that GLI2 induced a broad transcriptional program in PDA with a particular enrichment in EMT genes. Within this program we

identified several secreted proteins including OPN, which are induced following forced GLI2 expression in classical subtype cells. Accordingly, basal-like PDA cells express higher levels of OPN and several of its known receptors, including CD44 and integrin β 3. Our studies also suggest that OPN, like GLI2, is a key determinant of cellular reprogramming. As with GLI2, CRISPR mediated knockout of OPN in basal-like cells led to a failure to maintain the basal-like state and induced a classical subtype switch. Importantly, loss of OPN in basal-like PDA cells completely suppressed primary and metastatic tumor growth indicating that maintenance of the basal-like state is required for facilitating rapid *in vivo* tumor growth.

Notably, OPN has been linked to aggressive disease features including increased stemness, migration, EMT and drug resistance in several other cancer settings (Rangaswami et al. 2006; Orian-Rousseau 2010; Das et al. 2013; Wang et al. 2015; Zhao et al. 2018). In the context of PDA, early studies showed that OPN was over-expressed in patient tumors and could promote the growth of PDA cells (Koopmann et al. 2004; Kolb et al. 2005). Subsequent studies measuring serum OPN have suggested that elevated levels can distinguish PDA from chronic pancreatitis and healthy control subjects (Koopmann et al. 2004; Poruk et al. 2013; Cao et al. 2018). Whether OPN can serve as a faithful diagnostic and/or prognostic biomarker of aggressive disease and more specifically, the basal-like subtype will be an important future direction. Our data also shows that exogenous OPN can drive a classical to basal-like subtype switch. This finding suggests the intriguing possibility that GLI2-dependent induction of secreted factors may serve as a juxtacrine or paracrine mechanism to instruct neighboring tumor cells to establish and/or sustain a basal-like cell state. Tumor associated stromal cells in PDA

such as activated macrophages (Koopmann et al. 2004) and pancreatic stellate cells (Cao et al. 2018) can also secrete OPN and therefore potentially promote a basal-like switch. Similarly, in other tumor models such as glioblastoma multiforme and bladder cancer, infiltrating macrophage-secreted OPN can promote and sustain tumor cell growth, invasion, and stimulate angiogenesis (Ahmed et al. 2016; Chen et al. 2019). Tumor-cell derived OPN has also been reported to act in a paracrine fashion on normal mammary fibroblasts to promote an activated CAF phenotype in breast tumors (Sharon et al. 2015). Thus, the ability to locally reprogram neighboring epithelial or stromal cells to a more aggressive cell state may contribute to disease progression. In contrast to OPN, tumor derived SHH is associated with the classical subtype of PDA and was shown to restrain tumor growth (Lee et al. 2014; Mathew et al. 2014; Rhim et al. 2014; Liu et al. 2016). Recent studies in bladder cancer suggest that secreted SHH functions to activate the release of stromal derived paracrine cues that promote epithelial differentiation of tumor cells (Shin et al. 2014). Consistent with this finding, our data in PDA show that high SHH levels correlate with the well-differentiated classical subtype of PDA and longer disease-free survival of PDA patients. Taken together, these findings indicate opposite effects of OPN and SHH on PDA differentiation status and growth and suggest a potential hierarchy between secreted cues may help to establish subtype identity in PDA.

Recent studies have established that PDA subtypes have distinct epigenetic landscapes that underlie their specific transcriptional signatures (Lomberk et al. 2016; Andricovich et al. 2018; Lomberk et al. 2018; Somerville et al. 2018). Of note, specific chromatin states were linked to pathways known to be dysregulated during pancreatic carcinogenesis, including the hedgehog pathway. Interestingly, *SMO* and *PTCH1*

appeared strongly inhibited by the presence of repressive marks over their promoters and gene bodies, while *SHH* was identified as being significantly activated by epigenetic alterations in classical subtype samples, consistent with our analysis that *GLI2* appears to be regulated independent of *SMO* activation and that *SHH* expression marks the classical subtype (Lomberk et al. 2018). Interestingly, this study showed the basal-like subtype to be associated with only a few super-enhancers (30) compared to those identified in the classical subtype (250), and no basal-like specific transcription factors were identified (Lomberk et al. 2018). However, *MET*, the hepatocyte growth factor receptor, was associated with the regulation of basal-like super-enhancers, while *MYC*, *MYBL1*, *E2F1* and *SNAI2*, transcription factors involved in proliferation and EMT, were identified as acting downstream of *MET* (Lomberk et al. 2018). One explanation for the apparent absence of basal-like specific transcription factors could be the small sample size of 24 patient derived tumor xenografts (PDTX) used in this study, and of those only 6 were identified as being basal-like. Therefore, a more extensive analysis is required to accurately parse out how epigenetic components define the basal-like subtype, and how *GLI2* is integrated in these gene networks.

Other studies have identified *TP63* as an important mediator of enhancer reprogramming in a subset of basal-like/squamous PDA, consistent with this transcription factor functioning as a master regulator of squamous differentiation (Andricovich et al. 2018; Somerville et al. 2018). These findings suggest the intriguing possibility that multiple molecular drivers exist to define the aggressive basal-like subtype, and that a subset driven by *TP63* present with a particularly squamous-like phenotype. Indeed, Somerville et al. identified only two human PDA cell lines that expressed p63 isoforms,

where MiaPaca cells expressed the tumor-suppressive TAp63 variant while BXPC3 cells expressed the oncogenic Δ Np63 isoform. We verified that TAp63 is expressed in MiaPaca and additionally in Panc1 cells and found Panc0327 cells to be the only KRAS mutant cell line to express the pro-tumorigenic Δ Np63 (data not shown). Collectively, these findings suggest that TP63 may mediate squamous differentiation in a portion of basal-like PDA tumors. Whether GLI2 overlaps with TP63 function in basal-like/squamous samples remains unknown and highlights the possibility that multiple drivers may coordinately promote EMT and squamous differentiation to promote an aggressive basal-like state. Future work is required to comprehensively identify all potential subsets of basal-like identity that are driven by particular epigenetic states or transcriptional drivers. Whether these subsets of basal-like tumors are differentially affected by various chemotherapeutic regimens or targeted therapies also remains to be investigated. Overall, the impact of GLI2 on chromatin states and the specific interplay between GLI2 and other transcription factors and epigenetic regulators will be important to address in future studies to fully decipher the circuitry driving subtype switching in PDA.

The ability of cancer cells to adaptively interconvert between states that rely on different molecular circuits to support growth and survival provides a potential mechanism for treatment failure and tumor relapse (Polyak and Weinberg 2009). Recently, GLI transcription factors were shown to directly promote SOX2 transcription in PDA cell lines, which promoted resistance to gemcitabine. Depletion of GLI-SOX2 signaling re-sensitized resistant cells to gemcitabine treatment (Jia et al. 2019), providing further evidence that targeting GLI2-mediated signaling could be advantageous in aggressive PDA tumors. In addition to PDA, a prior study has linked elevated GLI expression to

resistance to therapy in patients with acute myeloid leukemia (AML) (Zahreddine et al. 2014). Reciprocally, switching off GLI activity in basal cell carcinoma of the skin was associated with a cell identity switch involving induction of GATA6 (Biehs et al. 2018). Overall, these studies suggest that GLI2-driven subtype switching facilitates therapeutic resistance or bypass of oncogene addiction and may have additional relevance in other cancers. Our data indicates that activation of a GLI-OPN circuit is a novel mechanism of acquired resistance to KRAS* inhibition. Upon KRAS* loss, GLI2 is induced and substitutes for KRAS* suppression by promoting a basal-like switch. A prediction based on these observations is that cells with pre-existing high GLI activity would show intrinsic resistance to KRAS* inhibition and potentially other oncogenic drivers. As strategies to target oncogenic KRAS are currently in development, co-targeting of GLI – and/or OPN in PDA - may be necessary to achieve durable therapeutic responses.

In conclusion, we have identified a high level of intrinsic plasticity between PDA subtypes mediated by GLI proteins and uncovered a surprising and unconventional role for these transcription factors in maintenance of the basal-like state. Blocking the ability of tumor cells to dynamically switch between cell states via inhibition of GLI proteins, OPN and other master regulators of cellular plasticity (Andricovich et al. 2018; Somerville et al. 2018) will be an important future direction in combating intrinsic and acquired resistance to therapy in PDA and other cancers. Our work also raises the possibility of using the unique susceptibilities that may exist in PDA subtypes to treat patients with appropriate therapeutic regimens. The ability to effectively stratify patients based on subtype to uncover unique vulnerabilities to known drugs has not been performed and remains an exciting and critical next step in improving survival outcomes of PDA patients.

References:

- Ahmed M, Sottnik JL, Dancik GM, Sahu D, Hansel DE, Theodorescu D, Schwartz MA. 2016. An Osteopontin/CD44 Axis in RhoGDI2-Mediated Metastasis Suppression. *Cancer Cell* **30**: 432-443.
- Aiello NM, Brabletz T, Kang Y, Nieto MA, Weinberg RA, Stanger BZ. 2017. Upholding a role for EMT in pancreatic cancer metastasis. *Nature* **547**: E7-E8.
- Aiello NM, Maddipati R, Norgard RJ, Balli D, Li J, Yuan S, Yamazoe T, Black T, Sahmoud A, Furth EE et al. 2018. EMT Subtype Influences Epithelial Plasticity and Mode of Cell Migration. *Dev Cell* **45**: 681-695 e684.
- Alexaki VI, Javelaud D, Van Kempen LC, Mohammad KS, Dennler S, Luciani F, Hoek KS, Juarez P, Goydos JS, Fournier PJ et al. 2010. GLI2-mediated melanoma invasion and metastasis. *J Natl Cancer Inst* **102**: 1148-1159.
- Alizadeh AA, Eisen MB, Davis RE, Ma C, Lossos IS, Rosenwald A, Boldrick JC, Sabet H, Tran T, Yu X et al. 2000. Distinct types of diffuse large B-cell lymphoma identified by gene expression profiling. *Nature* **403**: 503-511.
- Andricovich J, Perkail S, Kai Y, Casasanta N, Peng W, Tzatsos A. 2018. Loss of KDM6A Activates Super-Enhancers to Induce Gender-Specific Squamous-like Pancreatic Cancer and Confers Sensitivity to BET Inhibitors. *Cancer Cell* **33**: 512-526 e518.
- Auciello FR, Bulusu V, Oon C, Tait-Mulder J, Berry M, Bhattacharyya S, Tumanov S, Allen-Petersen BL, Link J, Kendsersky ND et al. 2019. A Stromal Lysolipid-Autotaxin Signaling Axis Promotes Pancreatic Tumor Progression. *Cancer Discov* **9**: 617-627.

Aung KL, Fischer SE, Denroche RE, Jang GH, Dodd A, Creighton S, Southwood B, Liang SB, Chadwick D, Zhang A et al. 2018. Genomics-Driven Precision Medicine for Advanced Pancreatic Cancer: Early Results from the COMPASS Trial. *Clin Cancer Res* **24**: 1344-1354.

Bailey JM, Hendley AM, Lafaro KJ, Pruski MA, Jones NC, Alsina J, Younes M, Maitra A, McAllister F, Iacobuzio-Donahue CA et al. 2016a. p53 mutations cooperate with oncogenic Kras to promote adenocarcinoma from pancreatic ductal cells. *Oncogene* **35**: 4282-4288.

Bailey P Chang DK Nones K Johns AL Patch AM Gingras MC Miller DK Christ AN Bruxner TJ Quinn MC et al. 2016b. Genomic analyses identify molecular subtypes of pancreatic cancer. *Nature* **531**: 47-52.

Berman DM, Karhadkar SS, Maitra A, Montes De Oca R, Gerstenblith MR, Briggs K, Parker AR, Shimada Y, Eshleman JR, Watkins DN et al. 2003. Widespread requirement for Hedgehog ligand stimulation in growth of digestive tract tumours. *Nature* **425**: 846-851.

Biankin AV Waddell N Kassahn KS Gingras MC Muthuswamy LB Johns AL Miller DK Wilson PJ Patch AM Wu J et al. 2012. Pancreatic cancer genomes reveal aberrations in axon guidance pathway genes. *Nature* **491**: 399-405.

Biehs B, Dijkgraaf GJP, Piskol R, Alicke B, Boumahdi S, Peale F, Gould SE, de Sauvage FJ. 2018. A cell identity switch allows residual BCC to survive Hedgehog pathway inhibition. *Nature* **562**: 429-433.

Black PC, Brown GA, Inamoto T, Shrader M, Arora A, Siefker-Radtke AO, Adam L, Theodorescu D, Wu X, Munsell MF et al. 2008. Sensitivity to epidermal growth factor

receptor inhibitor requires E-cadherin expression in urothelial carcinoma cells. *Clin Cancer Res* **14**: 1478-1486.

Boj SF, Hwang CI, Baker LA, Chio, II, Engle DD, Corbo V, Jager M, Ponz-Sarvise M, Tiriac H, Spector MS et al. 2015. Organoid models of human and mouse ductal pancreatic cancer. *Cell* **160**: 324-338.

Byers LA, Diao L, Wang J, Saintigny P, Girard L, Peyton M, Shen L, Fan Y, Giri U, Tumula PK et al. 2013. An epithelial-mesenchymal transition gene signature predicts resistance to EGFR and PI3K inhibitors and identifies Axl as a therapeutic target for overcoming EGFR inhibitor resistance. *Clin Cancer Res* **19**: 279-290.

Cancer Genome Atlas Research N. 2014. Comprehensive molecular characterization of urothelial bladder carcinoma. *Nature* **507**: 315-322.

- . 2017. Integrated Genomic Characterization of Pancreatic Ductal Adenocarcinoma. *Cancer Cell* **32**: 185-203 e113.

Cao J, Li J, Sun L, Qin T, Xiao Y, Chen K, Qian W, Duan W, Lei J, Ma J et al. 2018. Hypoxia-driven paracrine osteopontin/integrin alphavbeta3 signaling promotes pancreatic cancer cell epithelial-mesenchymal transition and cancer stem cell-like properties by modulating forkhead box protein M1. *Mol Oncol*.

Catenacci DV, Junttila MR, Karrison T, Bahary N, Horiba MN, Nattam SR, Marsh R, Wallace J, Kozloff M, Rajdev L et al. 2015. Randomized Phase Ib/II Study of Gemcitabine Plus Placebo or Vismodegib, a Hedgehog Pathway Inhibitor, in Patients With Metastatic Pancreatic Cancer. *J Clin Oncol* **33**: 4284-4292.

- Chen P, Zhao D, Li J, Liang X, Li J, Chang A, Henry VK, Lan Z, Spring DJ, Rao G et al. 2019. Symbiotic Macrophage-Glioma Cell Interactions Reveal Synthetic Lethality in PTEN-Null Glioma. *Cancer Cell* **35**: 868-884 e866.
- Collisson EA, Bailey P, Chang DK, Biankin AV. 2019. Molecular subtypes of pancreatic cancer. *Nat Rev Gastroenterol Hepatol* **16**: 207-220.
- Collisson EA, Sadanandam A, Olson P, Gibb WJ, Truitt M, Gu S, Cooc J, Weinkle J, Kim GE, Jakkula L et al. 2011. Subtypes of pancreatic ductal adenocarcinoma and their differing responses to therapy. *Nat Med* **17**: 500-503.
- Curtis C, Shah SP, Chin SF, Turashvili G, Rueda OM, Dunning MJ, Speed D, Lynch AG, Samarajiwa S, Yuan Y et al. 2012. The genomic and transcriptomic architecture of 2,000 breast tumours reveals novel subgroups. *Nature* **486**: 346-352.
- Dallas NA, Xia L, Fan F, Gray MJ, Gaur P, van Buren G, 2nd, Samuel S, Kim MP, Lim SJ, Ellis LM. 2009. Chemoresistant colorectal cancer cells, the cancer stem cell phenotype, and increased sensitivity to insulin-like growth factor-I receptor inhibition. *Cancer Res* **69**: 1951-1957.
- Damrauer JS, Hoadley KA, Chism DD, Fan C, Tiganelli CJ, Wobker SE, Yeh JJ, Milowsky MI, Iyer G, Parker JS et al. 2014. Intrinsic subtypes of high-grade bladder cancer reflect the hallmarks of breast cancer biology. *Proc Natl Acad Sci U S A* **111**: 3110-3115.
- Das S, Harris LG, Metge BJ, Liu S, Riker AI, Samant RS, Shevde LA. 2009. The hedgehog pathway transcription factor GLI1 promotes malignant behavior of cancer cells by up-regulating osteopontin. *J Biol Chem* **284**: 22888-22897.

- Das S, Samant RS, Shevde LA. 2013. Nonclassical activation of Hedgehog signaling enhances multidrug resistance and makes cancer cells refractory to Smoothed-tubulin-targeting Hedgehog inhibition. *J Biol Chem* **288**: 11824-11833.
- De Sousa EMF, Wang X, Jansen M, Fessler E, Trinh A, de Rooij LP, de Jong JH, de Boer OJ, van Leersum R, Bijlsma MF et al. 2013. Poor-prognosis colon cancer is defined by a molecularly distinct subtype and develops from serrated precursor lesions. *Nat Med* **19**: 614-618.
- Dennler S, Andre J, Alexaki I, Li A, Magnaldo T, ten Dijke P, Wang XJ, Verrecchia F, Mauviel A. 2007. Induction of sonic hedgehog mediators by transforming growth factor-beta: Smad3-dependent activation of Gli2 and Gli1 expression in vitro and in vivo. *Cancer Res* **67**: 6981-6986.
- Frederick BA, Helfrich BA, Coldren CD, Zheng D, Chan D, Bunn PA, Jr., Raben D. 2007. Epithelial to mesenchymal transition predicts gefitinib resistance in cell lines of head and neck squamous cell carcinoma and non-small cell lung carcinoma. *Mol Cancer Ther* **6**: 1683-1691.
- Genovese G, Carugo A, Tepper J, Robinson FS, Li L, Svelto M, Nezi L, Corti D, Minelli R, Pettazzoni P et al. 2017. Synthetic vulnerabilities of mesenchymal subpopulations in pancreatic cancer. *Nature* **542**: 362-366.
- Gidekel Friedlander SY, Chu GC, Snyder EL, Girnius N, Dibelius G, Crowley D, Vasile E, DePinho RA, Jacks T. 2009. Context-dependent transformation of adult pancreatic cells by oncogenic K-Ras. *Cancer Cell* **16**: 379-389.

- Groger CJ, Grubinger M, Waldhor T, Vierlinger K, Mikulits W. 2012. Meta-analysis of gene expression signatures defining the epithelial to mesenchymal transition during cancer progression. *PLoS One* **7**: e51136.
- Habbe N, Shi G, Meguid RA, Fendrich V, Esni F, Chen H, Feldmann G, Stoffers DA, Konieczny SF, Leach SD et al. 2008. Spontaneous induction of murine pancreatic intraepithelial neoplasia (mPanIN) by acinar cell targeting of oncogenic Kras in adult mice. *Proc Natl Acad Sci U S A* **105**: 18913-18918.
- Han B, Qu Y, Jin Y, Yu Y, Deng N, Wawrowsky K, Zhang X, Li N, Bose S, Wang Q et al. 2015. FOXC1 Activates Smoothed-Independent Hedgehog Signaling in Basal-like Breast Cancer. *Cell Rep* **13**: 1046-1058.
- Hruban RH, Adsay NV, Albores-Saavedra J, Anver MR, Biankin AV, Boivin GP, Furth EE, Furukawa T, Klein A, Klimstra DS et al. 2006. Pathology of genetically engineered mouse models of pancreatic exocrine cancer: consensus report and recommendations. *Cancer Res* **66**: 95-106.
- Hruban RH, Takaori K, Klimstra DS, Adsay NV, Albores-Saavedra J, Biankin AV, Biankin SA, Compton C, Fukushima N, Furukawa T et al. 2004. An Illustrated Consensus on the Classification of Pancreatic Intraepithelial Neoplasia and Intraductal Papillary Mucinous Neoplasms. *Am J Surg Pathol* **28**: 977-987.
- Huang L, Holtzinger A, Jagan I, BeGora M, Lohse I, Ngai N, Nostro C, Wang R, Muthuswamy LB, Crawford HC et al. 2015. Ductal pancreatic cancer modeling and drug screening using human pluripotent stem cell- and patient-derived tumor organoids. *Nat Med* **21**: 1364-1371.

Huang RY, Wong MK, Tan TZ, Kuay KT, Ng AH, Chung VY, Chu YS, Matsumura N, Lai HC, Lee YF et al. 2013. An EMT spectrum defines an anoikis-resistant and spheroidogenic intermediate mesenchymal state that is sensitive to e-cadherin restoration by a src-kinase inhibitor, saracatinib (AZD0530). *Cell Death Dis* **4**: e915.

Hui CC, Angers S. 2011. Gli proteins in development and disease. *Annu Rev Cell Dev Biol* **27**: 513-537.

Janes MR, Zhang J, Li LS, Hansen R, Peters U, Guo X, Chen Y, Babbar A, Firdaus SJ, Darjania L et al. 2018. Targeting KRAS Mutant Cancers with a Covalent G12C-Specific Inhibitor. *Cell* **172**: 578-589 e517.

Ji Z, Mei FC, Xie J, Cheng X. 2007. Oncogenic KRAS activates hedgehog signaling pathway in pancreatic cancer cells. *J Biol Chem* **282**: 14048-14055.

Jia Y, Gu D, Wan J, Yu B, Zhang X, Chiorean EG, Wang Y, Xie J. 2019. The role of GLI-SOX2 signaling axis for gemcitabine resistance in pancreatic cancer. *Oncogene* **38**: 1764-1777.

Jones S, Zhang X, Parsons DW, Lin JC, Leary RJ, Angenendt P, Mankoo P, Carter H, Kamiyama H, Jimeno A et al. 2008. Core signaling pathways in human pancreatic cancers revealed by global genomic analyses. *Science* **321**: 1801-1806.

Jordan NV, Johnson GL, Abell AN. 2011. Tracking the intermediate stages of epithelial-mesenchymal transition in epithelial stem cells and cancer. *Cell Cycle* **10**: 2865-2873.

Jordan VC. 2003. Tamoxifen: a most unlikely pioneering medicine. *Nat Rev Drug Discov* **2**: 205-213.

Kapoor A, Yao W, Ying H, Hua S, Liewen A, Wang Q, Zhong Y, Wu CJ, Sadanandam A, Hu B et al. 2014. Yap1 activation enables bypass of oncogenic Kras addiction in pancreatic cancer. *Cell* **158**: 185-197.

Kemper K, de Goeje PL, Peeper DS, van Amerongen R. 2014. Phenotype switching: tumor cell plasticity as a resistance mechanism and target for therapy. *Cancer Res* **74**: 5937-5941.

Kijewska M, Kocyk M, Kloss M, Stepniak K, Korwek Z, Polakowska R, Dabrowski M, Gieryng A, Wojtas B, Ciechomska IA et al. 2017. The embryonic type of SPP1 transcriptional regulation is re-activated in glioblastoma. *Oncotarget* **8**: 16340-16355.

Kolb A, Kleeff J, Guweidhi A, Esposito I, Giese NA, Adwan H, Giese T, Büchler MW, Berger MR, Friess H. 2005. Osteopontin influences the invasiveness of pancreatic cancer cells and is increased in neoplastic and inflammatory conditions. *Cancer Biology & Therapy* **4**: 740-746.

Konieczkowski DJ, Johannessen CM, Abudayyeh O, Kim JW, Cooper ZA, Piris A, Frederick DT, Barzily-Rokni M, Straussman R, Haq R et al. 2014. A melanoma cell state distinction influences sensitivity to MAPK pathway inhibitors. *Cancer Discov* **4**: 816-827.

Koopmann J, Fedarko NS, Jain A, Maitra A, Iacobuzio-Donahue C, Rahman A, Hruban RH, Yeo CJ, Goggins M. 2004. Evaluation of Osteopontin as Biomarker for Pancreatic Adenocarcinoma. *Cancer Epidemiol Biomarkers Prev* **13**: 487-491.

Kopp JL, von Figura G, Mayes E, Liu FF, Dubois CL, Morris JPt, Pan FC, Akiyama H, Wright CV, Jensen K et al. 2012. Identification of Sox9-dependent acinar-to-ductal

- reprogramming as the principal mechanism for initiation of pancreatic ductal adenocarcinoma. *Cancer Cell* **22**: 737-750.
- Kottakis F, Bardeesy N. 2015. Gene signatures from pancreatic cancer tumor and stromal cells predict disease outcome. *Nat Genet* **47**: 1102-1103.
- Krebs AM, Mitschke J, Lasierra Losada M, Schmalhofer O, Boerries M, Busch H, Boettcher M, Mougiakakos D, Reichardt W, Bronsert P et al. 2017. The EMT-activator Zeb1 is a key factor for cell plasticity and promotes metastasis in pancreatic cancer. *Nat Cell Biol* **19**: 518-529.
- Lafaro KJ, Melstrom LG. 2019. The Paradoxical Web of Pancreatic Cancer Tumor Microenvironment. *Am J Pathol* **189**: 44-57.
- Lambertini M, Ponde NF, Solinas C, de Azambuja E. 2017. Adjuvant trastuzumab: a 10-year overview of its benefit. *Expert Rev Anticancer Ther* **17**: 61-74.
- Lauth M, Bergstrom A, Shimokawa T, Toftgard R. 2007. Inhibition of GLI-mediated transcription and tumor cell growth by small-molecule antagonists. *Proc Natl Acad Sci U S A* **104**: 8455-8460.
- Lee GY, Kenny PA, Lee EH, Bissell MJ. 2007. Three-dimensional culture models of normal and malignant breast epithelial cells. *Nat Methods* **4**: 359-365.
- Lee JJ, Perera RM, Wang H, Wu DC, Liu XS, Han S, Fitamant J, Jones PD, Ghanta KS, Kawano S et al. 2014. Stromal response to Hedgehog signaling restrains pancreatic cancer progression. *Proc Natl Acad Sci U S A* **111**: E3091-3100.
- Liang X, Potter J, Kumar S, Zou Y, Quintanilla R, Sridharan M, Carte J, Chen W, Roark N, Ranganathan S et al. 2015. Rapid and highly efficient mammalian cell engineering via Cas9 protein transfection. *J Biotechnol* **208**: 44-53.

- Liu X, Pitarresi JR, Cuitino MC, Kladney RD, Woelke SA, Sizemore GM, Nayak SG, Egriboz O, Schweickert PG, Yu L et al. 2016. Genetic ablation of Smoothed in pancreatic fibroblasts increases acinar-ductal metaplasia. *Genes Dev* **30**: 1943-1955.
- Lomberk G, Blum Y, Nicolle R, Nair A, Gaonkar KS, Marisa L, Mathison A, Sun Z, Yan H, Elarouci N et al. 2018. Distinct epigenetic landscapes underlie the pathobiology of pancreatic cancer subtypes. *Nat Commun* **9**: 1978.
- Lomberk GA, Iovanna J, Urrutia R. 2016. The promise of epigenomic therapeutics in pancreatic cancer. *Epigenomics* **8**: 831-842.
- Lou K, Steri V, Ge AY, Hwang YC, Yogodzinski CH, Shkedi AR, Choi ALM, Mitchell DC, Swaney DL, Hann B et al. 2019. KRASG12C inhibition produces a driver-limited state revealing collateral dependencies. *Sci Signal* **12**: 1-15.
- Marisa L, de Reynies A, Duval A, Selves J, Gaub MP, Vescovo L, Etienne-Grimaldi MC, Schiappa R, Guenot D, Ayadi M et al. 2013. Gene expression classification of colon cancer into molecular subtypes: characterization, validation, and prognostic value. *PLoS Med* **10**: e1001453.
- Martinelli P, Carrillo-de Santa Pau E, Cox T, Sainz B, Jr., Dusetti N, Greenhalf W, Rinaldi L, Costello E, Ghaneh P, Malats N et al. 2017. GATA6 regulates EMT and tumour dissemination, and is a marker of response to adjuvant chemotherapy in pancreatic cancer. *Gut* **66**: 1665-1676.
- Mathew E, Zhang Y, Holtz AM, Kane KT, Song JY, Allen BL, Pasca di Magliano M. 2014. Dosage-dependent regulation of pancreatic cancer growth and angiogenesis by hedgehog signaling. *Cell Rep* **9**: 484-494.

- Moffitt RA, Marayati R, Flate EL, Volmar KE, Loeza SG, Hoadley KA, Rashid NU, Williams LA, Eaton SC, Chung AH et al. 2015. Virtual microdissection identifies distinct tumor- and stroma-specific subtypes of pancreatic ductal adenocarcinoma. *Nat Genet* **47**: 1168-1178.
- Morris JP, Wang SC, Hebrok M. 2010. KRAS, Hedgehog, Wnt and the twisted developmental biology of pancreatic ductal adenocarcinoma. *Nature Reviews Cancer* **10**: 683-695.
- Neelakantan D, Zhou H, Oliphant MUJ, Zhang X, Simon LM, Henke DM, Shaw CA, Wu MF, Hilsenbeck SG, White LD et al. 2017. EMT cells increase breast cancer metastasis via paracrine GLI activation in neighbouring tumour cells. *Nat Commun* **8**: 15773.
- Nieto MA. 2013. Epithelial plasticity: a common theme in embryonic and cancer cells. *Science* **342**: 1234850.
- Nolan-Stevaux O, Lau J, Truitt ML, Chu GC, Hebrok M, Fernandez-Zapico ME, Hanahan D. 2009. GLI1 is regulated through Smoothed-independent mechanisms in neoplastic pancreatic ducts and mediates PDAC cell survival and transformation. *Genes Dev* **23**: 24-36.
- Olive KP, Jacobetz MA, Davidson CJ, Gopinathan A, McIntyre D, Honess D, Madhu B, Goldgraben MA, Caldwell ME, Allard D et al. 2009. Inhibition of Hedgehog Signaling Enhances Delivery of Chemotherapy in a Mouse Model of Pancreatic Cancer. *Science* **324**: 1457-1461.
- Orian-Rousseau V. 2010. CD44, a therapeutic target for metastasising tumours. *Eur J Cancer* **46**: 1271-1277.

- Oser MG, Niederst MJ, Sequist LV, Engelman JA. 2015. Transformation from non-small-cell lung cancer to small-cell lung cancer: molecular drivers and cells of origin. *The Lancet Oncology* **16**: e165-e172.
- Ostrem JM, Peters U, Sos ML, Wells JA, Shokat KM. 2013. K-Ras(G12C) inhibitors allosterically control GTP affinity and effector interactions. *Nature* **503**: 548-551.
- Ozdemir BC, Pentcheva-Hoang T, Carstens JL, Zheng X, Wu CC, Simpson TR, Laklai H, Sugimoto H, Kahlert C, Novitskiy SV et al. 2014. Depletion of carcinoma-associated fibroblasts and fibrosis induces immunosuppression and accelerates pancreas cancer with reduced survival. *Cancer Cell* **25**: 719-734.
- Parker JS, Mullins M, Cheang MC, Leung S, Voduc D, Vickery T, Davies S, Fauron C, He X, Hu Z et al. 2009. Supervised risk predictor of breast cancer based on intrinsic subtypes. *J Clin Oncol* **27**: 1160-1167.
- Pasca di Magliano M, Sekine S, Ermilov A, Ferris J, Dlugosz AA, Hebrok M. 2006. Hedgehog/Ras interactions regulate early stages of pancreatic cancer. *Genes Dev* **20**: 3161-3173.
- Patricelli MP, Janes MR, Li LS, Hansen R, Peters U, Kessler LV, Chen Y, Kucharski JM, Feng J, Ely T et al. 2016. Selective Inhibition of Oncogenic KRAS Output with Small Molecules Targeting the Inactive State. *Cancer Discovery* **6**: 316-329.
- Perera RM, Bardeesy N. 2015. Pancreatic Cancer Metabolism: Breaking It Down to Build It Back Up. *Cancer Discov* **5**: 1247-1261.
- Perera RM, Stoykova S, Nicolay BN, Ross KN, Fitamant J, Boukhali M, Lengrand J, Deshpande V, Selig MK, Ferrone CR et al. 2015. Transcriptional control of

- autophagy-lysosome function drives pancreatic cancer metabolism. *Nature* **524**: 361-365.
- Perou CM. 2010. Molecular Stratification of Triple-Negative Breast Cancers. *The Oncologist* **15**: 39-48.
- Perou CM, Sorlie T, Eisen MB, van de Rijn M, Jeffrey SS, Rees CA, Pollack JR, Ross DT, Johnsen H, Akslen LA et al. 2000. Molecular portraits of human breast tumours. *Nature* **406**: 747-752.
- Pietras A, Katz AM, Ekstrom EJ, Wee B, Halliday JJ, Pitter KL, Werbeck JL, Amankolor NM, Huse JT, Holland EC. 2014. Osteopontin-CD44 signaling in the glioma perivascular niche enhances cancer stem cell phenotypes and promotes aggressive tumor growth. *Cell Stem Cell* **14**: 357-369.
- Polyak K, Weinberg RA. 2009. Transitions between epithelial and mesenchymal states: acquisition of malignant and stem cell traits. *Nat Rev Cancer* **9**: 265-273.
- Poruk KE, Firpo MA, Scaife CL, Adler DG, Emerson LL, Boucher KM, Mulvihill SJ. 2013. Serum Osteopontin and Tissue Inhibitor of Metalloproteinase 1 as Diagnostic and Prognostic Biomarkers for Pancreatic Adenocarcinoma. *Pancreas* **42**: 193-197.
- Prasad NB, Biankin AV, Fukushima N, Maitra A, Dhara S, Elkahloun AG, Hruban RH, Goggins M, Leach SD. 2005. Gene expression profiles in pancreatic intraepithelial neoplasia reflect the effects of Hedgehog signaling on pancreatic ductal epithelial cells. *Cancer Res* **65**: 1619-1626.
- Provenzano PP, Cuevas C, Chang AE, Goel VK, Von Hoff DD, Hingorani SR. 2012. Enzymatic targeting of the stroma ablates physical barriers to treatment of pancreatic ductal adenocarcinoma. *Cancer Cell* **21**: 418-429.

- Rahib L, Smith BD, Aizenberg R, Rosenzweig AB, Fleshman JM, Matrisian LM. 2014. Projecting cancer incidence and deaths to 2030: the unexpected burden of thyroid, liver, and pancreas cancers in the United States. *Cancer Res* **74**: 2913-2921.
- Rajurkar M, De Jesus-Monge WE, Driscoll DR, Appleman VA, Huang H, Cotton JL, Klimstra DS, Zhu LJ, Simin K, Xu L et al. 2012. The activity of Gli transcription factors is essential for Kras-induced pancreatic tumorigenesis. *Proc Natl Acad Sci U S A* **109**: E1038-1047.
- Rangaswami H, Bulbule A, Kundu GC. 2006. Osteopontin: role in cell signaling and cancer progression. *Trends Cell Biol* **16**: 79-87.
- Regl G, Kasper M, Schnidar H, Eichberger T, Neill GW, Philpott MP, Esterbauer H, Hauser-Kronberger C, Frischauf A-M, Aberger F. 2004. Activation of the BCL2 Promoter in Response to Hedgehog/GLI Signal Transduction Is Predominantly Mediated by GLI2. *Cancer Research* **64**: 7724-7731.
- Reichert M, Bakir B, Moreira L, Pitarresi JR, Feldmann K, Simon L, Suzuki K, Maddipati R, Rhim AD, Schlitter AM et al. 2018. Regulation of Epithelial Plasticity Determines Metastatic Organotropism in Pancreatic Cancer. *Dev Cell* **45**: 696-711 e698.
- Rhim AD, Mirek ET, Aiello NM, Maitra A, Bailey JM, McAllister F, Reichert M, Beatty GL, Rustgi AK, Vonderheide RH et al. 2012. EMT and dissemination precede pancreatic tumor formation. *Cell* **148**: 349-361.
- Rhim AD, Oberstein PE, Thomas DH, Mirek ET, Palermo CF, Sastra SA, Dekleva EN, Saunders T, Becerra CP, Tattersall IW et al. 2014. Stromal elements act to restrain, rather than support, pancreatic ductal adenocarcinoma. *Cancer Cell* **25**: 735-747.

- Robbins DJ, Fei DL, Riobo NA. 2012. The Hedgehog signal transduction network. *Sci Signal* **5**: re6.
- Ryan DP, Hong TS, Bardeesy N. 2014. Pancreatic adenocarcinoma. *N Engl J Med* **371**: 1039-1049.
- Sadanandam A, Lyssiotis CA, Homicsko K, Collisson EA, Gibb WJ, Wullschleger S, Ostos LC, Lannon WA, Grotzinger C, Del Rio M et al. 2013. A colorectal cancer classification system that associates cellular phenotype and responses to therapy. *Nat Med* **19**: 619-625.
- Sasaki H, Hui C, Nakafuku M, Kondoh H. 1997. A binding site for Gli proteins is essential for HNF-3beta floor plate enhancer activity in transgenics and can respond to Shh in vitro. *Development* **124**: 1313-1322.
- Seino T, Kawasaki S, Shimokawa M, Tamagawa H, Toshimitsu K, Fujii M, Ohta Y, Matano M, Nanki K, Kawasaki K et al. 2018. Human Pancreatic Tumor Organoids Reveal Loss of Stem Cell Niche Factor Dependence during Disease Progression. *Cell Stem Cell* **22**: 454-467.e456.
- Sequist LV, Waltman BA, Dias-Santagata D, Digumarthy S, Turke AB, Fidias P, Bergethon K, Shaw AT, Gettinger S, Cospers AK et al. 2011. Genotypic and Histological Evolution of Lung Cancers Acquiring Resistance to EGFR Inhibitors. *Sci Transl Med* **3**: 75ra26.
- Shao DD, Xue W, Krall EB, Bhutkar A, Piccioni F, Wang X, Schinzel AC, Sood S, Rosenbluh J, Kim JW et al. 2014. KRAS and YAP1 converge to regulate EMT and tumor survival. *Cell* **158**: 171-184.

- Sharon Y, Raz Y, Cohen N, Ben-Shmuel A, Schwartz H, Geiger T, Erez N. 2015. Tumor-derived osteopontin reprograms normal mammary fibroblasts to promote inflammation and tumor growth in breast cancer. *Cancer Res* **75**: 963-973.
- Sherman MH, Yu RT, Engle DD, Ding N, Atkins AR, Tiriach H, Collisson EA, Connor F, Van Dyke T, Kozlov S et al. 2014. Vitamin D receptor-mediated stromal reprogramming suppresses pancreatitis and enhances pancreatic cancer therapy. *Cell* **159**: 80-93.
- Shibue T, Weinberg RA. 2017. EMT, CSCs, and drug resistance: the mechanistic link and clinical implications. *Nat Rev Clin Oncol* **14**: 611-629.
- Shin K, Lim A, Zhao C, Sahoo D, Pan Y, Spiekerkoetter E, Liao JC, Beachy PA. 2014. Hedgehog signaling restrains bladder cancer progression by eliciting stromal production of urothelial differentiation factors. *Cancer Cell* **26**: 521-533.
- Singh A, Greninger P, Rhodes D, Koopman L, Violette S, Bardeesy N, Settleman J. 2009. A gene expression signature associated with "K-Ras addiction" reveals regulators of EMT and tumor cell survival. *Cancer Cell* **15**: 489-500.
- Singh A, Settleman J. 2010. EMT, cancer stem cells and drug resistance: an emerging axis of evil in the war on cancer. *Oncogene* **29**: 4741-4751.
- Sipos B, Frank S, Gress T, Hahn S, Kloppel G. 2009. Pancreatic intraepithelial neoplasia revisited and updated. *Pancreatology* **9**: 45-54.
- Somerville TDD, Xu Y, Miyabayashi K, Tiriach H, Cleary CR, Maia-Silva D, Milazzo JP, Tuveson DA, Vakoc CR. 2018. TP63-Mediated Enhancer Reprogramming Drives the Squamous Subtype of Pancreatic Ductal Adenocarcinoma. *Cell Rep* **25**: 1741-1755 e1747.

Sorlie T, Perou CM, Tibshirani R, Aas T, Geisler S, Johnsen H, Hastie T, Eisen MB, van de Rijn M, Jeffrey SS et al. 2001. Gene expression patterns of breast carcinomas distinguish tumor subclasses with clinical implications. *Proc Natl Acad Sci U S A* **98**: 10869-10874.

Sorlie T, Tibshirani R, Parker J, Hastie T, Marron JS, Nobel A, Deng S, Johnsen H, Pesich R, Geisler S et al. 2003. Repeated observation of breast tumor subtypes in independent gene expression data sets. *Proc Natl Acad Sci U S A* **100**: 8418-8423.

Sotiriou C, Pusztai L. 2009. Gene-Expression Signatures in Breast Cancer. *N Engl J Med* **360**: 790-800.

Thayer SP, di Magliano MP, Heiser PW, Nielsen CM, Roberts DJ, Lauwers GY, Qi YP, Gysin S, Fernandez-del Castillo C, Yajnik V et al. 2003. Hedgehog is an early and late mediator of pancreatic cancer tumorigenesis. *Nature* **425**: 851-856.

Thiery JP, Acloque H, Huang RY, Nieto MA. 2009. Epithelial-mesenchymal transitions in development and disease. *Cell* **139**: 871-890.

Thomson S, Buck E, Petti F, Griffin G, Brown E, Ramnarine N, Iwata KK, Gibson N, Haley JD. 2005. Epithelial to mesenchymal transition is a determinant of sensitivity of non-small-cell lung carcinoma cell lines and xenografts to epidermal growth factor receptor inhibition. *Cancer Res* **65**: 9455-9462.

Tiriac H, Belleau P, Engle DD, Plenker D, Deschenes A, Somerville TDD, Froeling FEM, Burkhart RA, Denroche RE, Jang GH et al. 2018. Organoid Profiling Identifies Common Responders to Chemotherapy in Pancreatic Cancer. *Cancer Discov* **8**: 1112-1129.

- Uramoto H, Iwata T, Onitsuka T, Shimokawa H, Hanagiri T, Oyama T. 2010. Epithelial-Mesenchymal Transition in EGFR-TKI Acquired Resistant Lung Adenocarcinoma. *Anticancer Research* **30**: 2513-2518.
- Viswanathan VS, Ryan MJ, Dhruv HD, Gill S, Eichhoff OM, Seashore-Ludlow B, Kaffenberger SD, Eaton JK, Shimada K, Aguirre AJ et al. 2017. Dependency of a therapy-resistant state of cancer cells on a lipid peroxidase pathway. *Nature* **547**: 453-457.
- Waddell N, Pajic M, Patch AM, Chang DK, Kassahn KS, Bailey P, Johns AL, Miller D, Nones K, Quek K et al. 2015. Whole genomes redefine the mutational landscape of pancreatic cancer. *Nature* **518**: 495-501.
- Wang L, Yang H, Abel EV, Ney GM, Palmboos PL, Bednar F, Zhang Y, Leflein J, Waghray M, Owens S et al. 2015. ATDC induces an invasive switch in KRAS-induced pancreatic tumorigenesis. *Genes Dev* **29**: 171-183.
- Weber GF, Ashkar S, Glimcher MJ, Cantor H. 1996. Receptor-ligand interaction between CD44 and osteopontin (Eta-1). *Science* **271**: 509-512.
- Wellner U, Schubert J, Burk UC, Schmalhofer O, Zhu F, Sonntag A, Waldvogel B, Vannier C, Darling D, zur Hausen A et al. 2009. The EMT-activator ZEB1 promotes tumorigenicity by repressing stemness-inhibiting microRNAs. *Nat Cell Biol* **11**: 1487-1495.
- Whittle MC, Hingorani SR. 2019. Fibroblasts in Pancreatic Ductal Adenocarcinoma: Biological Mechanisms and Therapeutic Targets. *Gastroenterology* **156**: 2085-2096.

- Witkiewicz AK, McMillan EA, Balaji U, Baek G, Lin WC, Mansour J, Mollaei M, Wagner KU, Koduru P, Yopp A et al. 2015. Whole-exome sequencing of pancreatic cancer defines genetic diversity and therapeutic targets. *Nat Commun* **6**: 6744.
- Witta SE, Gemmill RM, Hirsch FR, Coldren CD, Hedman K, Ravdel L, Helfrich B, Dziadziuszko R, Chan DC, Sugita M et al. 2006. Restoring E-cadherin expression increases sensitivity to epidermal growth factor receptor inhibitors in lung cancer cell lines. *Cancer Res* **66**: 944-950.
- Xu X, Zhou Y, Xie C, Wei SM, Gan H, He S, Wang F, Xu L, Lu J, Dai W et al. 2012. Genome-wide screening reveals an EMT molecular network mediated by Sonic hedgehog-Gli1 signaling in pancreatic cancer cells. *PLoS One* **7**: e43119.
- Yang J, Weinberg RA. 2008. Epithelial-mesenchymal transition: at the crossroads of development and tumor metastasis. *Dev Cell* **14**: 818-829.
- Yauch RL, Januario T, Eberhard DA, Cavet G, Zhu W, Fu L, Pham TQ, Soriano R, Stinson J, Seshagiri S et al. 2005. Epithelial versus mesenchymal phenotype determines in vitro sensitivity and predicts clinical activity of erlotinib in lung cancer patients. *Clin Cancer Res* **11**: 8686-8698.
- Ying H, Dey P, Yao W, Kimmelman AC, Draetta GF, Maitra A, DePinho RA. 2016. Genetics and biology of pancreatic ductal adenocarcinoma. *Genes Dev* **30**: 355-385.
- Ying H, Kimmelman AC, Lyssiotis CA, Hua S, Chu GC, Fletcher-Sananikone E, Locasale JW, Son J, Zhang H, Coloff JL et al. 2012. Oncogenic Kras maintains pancreatic tumors through regulation of anabolic glucose metabolism. *Cell* **149**: 656-670.

- Yoon JW, Kita Y, Frank DJ, Majewski RR, Konicek BA, Nobrega MA, Jacob H, Walterhouse D, Iannaccone P. 2002. Gene expression profiling leads to identification of GLI1-binding elements in target genes and a role for multiple downstream pathways in GLI1-induced cell transformation. *J Biol Chem* **277**: 5548-5555.
- Yoshida T, Song L, Bai Y, Kinose F, Li J, Ohaegbulam KC, Munoz-Antonia T, Qu X, Eschrich S, Uramoto H et al. 2016. ZEB1 Mediates Acquired Resistance to the Epidermal Growth Factor Receptor-Tyrosine Kinase Inhibitors in Non-Small Cell Lung Cancer. *PLoS One* **11**: e0147344.
- Yu HA, Arcila ME, Rekhtman N, Sima CS, Zakowski MF, Pao W, Kris MG, Miller VA, Ladanyi M, Riely GJ. 2013. Analysis of tumor specimens at the time of acquired resistance to EGFR-TKI therapy in 155 patients with EGFR-mutant lung cancers. *Clin Cancer Res* **19**: 2240-2247.
- Zahreddine HA, Culjkovic-Kraljacic B, Assouline S, Gendron P, Romeo AA, Morris SJ, Cormack G, Jaquith JB, Cerchietti L, Cocolakis E et al. 2014. The sonic hedgehog factor GLI1 imparts drug resistance through inducible glucuronidation. *Nature* **511**: 90-93.
- Zhao H, Chen Q, Alam A, Cui J, Suen KC, Soo AP, Eguchi S, Gu J, Ma D. 2018. The role of osteopontin in the progression of solid organ tumour. *Cell Death Dis* **9**: 356.
- Zheng X, Carstens JL, Kim J, Scheible M, Kaye J, Sugimoto H, Wu CC, LeBleu VS, Kalluri R. 2015. Epithelial-to-mesenchymal transition is dispensable for metastasis but induces chemoresistance in pancreatic cancer. *Nature* **527**: 525-530.

Zipser MC, Eichhoff OM, Widmer DS, Schlegel NC, Schoenewolf NL, Stuart D, Liu W, Gardner H, Smith PD, Nuciforo P et al. 2011. A proliferative melanoma cell phenotype is responsive to RAF/MEK inhibition independent of BRAF mutation status. *Pigment Cell Melanoma Res* **24**: 326-333.

Publishing Agreement

It is the policy of the University to encourage the distribution of all theses, dissertations, and manuscripts. Copies of all UCSF theses, dissertations, and manuscripts will be routed to the library via the Graduate Division. The library will make all theses, dissertations, and manuscripts accessible to the public and will preserve these to the best of their abilities, in perpetuity.

Please sign the following statement:

I hereby grant permission to the Graduate Division of the University of California, San Francisco to release copies of my thesis, dissertation, or manuscript to the Campus Library to provide access and preservation, in whole or in part, in perpetuity.

Christina Adams
Author Signature

8/5/19
Date